Hot dip coating of high strength low carbon steels.

Lodwig, Geraint Wyn

EPSRC Engineering Doctorate Centre in Steel Technology

Hot Dip Coating Of High Strength Low Carbon Steels

by

Geraint Wyn Lodwig

A thesis submitted to the University of Wales for the degree of Doctor of Engineering (EngD)

2004

ProQuest LLC.
789 East Eisenhower Parkway
P.O. Box 1346
Ann Arbor, MI 48106 – 1346

DECLARATION

This work has not previously been accepted in substance for any degree and is not being concurrently submitted in candidature for any degree.

Candidate: Geraint Wyn Lodwig

Signed:... ..... Date:10.6.04

STATEMENT 1

This thesis is the result of my own investigations, except where otherwise stated. Other sources are acknowledged by explicit references. A list of references is appended.

Candidate: Geraint Wyn Lodwig

Signed:..... Date:10.6.04

STATEMENT 2

I hereby give consent for my thesis, if accepted, to be available for photocopying and for inter-library loans after expiry of a bar on access approved by the University of Wales on the special recommendation of the Constituent/Associated Institution.

Candidate: Geraint Wyn Lodwig

Signed:.. ..... Date:10.6.04

ABSTRACT

In response to increasing demand for high strength automotive steels, the development of galvanised dual phase steels has become more significant in recent years. At present, a requirement for galvanised high strength steels with tensile strengths in excess of 600 MPa exists within the automotive industry.

The present programme focuses on seven C-Mn based steels, each steel varying in key additions such as silicon, chromium, vanadium, molybdenum and niobium. A composition range wt% of C (0.07-0.2), Mn (1.3-1.5), Si (0.05-1.3), Cr (0.05-0.45), V (up to 0.01), Mo (up to 0.01) and Nb (0.001-0.01) was studied. In order to attain these wide-ranging steel chemistries, both commercially produced and laboratory cast steels were used for this project. All steels had the required chemistry for dual phase steel production, but only if a suitable annealing cycle was used. As a result, all steels were subjected to a range of annealing cycles on a laboratory-annealing simulator, based on current continuous annealing/galvanising line schedules utilised by the Corus Group.

Steels identified as dual phase steels from annealing experiments by microstructural and mechanical property analysis were subjected to laboratory galvanising. The zinc coating applied to these steels has been studied to evaluate the quality of the galvanised steel. This investigation, which has utilised a galvanising simulator, has demonstrated that during standard galvanising practices, problems known as de-wetting affected the coating quality. Unfortunately, this issue was most prevalent with the steels displaying the most suitable metallurgical properties. Nevertheless, the wetting performance could be vastly improved by varying processing conditions such as annealing furnace dew point and strip entry temperature.

ACKNOWLEDGEMENTS

The author would like to thank both Corus and the Engineering and Physical Sciences Research Council for the financial support offered throughout the course of the EngD programme. In addition, I would like to express my thanks to the staff at the University of Wales Swansea, Materials Research Centre. Particular thanks go to the staff of the Welsh Technology Centre and subsequently ECM^2 for their continued support in ensuring that the necessary facilities were available. Also, the support offered by the Metallic Coatings Section at WTC and in IJmuiden is appreciated.

Grateful thanks for the industrial supervision go to Dr. Stephen Price and Dr. Laurent Gavard. Their guidance throughout the project is greatly appreciated. Special thanks are offered to Professor Wilshire for the assistance with thesis preparation.

Thanks go to fellow EngD's for making the four years an enjoyable and unforgettable experience, particularly Simon, Ian, Hiram, Nicolas, Nathan and Paul. Their words of wisdom on a vast array of subjects were gratefully accepted.

Finally, I would like to thank my family and friends for the unwavering support given during the duration of the EngD degree. The support from my parents throughout my university days cannot be understated, especially the financial contribution made. Last, but not least, I wish to express a very big thank you to Nichola for her patience and understanding over the last few years, in particular during the long and testing months spent writing up.

CONTENTS

INTRODUCTORY COMMENTS

High strength and ultra high strength low carbon steels for automotive applications have been at the forefront of research and development in recent times. These steel grades are based on low-carbon steels and have tensile strengths ranging from around 500 MPa up to 1400 MPa. High strength steels (HSS) cover a broad range of steel grades, which can be a little unclear at times due to varying interpretations. For the purpose of this investigation, HSS grades will be described as those with ultimate tensile strengths up to 800 MPa. Steels with higher tensile strengths are usually classified as ultra high strength steels (UHSS). The main attraction is that they offer the possibility of lightweight steel vehicle bodies. The drive for these advanced high strength grades has mainly been provided from within the industry, with the potential threat posed by non-ferrous materials being seen as significant. However, external factors such as environmental legislation to reduce vehicle fuel emissions have also pressed both the steel producers and carmakers into reviewing the existing position. The ULSAB (Ultra Light Steel Automotive Body) projects, which were jointly supported by most major steel producers, demonstrated that the successful replacement of current low strength grades with thinner gauge high strength steels was possible. In fact, a 25% weight reduction was achieved, which was based on a standard family saloon car. Grades that make up the high strength steel family include established materials in the automotive sector such as solid solution strengthened steels, which rely on the strengthening effect of phosphorous, silicon, manganese etc., as well as newer materials like Transformation Induced Plasticity (TRIP) steels. A balance of conventional and new grades, high strength and ultra high strength was used to show the diverse properties required when considering application. Many metallurgical and mechanical issues were raised regarding the high strength steels, which have led to a demand for gaining further knowledge of these material grades. Possible issues surrounding the suitability for welding, galvanising and formability came to light, which is a part of the challenge to produce these new steel grades.

Most automotive steels are supplied to the manufacturers as coated products by means of a coating line. A range of coatings is used, which include zinc, zinc-iron and

aluminium via hot dip coating and electroplated zinc, with zinc coated products accounting for the majority of materials produced. The zinc coating prevents the steel from corroding by sacrificial protection and also by acting as a barrier between the steel and the environment. A galvanised (pure zinc coating) or galvannealed (zinc-iron alloy coating) coating can be produced by means of hot dip coating; with the component application usually governing product selection. As well as offering protection for the steel substrate, it is just as important that the appearance of the coating is aesthetically pleasing. The quality of surface finish achieved for the final product is critical, as material supplied to the manufacturer with surface defects will be rejected. Existing grades of steel such as High Strength Low Alloy (HSLA), Interstitial Free (IF) and mild steels have been galvanised/galvannealed without significant wetting problems, i.e., good zinc adhesion leading to good coating quality. However, with the highly alloyed high strength steels being developed, issues surrounding the ability of zinc to adhere to the steel have been raised. Steels high in manganese, silicon and chromium are known to form oxides on the steel surface that can subsequently cause de-wetting.

The primary objective of the present investigation is to balance the requirements regarding mechanical and metallurgical properties with those concerning coating issues. Highly alloyed steels, which would satisfy mechanical properties, could produce an unsatisfactory coating. Equally, a steel chemistry satisfying coating requirements may not achieve the desired mechanical properties.

1.0 LITERATURE REVIEW

Research into zinc-coated high-strength steel has been very well documented in recent years (Goodwin *et al.* 2000). The importance of these steel grades has driven many studies attempting to quantify the benefits of such products, as well highlighting any potential drawbacks. Both the steel makers and automotive manufacturers have jointly been striving to achieve commercially viable high-strength steels, a venture has subsequently re-focussed on coated high-strength steels. The following literature review will highlight the current situation and also give an insight into future developments.

1.1 FUNDAMENTAL PRINCIPLES

Before evaluating high strength steels, a firm understanding of the underlying metallurgical principles and mechanical properties is necessary in order to appreciate the purpose of these grades.

1.1.1 Ferrous Microstructures

The iron-carbon equilibrium diagram is an important system in gaining an understanding of steel metallurgy. It is worth noting that, the meta-stable equilibrium diagram between iron-iron carbide (cementite) is commonly used, not that of iron-carbon (graphite). This is because it is difficult to obtain the iron-carbon (graphite) equilibrium phase in low carbon steels. The iron-rich end of the equilibrium diagram, shown in figure 1.1, is the area of particular interest for low carbon steels. On cooling, the austenite transforms to ferrite plus pearlite (ferrite+cementite) in steels containing carbon between 0.02 and 0.8 weight %. The volume of ferrite and pearlite is determined by the lever rule which, in this case, indicates that an increase in carbon will increase the volume percentage of pearlite.

Transformation temperatures A_1 and A_3 shown in the phase diagram (figure 1.1) relate to equilibrium conditions for iron and carbon. The transformation temperatures have

three distinct values, denoted by Ae_x for equilibrium conditions (given on the phase diagram) and Ac_x and Ar_x that refer to heating and cooling respectively. The presence of certain alloying elements can change the transformation temperatures, which can be calculated by an empirical formula devised by Andrews (1965). The formula works from the alloying additions present (weight %) in the steel and is used as a guide for transformation temperatures.

$$A_1 = 723 - 10.7(Mn) - 16.9(Ni) + 29.1(Si) + 16.9(Cr) + 290(As) + 6.38(W) \quad \text{[equation 1.1]}$$

$$A_3 = 910 - 203(C)^{0.5} - 15.2(Ni) + 44.7(Si) + 104(V) + 31.5(Mo) + 13.1(W) \quad \text{[equation 1.2]}$$

Dilatometry can be used to determine the A_1 and A_3 temperatures experimentally by measuring volume changes as a function of temperature.

The equilibrium diagram describes the constituents formed during slow cooling. However, when rapid cooling is applied from the austenite region, the austenite can transform to bainite or martensite. The time temperature transformation (TTT) diagram illustrates the kinetics of the austenite transformation, and figure 1.2 shows a typical TTT for low carbon steel. It demonstrates that cooling rate from the austenite region affects whether ferrite-pearlite, bainite or martensite is formed. It should be noted that the steel chemistry is a factor that influences the TTT curve, with most additions pushing the curve to longer times, i.e., transformations taking place at lower cooling rates.

1.1.1.1 Ferrite

Low carbon steels can exist as a main body centred cubic (bcc) phase called ferrite, which is also known as α iron. Several morphologies of ferrite have been identified from the austenite transformation, namely, grain boundary allotriomorphs, Widmanstatten laths, intragrannular idiomorphs and intragrannular plates. The formation of these morphologies is dependent on transformation temperature, which

also determines the site of nucleation. Grain boundary allotriomorphs form at the highest temperatures (800-850 °C) and nucleate at the austenite grain boundaries. Widmanstatten laths also nucleate on austenite grain boundaries or on ferrite allotriomorphs. The intragrannular idiomorphs and plates both nucleate within the austenite grains, the main difference relating to the shape of the crystals (Honeycombe & Bhadeshia 1995).

Ferrite can be found as plate like structures that are known as acicular ferrite. The structure can be closely compared with bainite due to the interwoven structure that is formed. Acicular ferrite is one of the last phases to form during transformation from austenite on cooling and is more likely to be produced from large austenite grains (Porter & Easterling 1992).

A fully ferritic structure can be formed, but only with ultra low carbon steel, typically below 0.02 weight % carbon. Consequently, ferrite is usually present along with other phases. In ferritic steels, the size of the grains determines the yield stress, which is specified by the Hall-Petch empirical equation:

$$\sigma_y = \sigma_0 + k_y d^{-1/2}$$

[equation 1.3]

where σ_y = yield stress, σ_0 = friction stress opposing dislocation movement, k_y = constant of the steel and d = ferrite grain size.

1.1.1.2 Pearlite

Pearlite is a constituent of steel that is produced by a eutectoid reaction and usually consists of plates of ferrite and cementite (Fe_3C). The amount of pearlite formed depends on the carbon level, such that, at 0.8 weight % carbon, austenite transforms to a fully pearlitic structure. Typically, austenite to pearlite transformation takes place at temperatures in the region of 550-720 °C. It should be noted that the cooling rate must be relatively slow in order for pearlite to form, which can be seen from the TTT

diagram (figure 1.2). Specifically, a cooling rate that intersects the curve above the nose is required.

The pearlite forms via nucleation and growth, with nucleation occurring at austenite grain boundaries as hemispherical nodules. Growth takes place as parallel lamellae of alternate ferrite and cementite, with the spacing between the ferrite and cementite influencing strength and hardness of the steel. When the interlamellar spacing is small, the steel displays an increase in strength and hardness (Anderson 2003).

1.1.1.3 Bainite

On cooling from the austenite region, bainite is a product that forms at temperatures lower than the pearlite reaction. This can be seen from the TTT diagram (figure 1.2). The diagram clearly illustrates that, initially, a rapid cooling rate is required to avoid the nose of the curve, thus avoiding pearlite formation. Once the transformation reaction to pearlite is prevented, an isothermal hold is required so that the time needed for the bainite reaction is satisfied. Typically, austenite to bainite transformation takes place at temperatures in the region of 250-550 °C. It is between these temperatures that fine aggregates of ferrite plates and cementite particles are formed, i.e., bainite (Honeycombe & Bhadeshia 1995).

Two forms of bainite are observed, upper and lower bainite. At higher temperatures in the bainitic range (350-550 °C), upper bainite is formed. Upper bainite effectively forms in two stages, the first stage is the formation of bainitic ferrite as plates growing in clusters called sheaves. The ferrite has low carbon solubility, which means carbon enrichment of the remaining austenite takes place. At the next stage, the cementite precipitates from the austenite between the ferrite plates. Lower bainite forms at lower temperatures in the bainitic range (250-350 °C) and has a microstructure that is similar to that of upper bainite. However, the main difference is that cementite particles can form within the plates of ferrite, i.e., as well as precipitating from the carbon-rich austenite, the cementite can precipitate from the super-saturated ferrite (Honeycombe & Bhadeshia 1995).

The transformation temperatures for bainite start (B_s) and finish (B_f), which was shown on the TTT curve (figure 1.2), can be estimated based on the chemical composition (weight %) using the following equations (Steven *et al.* 1956):

$$B_s = 830 - 270(C) - 90(Mn) - 37(Ni) - 70(Cr) - 83(Mo)$$

[equation 1.4]

$$B_f = B_s - 120$$

[equation 1.5]

1.1.1.4 Martensite

The formation of martensite is a diffusionless transformation that takes place with certain steel chemistries and cooling rates, typically highly alloyed steels and rapid cooling rates from the austenite region. The martensite forms via a shear process, which is not accompanied by atomic diffusion. Hence, it is a structure that contains a super-saturated solid solution of carbon in iron. Examination of the TTT diagram (figure 1.2), demonstrates that continuous rapid cooling must take place into the martensite region so that martensite is produced. Once the martensite start (M_s) temperature is reached, martensite will form regardless of time held at this temperature, i.e., martensite formation is a function of the M_s temperature and not the time held at that temperature. Subsequently, by crossing the martensite finish (M_f) temperature, a fully martensitic structure will be formed, i.e., all austenite will have transformed to martensite. The transformation temperatures can vary because of alloy composition, but the M_s is typically between 200 and 500 °C for low carbon steels.

In low carbon steels, martensite is observed as laths grouped together usually in the same orientation and is the hardest phase that can be produced in steel. The martensite has a carbon content equivalent to the carbon rich austenite from which it has formed. An increase in carbon content produces an increase in strength.

The transformation temperatures for M_s and M_f can be estimated by the chemical composition (weight %) of the steel, this is shown in the following equations (Andrews 1965):

$$M_s = 539 - 423(C) - 30.3(Mn) - 12.1(Cr) - 17.7(Ni) - 7.5(Mo)$$

[equation 1.6]

$$M_f = M_s - 215$$

[equation 1.7]

1.1.1.5 Retained Austenite

In low carbon steels, under equilibrium conditions, the austenite phase is present in the temperature range, 723-1400 °C. It transforms to ferrite and/or pearlite under equilibrium conditions but, as discussed previously, can transform to bainite and/or martensite when distinct alloying and cooling are applied. In the previous sub-section (1.1.1.4), it was stated that certain alloying additions depress the martensite transformation temperatures. With reference to the TTT diagram (figure 1.2), if the M_s temperature is lowered sufficiently which subsequently lowers the M_f to below room temperature, then austenite does not transform. As explained in section 1.1.1.4, martensite formation is a function of the M_s temperature and not the time held at that temperature. Therefore, once this temperature is reached, the steel will contain retained austenite regardless of the cooling regime from there on in.

1.1.2 Steel Mechanical Properties

Mechanical properties such as yield strength, tensile strength and elongation are commonly used to gain knowledge for specific materials. Likewise, the plastic strain ratio (r value) and the work hardening coefficient (n value) are both important values when cold deformation is considered. The r value can be defined as:

$$r = \varepsilon_w / \varepsilon_t$$

[equation 1.8]

where ε_w = true strain in the width direction and ε_t = true strain in the thickness direction.

Given that the properties for steel are rarely isotropic, the r value is usually represented as the mean value, r_m, which is obtained by averaging the r values in the rolling, transverse and diagonal direction. The n value is related to the stress-strain curve when defined as:

$$\sigma = k\varepsilon^n$$

[equation 1.9]

where σ = true stress, k = constant and ε = true strain.

It is clear from equation 1.9 that the gradient of a double logarithmic plot of the stress-strain curve will provide the n value. The n value is usually represented along with a subscripted range of numbers, which refer to the calculated n value at a given strain range. This is undertaken because the logarithmic plot does not always produce a perfectly straight line.

Hardenability is a factor that is considered when dealing with engineering and high strength steels. The term hardenability can be defined as 'the capacity of a steel to transform partially or completely from austenite to some percentage of martensite at a given depth when cooled under some given condition' (Siebert et al. 1977). In other words, hardenability is the ability to produce martensite on cooling from the austenite field. It is effectively a measure of the kinetics of austenite decomposition.

1.2 HIGH STRENGTH STEEL DEMAND

There are a number of reasons for the development of high strength steels in the automotive industry. These include the possibility of Government legislation to reduce fuel emissions, the potential for cost effective weight reduction and the threat posed by other materials for use in automotive manufacture. The last decade in particular has seen a steady rise in vehicle weight due to additional safety features and luxury equipment. This can be validated since it has been reported that an average family car such as the Volkswagen Golf now weighs approximately 1000 kg as opposed to 750 kg twenty years ago (Winklegrund 1994).

1.2.1 Ultra Light Steel Automotive Body (ULSAB)

In order to comply with the legislation for reduced fuel emissions, the automotive industry targeted vehicle weight reduction as one possible solution. The Ultra Light Steel Automotive Body (ULSAB) project, involving a consortium comprising of 35 steel companies worldwide guided by Porsche Engineering Services, achieved a 25% body weight reduction through the substantial use of thinner gauge steels. The steel grades utilised during the ULSAB project are shown in figure 1.3. Thinner gauge material coupled with advances in other technologies such as hydroforming and steel sandwich have contributed to the lower weight. This weight loss was attained without jeopardising safety and does not have any major increased costs. Progress currently made in high strength steel development is significant with many steel-makers in the advanced stages of producing commercial grades highlighted in the project. Indeed, it has been suggested that by the year 2005, there will have been a considerable replacement of mild steels by high strength steels (Goodwin 1997).

The success of the ULSAB project promoted the development of the Ultra Light Steel Auto Closures (ULSAC), Ultra Light Steel Auto Suspensions (ULSAS) and ULSAB - Advanced Vehicle Concepts (AVC) projects. ULSAC focussed on innovative closure concepts that utilised frameless structures for doors, hoods, deck lids and hatchbacks and showed up to 46% lighter door structures than the average benchmarked

frameless doors. ULSAS concentrated on effective use of steel in producing lightweight, structurally-sound steel automotive suspensions that achieved up to 34% mass reductions over conventional steel systems. Finally, the ULSAB-AVC initiative is the most recent project, which offers steel solutions to meet demands for safe, affordable, fuel efficient and environmentally responsible vehicles for the 21st century (www.ulsab.org). The materials used in the ULSAB-AVC are shown in figure 1.4, indicating a considerable increase in high strength steel use when compared with the original project (figure 1.3).

1.2.2 Non – Ferrous Materials

The development of non-ferrous materials such as aluminium and plastics for car parts has meant that steel producers have acknowledged that steel is being challenged as the primary material for automotive manufacture.

1.2.2.1 Aluminium

Aluminium currently comprises about 6% of the car's weight, mainly for castings used in engine components (Matthews 1997). There have been limited attempts in the past to use aluminium strip for body panels but only in high-cost low-volume cars such as those produced by Porsche, Ferrari and Lagonda. However, in recent years, the development of the aluminium space frame has been very successful, which is shown as well as the steel body-in-white in figure 1.5 (www.uss.com). The Audi group have utilised this technology, with the A8, A6 and A2 cars all being manufactured primarily from aluminium. With claims that the new Audi A2, which is the worlds first mass produced aluminium car, can achieve fuel consumption of 80 miles per gallon, it certainly offers a genuine alternative (www.audi.co.uk). Questions have been raised regarding the viability of this technique, claiming that fuel savings are small and production costs are higher, thus not justifying the grounds for the change to aluminium (Matthews 1997). In fact, a comparison made between the Audi A8 and two high-strength steel manufactured luxury cars – BMW 7 Series and Lexus LS430 – found that, the Audi did not achieve significant weight reduction, was

not more fuel-efficient and, most importantly, had the highest on-the-road price tag (www.uss.com).

Public perception that aluminium is a superior product to steel has also played into the hands of carmakers wishing to supply aluminium cars. Audi have marketed the lightweight aluminium spaceframe with reference to the NASA space programme, which implies it has enhanced properties. However, the superior mechanical properties offered by steel are not mentioned. Aluminium may be one-third the density of steel, but the components used must be produced with thicker gauges, which do not achieve a significant weight reduction. In addition, steel is easier to weld, has better crash resistance and, most surprisingly, is easier to recycle (www.uss.com).

1.2.2.2 Plastics

Plastic use in cars has increased significantly over the years and its main use is for interior parts, but successful use for exterior panels has been achieved. The GM Saturn has successfully used plastic panels attached to a steel frame and the Renault Espace has used a body made from laminated polyester, reinforced with glass fibre. With none of the major automotive manufacturers currently pursuing the development of mass-produced plastic cars, the role of plastics for the near future will continue to be for interior components. Furthermore, issues such as the complexity of manufacturing, high production costs and the problems associated with recycling complex polymers will limit the appeal for plastic cars (Matthews 1997).

1.3 HIGH STRENGTH STEEL GRADES

In markets other than automotive, there is a minimal requirement for HSS, examples of which include white goods, packaging, cladding and office furniture. Therefore, in this work, all characteristics will be geared specifically towards automotive application, i.e., non-automotive application will not be taken into account.

There are numerous processing routes that can be considered to attain a high strength steel grade, each giving specific mechanical and metallurgical properties. HSS grades, which were highlighted in the ULSAB projects, include solid solution strengthened, high strength low alloy (HSLA), bake hardenable (BH), dual phase (DP), transformation induced plasticity (TRIP) and martensitic steels. Figure 1.6 shows the strength to elongation properties associated with a range of HSS grades. These properties are very important factors when determining material application. It is therefore clear that the different types of steel offer a diverse range of properties that will favour or limit their use in certain parts of the automotive production.

1.3.1 Solid Solution Strengthened Steels

Solid solution strengthened steels are bolstered by specific alloy additions, examples of which are carbon, nitrogen, chromium, nickel, silicon, phosphorous and manganese (Llewellyn *et al.* 1998). These steels have properties in the range of yield strengths 200-300 MPa, tensile strengths 300-500 MPa, total elongation 25-40 % and n and r values of approximately 0.12-0.18 and 1.8 respectively.

There are essentially two modes of strengthening, interstitial and substitutional strengthening. Interstitial strengtheners are atoms significantly smaller than the iron atoms, such as carbon and nitrogen. These atoms are positioned in the interstitial sites within the iron matrix that impede dislocation movement, which in turn generates the strength increase. Substitutional strengthening elements such as phosphorous, manganese and silicon replace the iron atoms causing lattice distortion, which produces increased strength.

Phosphorous is commonly used for strengthening because it offers high increases in strength with relatively low additions. In fact, the strengthening effect achieved is generally an order of magnitude more than other commonly used substitutional additions. However, excess phosphorous can cause secondary cold work embrittlement, which is the brittle fracture that can occur with a secondary working operation. This problem is frequently associated with formed components fabricated in press shops. Manganese, silicon and chromium all give similar strengthening rates per % addition. However, they all form oxides that are more stable than iron oxide, which can generate problems during coating operations. Moreover, the addition of manganese produces a fine grain size that improves the ultimate tensile strength and the plastic strain ratio (r). Figure 1.7 shows the increase in strength when specific additions of solid solution strengthening elements are added.

1.3.2 High Strength Interstitial Free (IF) Steels

Typically, IF steels have r values of 1.2-1.8 and n values of around 0.2. When compared to solid solution strengthened steel, the n value is higher, whereas the r value is about the same. With tensile strengths in the region of 350-500 MPa and total elongation values between 30-40 %, high strength IF steels have been developed primarily for highly formed components such as outer automotive panels. Interstitial free (IF) steels are grades that contain minimal amounts of interstitial elements such as carbon and nitrogen. Lower strength IF steels are recognised for their excellent formability. Therefore, the addition of solid solution strengthening elements like silicon, phosphorous and manganese can create high strength IF steels, without significantly decreasing formability.

1.3.3 Micro-alloyed / High Strength Low Alloy (HSLA) Steels

HSLA steels have mechanical properties in the range of yield strengths 250-350 MPa, tensile strengths 300-550 MPa, total elongation 20-35 % and r and n values of approximately 1-1.6 and 0.12-0.18 respectively. Micro-alloyed steels are usually based on carbon manganese grades with additions of elements like niobium, titanium

and/or vanadium that form carbides and/or nitrides resulting in precipitation hardening. Typically, fine particles such as NbCN, TiN or V_4C_3 precipitates are formed. As well as strengthening caused by precipitation hardening, grain refinement of the ferrite also contributes to an increase in strength.

Austenite properties before hot rolling in HSLA steels can also cause an increase in strength. Prior to hot rolling, micro-alloying elements are only partially soluble at the slab reheating temperature and fine Nb(CN) particles, for example, that remain out of solution will refine the austenite grains. This will lead to a finer austenite structure because it will change the recrystallisation behaviour during hot rolling. The elements that have dissolved at reheating will form fine precipitates of carbides or carbonitrides during austenite to ferrite transformation, which also causes a strengthening effect (Llewellyn *et al.* 1998). However, this final strengthening effect is lost after cold rolling and annealing because the fine grains coarsen, unless the steel is austenised during the annealing process.

1.3.4 Bake Hardened (BH) Steels

Bake hardened steels have properties in the range of yield strengths 200-250 MPa, tensile strengths 300-400 MPa, total elongation 30-45 % and r and n values of approximately 1.6-1.8 and 0.13-0.19 respectively. The strengthening mechanism achieved with bake hardenable steels occurs after the material has been formed to its final shape, which is effectively a beneficial strain ageing process. Before the steel is formed, properties are akin to a low strength high formability material. However, once the steel has been formed and subsequently heat treated (during paint shop process), an increase in strength of up to 60 MPa can be achieved. As a result, BH steels combine good formability before pressing with a component that exhibits good resistance to deformation in the pressed condition that has a positive effect on dent resistance. The bake hardening is achieved when sufficient interstitial elements like carbon present in solid solution segregate and pin dislocation generation during forming.

1.3.5 Dual Phase (DP) Steels

Given that the classification of DP steels is very broad, mechanical properties can vary considerably; yield strength can range from 280-600 MPa and tensile strength from 500-1000 MPa. Additionally, total elongation can range from 12-35 %, with r and n values in the region of 1 and 0.1-0.2 respectively. Consequently, DP steels can be considered as both high strength and ultra high strength steels. Dual phase steels are essentially comprised of a microstructure containing a fraction martensite and mostly ferrite. These steels are produced when a combination of rapid cooling rates from the annealing temperature and a suitable chemistry to suppress pearlite and bainite formation is utilised. Elements commonly used include carbon, manganese, chromium and molybdenum. By suppressing the pearlite and bainite formation, austenite is retained to lower temperature during cooling that increases the likelihood of a diffusionless transformation to martensite.

DP steels, which can range from 5 to 70 % martensite, are usually cooled from the intercritical ($\alpha+\gamma$) region. Therefore, a structure with large volumes of martensite would require a higher annealing temperature in order for a larger proportion of austenite to transform to martensite, i.e., higher annealing temperatures would equate to more austenite. Likewise, lower annealing temperatures would generate less austenite which, would yield smaller volumes of martensite. However, the higher annealing temperatures can have an adverse effect on hardenability for low carbon steel, i.e., the austenite is lower in carbon, resulting in a decrease in hardenability. The opposite is true at lower intercritical temperatures, the austenite volume fraction is low which, consequently means that its carbon levels are high, thus increasing hardenability (Llewellyn *et al.* 1996). Several authors have suggested that optimum mechanical properties are attributed to grades that have an 80-20 ferrite–martensite ratio.

The strengthening effect is attributed to the hard martensitic grains that form on ferrite grain boundaries. A combination of the ductile ferrite phase and hard martensite give these grades high strength and relatively high total elongation. Additional properties associated with DP steels are high rate of work hardening, low yield to tensile ratio

and continuous yielding, i.e., no yield point phenomenon. The continuous yielding can be attributed to the role played by carbon in DP steels. Discontinuous yielding is a phenomenon in low carbon steels that is attributed to the carbon (or nitrogen) pinning dislocations, however, in DP steels the majority of carbon is in supersaturated solid solution within the martensite. Therefore, the low solute carbon in the ferrite matrix cannot pin the dislocations, thus causing the continuous yielding effect.

1.3.6 Transformation Induced Plasticity (TRIP) Steels

Mechanical properties achieved with TRIP steel grades are in the order of yield strength 400-600 MPa, tensile strength 600-1000 MPa and total elongation of 20-40 %. More significantly, the n value can be expected to be around 0.2 and r value roughly 1.0. Microstructures of Transformation Induced Plasticity (TRIP) steels consist of martensite and/or bainite, ferrite and retained austenite. Owing to the multiple phases present, TRIP steels are in some cases identified as multi-phase steels. A typical TRIP grade could exhibit approximately 70% ferrite, 20% bainite and 10% martensite and/or retained austenite. As well as displaying a dual phase strengthening mechanism, TRIP steels have the added advantage of greater total elongation values. The enhancement in properties is attributed to the retained austenite in the microstructure. The mechanically metastable retained austenite transforms to martensite during deformation leading to an increase in work hardening rate. This can occur during a process such as forming or in service, e.g., in a crash. It is therefore clear why TRIP steels are being investigated for crash performance.

In order to obtain TRIP microstructures, substantial austenite stabilisers must be present along with an intermediate hold during cooling. Additions such as silicon, phosphorous and aluminium are required to prevent the formation of unwanted cementite (Fe_3C) leading to a primarily martensitic phase formation (Heller *et al.* 2000). Mintz (2001) reports that the addition of molybdenum can be used as an alternative austenite stabiliser because it offers slightly better austenite retaining properties. Silicon is used most often for stabilising austenite in TRIP steels, but several researchers have substituted the silicon with aluminium (Traint *et al.* 2002, Mahieu *et al.* 2000). However, tensile properties of the aluminium TRIP steels failed

to attain the levels that the silicon TRIP steels achieved. Given the role played by nickel in stainless steels, it is an addition worth considering. However, the substantial increase in cost would make nickel an impractical option (Maruta 1999).

Once cooling begins, ferrite formation proceeds with carbon being expelled into the remaining austenite. Following initial rapid cooling from the intercritical temperature, the steel is held for a set time below the bainite start temperature. This isothermal hold allows bainitic transformation and further carbon enrichment of the retained austenite.

1.3.7 Martensitic Steels

Martensitic steels display very high tensile strengths (1200-1500 MPa) coupled with extremely low total elongation values (2-7 %), in addition, the r and n values are very low (typically 0.9 and 0.07 respectively). As a result of the poor forming quality, martensitic steels would in general be used for non/low formed structural parts. Steel grades identified as martensitic are composed entirely of a martensite microstructure. Martensite is the hardest phase in steels and is formed during a diffusionless transformation of austenite below the martensite start temperature. Similarities can be drawn with DP steels (section 1.3.5), due to the rapid cooling rate and highly alloyed steel required. However, the principal difference is the annealing temperature. Unlike DP steels, which are cooled from an intercritical temperature, martensitic steels are cooled from the fully austenitic region, preventing the possibility of ferrite formation. Alloying additions required include manganese, chromium, silicon and molybdenum, but of greater significance is the carbon level. An increase in carbon level results in an increase in hardenability and also strengthens the martensite (Honeycombe & Bhadeshia 1995).

1.3.8 High Strength Steel Review

Following this summary of HSS grades, it can be concluded that solid solution strengthened, HSIF and HSLA steels generally do not have the desired mechanical

properties when compared with the higher strength grades. Also, galvanisability of solid solution strengthened, HSIF and HSLA grades has been investigated thoroughly, whereas coated DP, TRIP and martensitic grades have not. However, martensitic grades would be extremely difficult to produce on continuous galvanising lines due to current practical limitations, i.e., the low formable strip would be difficult to process through the line. In addition, because they are considered as ultra HSS, investigations into HSS would be the most feasible first step.

In view of the fact that the newer generation of HSS (DP & TRIP) have not been extensively researched and offer superior mechanical properties, they seem the obvious choice for this investigation. Nevertheless, given that DP steels are the most desired steel for automotive application in the foreseeable future, an investigation into the galvanisability of DP seems the most feasible study.

1.4 DUAL PHASE STEELS

An overview of dual phase steels was given in section 1.3.5. However, the purpose of this chapter is to give an in depth account of properties, chemistry and processing conditions.

Dual phase steels are fast becoming a very important grade of steel for automotive manufacture because of the combination of high strength and good formability. These properties make dual phase steels a very attractive option for reducing vehicle weight. Indeed, the ULSAB-AVC project highlighted six DP grades making up almost 75 % of total material used in the body. As the name suggests, this particular grade of steel consists of two phases, namely, a ferrite matrix dispersed with martensite, where martensite acts as the main strengthening agent.

1.4.1 Chemical Composition

DP steels have chemistries selected specifically for the successful production of a ferrite and martensite microstructure. Both the thermodynamics and kinetics must be appreciated to fully understand the role of additions to the steel. In order to produce the required microstructure, pearlite and bainite formation must be avoided through the use of austenite stabilisers and cementite inhibitors or kinetic retardators. The term austenite stabilisers is given to elements that delay the austenite transformation to ferrite and are vitally important when producing dual phase steels. Ferrite formers also play an important role during dual phase production. The role played by the various additions is shown in figure 1.8, which is a schematic representation of the effect that alloying elements have on transformation kinetics (Heller *et al.* 2001). As well as describing the influence that alloying additions have on transformation kinetics, an overview of the effects that additions have on overall steel properties will also be given.

1.4.1.1 Thermodynamics

Alloying additions can influence the equilibrium diagram in effectively two ways, either by expanding or contracting the austenite range. The expansion of the austenite field is achieved through the addition of carbon, nitrogen, manganese and nickel to name but a few, which are commonly described as austenite stabilisers. As well as expanding the austenite field, additions such as manganese and nickel depress the A_1 and A_3 transformation to lower temperatures, hence justifying the term austenite stabilisers. Conversely, additions such as silicon, aluminium, vanadium, molybdenum, chromium and titanium contract the austenite field and are therefore often referred to as ferrite formers, i.e., austenite to ferrite transformation would take place at higher temperatures (Honeycombe & Bhadeshia 1995).

The amount of carbon in the steel influences total volume fraction of martensite, given that martensite is usually a carbon rich constituent of steel. Carbon has the greatest influence of all alloying additions where martensite transformation temperatures are concerned, the higher the amount of carbon the lower the transformation temperatures. This can be explained because an increase in the amount of carbon will suppress the formation of ferrite. Carbon steels that contain manganese are often used for DP steel production. Indeed, there are very few industrially produced DP steels that do not contain manganese. Austenite stabilisation is achieved because the manganese has a higher solubility in austenite compared with ferrite. Thus, the transformation to ferrite is delayed. The formation of pearlite and bainite is also retarded with carbon steels containing manganese.

Additions described as ferrite formers (silicon, aluminium, vanadium, molybdenum, chromium and titanium) act in a manner opposite to that described for additions such as manganese and carbon. Indeed, the ferrite formers can cause the austenite region to contract to very small temperature carbon ranges which, in some cases, can result in a continuous δ and α phase. As well as the contraction of the austenite field, higher transformation temperatures are also a feature of steels containing ferrite formers. It is therefore clear that levels of elements that promote ferrite formation should be selected with caution. This is substantiated by examining equations 1.1 and 1.2,

which show that high additions of the ferrite formers will draw the A_1 and A_3 closer together.

1.4.1.2 Kinetics

During cooling from the intercritical temperature, the steel chemistry influences the kinetics of the decomposition of austenite. This is often referred to as hardenability and most alloy additions will increase the hardenability of the steel, so that martensite would be formed on cooling. Essentially, most alloy additions will reduce the nucleation and growth rates for pearlite. Two reasons for this are proposed; the alloy additions can limit volume diffusion of the carbon that in turn reduces pearlite growth rate and a slow rate of diffusion can be attributed to alloy segregation during phase transformation. The segregation, which is often referred to as partitioning, is behaviour usually associated with steels that contain manganese (Le Jeune 2000).

There are a couple of exceptions to the rule that all alloy additions increase hardenability, namely cobalt and aluminium. In effect, these additions do not retard the austenite to pearlite transformation as with most other additions. In other words, these additions do not assist in forming martensite.

Carbon has the greatest influence on the hardenability because it is the element that ultimately determines the hardness of the steel. Evidence of this effect can be seen when considering equation 1.6, which clearly shows carbon to have the greatest influence on the results of that equation. Clearly, ultra-low-carbon steel would not produce dual phase steel because of the inability to produce martensite. Other key additions that increase the hardenability are manganese, nickel, chromium, molybdenum and silicon (Llewellyn *et al.* 1998).

1.4.1.3 General Properties

The role performed by the additions with regards to thermodynamics and kinetics have been discussed, but some of these additions also posses other beneficial

properties. Both chromium and molybdenum can limit the tempering of martensite if the steel is subjected to further heat treatment. However, both are costly additions for mass produced steels which, in view of the constant cost saving initiatives employed in the current market place, make their use more difficult to justify. Even so, molybdenum has the advantage over other additions in that it does not produce surface oxides, which are produced with additions such as chromium, silicon and manganese.

1.4.2 Processing Conditions

Dual phase steels can be produced as hot rolled or cold rolled and annealed products. If the dual phase steel is produced as hot rolled, then the cooling rate is controlled on the run out table, i.e., the section containing water jets and sprays to control cooling rate after the final reduction before coiling. Initially, the majority of the austenite is transformed to ferrite, leaving some remaining carbon-rich austenite. The rapid cool then transforms the remaining austenite to martensite. Furthermore, the hot mill processing conditions can affect the properties of the cold rolled and annealed product. Rege *et al.* (2002) investigated the influence of varying coiling temperatures on the mechanical properties of the final annealed product. They found that higher coiling temperatures after hot rolling had a detrimental effect on a dual phase steel grade, which had a tensile strength in excess of 600 MPa (DP600), that was subsequently cold rolled and annealed. The higher coiling temperature produced more martensite in the annealed steel, which severely affected formability even though tensile strengths were higher. The authors concluded that this was in fact an adverse effect, which could be interpreted as a positive result if a high strength-low ductility product was desired.

To produce as cold rolled and annealed dual phase steels, initially, the steel is processed through the hot and cold mills with standard methods. However, when the steel is annealed after cold rolling, the temperature is increased above the A_1 into the two-phase ($\alpha+\gamma$) region of the iron-carbon phase diagram (figure 1.1). Both austenite and ferrite are present at this stage, with volume of each phase determined primarily

by holding temperature. The steel is then cooled to ambient temperature where the cooling rate applied determines the final microstructure.

The rate at which cooling takes place is very important in determining the final microstructure of the steel. If the cooling rate is too slow then, as shown in figure 1.8, the austenite will transform to pearlite or bainite, which does not show the same strengthening ability as martensite. The annealing times and temperatures are also important factors in dual phase production. The intercritical annealing temperature ultimately determines the amount of austenite present, which consequently affects the hardenability (Sarwar *et al.* 1998).

An attempt to quantify the cooling rate (CR) required to produce 5 vol % martensite was made by Rigsbee *et al.* (1979) and Tanaka *et al.* (1979). Both calculations are shown in equations 1.10 (Rigsbee) and 1.11 (Tanaka) and are effectively measures of hardenability, in relation to the weight % of added elements.

$$\text{Log CR (°C/s)} = 4.93 - 1.7(\text{Mn}) - 1.34(\text{Si}) - 5.86(\text{C}) \qquad \text{[equation 1.10]}$$

$$\text{Log CR (°C/s)} = 3.95 - 1.73 \times (\text{Mn} - 0.26(\text{Si}) + 3.5(\text{P}) - 1.3(\text{Cr}) + 2.67(\text{Mo})) \qquad \text{[equation 1.11]}$$

Neither equation seems to be entirely accurate because of the omission of key elements, i.e., Rigsbee *et al.* did not consider crucial additions such as phosphorous, chromium and molybdenum, whereas Tanaka *et al.* failed to include carbon. This suggests that these equations are useful tools in assessing steel chemistry, but should not be used as a definitive guide.

It should be noted that when the DP steel has cooled to ambient temperature from the annealing temperature and is subsequently re-heated, martensite tempering could occur. Tempering is best described, as the rejection of carbon from martensite that is caused by diffusion of carbon atoms from the martensite to form carbides. In many cases, this procedure would be advantageous because it can make the martensite less brittle. However, with regard to dual phase steels, it could have an adverse effect on

DP metallurgy and properties, i.e., mechanical properties such as tensile strength could be lowered due to tempering. There are different degrees of tempering, which are specific to certain temperature ranges. Temperatures at which tempering occurs are usually between 200 °C up to the A_1. A selection of elemental additions can minimise the effect of tempering, such as molybdenum chromium and manganese (Thomson *et al.* 1995).

1.4.3 DP Microstructure

Dual phase steels produced by cold reduction and intercritical annealing, have elongated microstructures prior to annealing. The ferrite grains begin recovery and recrystallisation before the intercritical temperature is reached. On heating into the intercritical region, austenite grain growth is initiated at cementite particles located at ferrite grain boundaries. Austenite continues to grow along the ferrite grain boundaries, and if the temperature is high enough, austenite will begin to grow into the ferrite matrix (Le Jeune 2000). It should be noted that, the amount of prior cold reduction also influences austenite growth. A greater amount of cold reduction will potentially create more sites for nucleation, resulting in an increased rate of austenite formation (El-Sesy *et al.* 1990).

Prior to cooling, the steel will contain a ferrite-austenite microstructure in a ratio determined by the annealing temperature, time and the amount cold working applied. If cooling rate is high enough, the austenite will transform to martensite producing the desired dual phase microstructure. Once cooled to ambient temperature, microstructural evaluation of DP steels reveals a ferrite and martensite structure, which is made up of ferrite grains with martensite dispersed around the ferrite, i.e., at points where the austenite was prior to cooling. Therefore, martensite is usually found as small islands situated on the ferrite grain boundaries, they are more likely to have formed on the tri-points of ferrite grain boundaries. The martensitic grains are significantly smaller than the ferrite grains, typically ferrite grains would be in the range of 5 and 15 μm in diameter whereas martensite would be closer to 1 μm.

Ferrite in DP steels is likely to consist of grains formed during annealing (recrystallised ferrite) and 'new' grains formed during cooling usually referred to as transformed ferrite. The volume fraction of the two types of ferrite would depend on annealing temperature and holding time, cooling rate and steel chemistry. A higher annealing temperature would yield more 'new' ferrite, due to more austenite present before cooling. Conversely, a rapid cooling rate would yield less new ferrite because the faster cooling would transform more austenite to martensite instead of ferrite.

The formation of a pure DP microstructure without any other second phases is very unlikely. More often than not, a small percentage of non-martensitic second phase will be observed, which in most cases is identified as bainite and/or pearlite. However, depending on processing conditions and chemistry, retained austenite can also be observed giving a slight TRIP steel effect (Vrieze *et al.* 2000). The presence of small volumes of non-martensitic second phases will not have an adverse influence on the steel properties. Nevertheless, if comparable volumes of martensite and non-martensitic second phases are observed, there will be change in steel properties.

1.4.4 Mechanical Properties

Dual phase steels are characterised by continuous yielding behaviour, low proof stress to tensile ratio and a high work hardening rate, giving this type of steel very good strength and ductility. The microstructure of the dual phase steel ultimately determines the material mechanical properties. The strength and ductility of the dual phase can be compared to that of a composite, because the properties of the second phase control the tensile strength while work hardening and ductility are controlled by factors that include the second phase (Evans *et al.*1997).

Continuous yielding can be attributed to the martensite in dual phase steels. Martensite is a super-saturated solid solution, which means there is less carbon in the interstitial sites. Thus, because of the low solute carbon content, dislocations that would usually be pinned are not, as a result continuous yielding is observed. During the austenite to martensite transformation, a volume change occurs. This volume change creates localised stress fields in the ferrite matrix, which gives rise to a high

uniform elongation and hence good ductility. The yielding behaviour and tensile strength is directly related to the amount of martensite that forms (Evans *et al.* 1997).

1.5 HOT DIP COATING

Coated steel products have been used for many years in several market sectors that include automotive, construction, packaging and white goods (domestic appliances). Most coated steels are used to protect the substrate from the corrosive environment. For automotive products, the coating is most frequently applied by means of a continuous processing line by electroplating or hot dipping. Traditionally, hot dipped products tended to be utilised for body and interior panels, whereas electroplated steels were used for exterior panels (also known as exposed parts). Even though electroplated products are very high quality, the higher costs associated with production have limited their application to surface-quality-sensitive outer body panels. Recent improvements in hot dip coating practices have enabled the development and production of the 'full finish galvanised product', which is proposed to supply material for outer panels, thereby reducing total expenditure.

Most products for the automotive sector are zinc coated and are more commonly known as galvanised steel. However, there are a few exceptions, namely aluminium coated steel supplied for exhaust systems. The galvanising process can be modified to produce an iron-zinc intermetallic coating identified as 'galvanneal'. Both types of coating are used for the automotive industry; with end product application usually determining which product is used (Llewellyn *et al.* 1998).

1.5.1 Galvanic Protection

Before the steel can be used for automotive manufacture, it must be coated in order to protect against corrosion. With long-term guarantees against corrosion issued by several carmakers, it is vitally important that there is no possibility of premature corrosion failure. The most common way of protecting the steel in the automotive industry is with zinc, both hot dipping and electroplating are used to apply the coating. Zinc is an excellent form of protection for the steel as it offers both barrier and sacrificial protection. A physical barrier is formed between the steel and the environment preventing the steel from contacting the corrosive environment.

However, the major advantage is that it also offers sacrificial protection, which means that the steel is protected from corrosion if the barrier is broken.

Sacrificial protection, which is also known as galvanic protection, is a process governed by the difference in standard electrode potentials (E^o) of the metals concerned. The metal with the largest negative standard electrode potential will act as the anode and the least negative will serve as the cathode. With iron and zinc, the zinc is more negative (Zn/Zn^{2+} E^o = - 0.763) than the iron (Fe/Fe^{2+} E^o = - 0.44), therefore the zinc becomes the sacrificial anode where metal dissolution takes place and iron is cathodically protected. The Pourbaix diagram for iron (figure 1.9) demonstrates that under neutral conditions active corrosion takes place. However, zinc presence will drive the iron into the immune region where it is thermodynamically stable (McMurray 1999).

1.5.2 Wettability

Whether the zinc coating will adhere to the surface of the steel will depend on the wettability of the steel. This can be related to the surface tension of the zinc on the steel surface, which was first discussed by Young and Laplace for liquids. Figure 1.10 illustrates the different interfacial tensions acting on a liquid droplet in equilibrium on a solid surface. The contact angle of the droplet is determined by the equilibrium between the tensions of the three interfaces, which refers to the Young's relation and is given by equation 1.12 (Berenger & Charbonnier 1992).

$$\lambda_{LV} \cos \theta = \lambda_{SV} - \lambda_{SL}$$

[equation 1.12]

where λ_{LV} = liquid/vapour interface, λ_{SV} = solid/vapour interface, λ_{SL} = solid/liquid interface and θ = contact angle.

Equation 1.12 describes the situation under equilibrium conditions. However, given that the galvanising process is not an equilibrium situation, the schematic principle of

tensiometric method of surface tension measurement should be considered (figure 1.11), which is given by the following equation.

$$F = -\rho g d S + \lambda_{LV} d \cos \theta$$

[equation 1.13]

where ρ = specimen density, g = gravity, d = perimeter of the specimen, S = surface area of contact, λ_{LV} = liquid/vapour interface and θ = contact angle.

The contact angle corresponds to the wetting performance expected between the solid and liquid. When $\theta = 0$, perfect wetting is achieved, good wetting will occur when θ is between 0 and 90°, when θ is between 90° and 180° poor wetting occurs and complete absence of wetting will take place if θ is greater than 180°. The contact angle can be determined either by static or dynamic measurements. A standard static test used is the sessile drop technique, which involves the measurement of the contact angle of the liquid droplet in relation to the solid surface. There are numerous tests used for dynamic testing, these include tensiometry, menisographic balance, Wilhemly balance and reactive wetting. The dynamic measurements offer a more realistic measure of wettability when considering the galvanising process, i.e., it allows for the movement of strip from the liquid zinc (figure 1.11).

A number of factors will influence the wetting behaviour of the zinc on the steel substrate, which include the steel chemistry, surface texture and the atmosphere. These effects will be described in sections 1.5.5 and 1.5.6.

1.5.3 The Galvanising Process

Industrial galvanising relies on a continuous processing line in order to produce coated strip steel (figure 1.12). Initially, the incoming coil is welded to the next coil in order to have a continuous process. To accommodate the very slow line speed required for the weld to be made, the line must incorporate an accumulator. The accumulator allows the strip within the main part of the galvanising line to be

processed at a constant speed while the two coils are welded together (or sheared at the exit section). Accumulators are located at the entry and exit section of the galvanising line.

A pre-cleaning section is often utilised in preparation for dipping, which includes electrolytic degreasing and pickling. This step removes oils and other residues present after the rolling process or oxides that form due to corrosion or heat scale. Once the steel has been cleaned, it enters the annealing furnace where any remaining surface oxides are reduced. To prevent the steel oxidising, certain conditions are required, an inert furnace atmosphere is required that usually consists of a nitrogen-hydrogen mix with about 95% nitrogen. As well as reducing the oxides, the furnace acts as an annealing furnace so that recrystallisation and grain growth can occur to counter the effects of cold rolling. For annealing to occur, furnace temperature is usually in the region of 700-800 °C.

After leaving the furnace, the steel strip is passed through a ceramic snout before entering the zinc bath. Strip entry temperature is an important factor with 465 °C aimed for. The temperature of the bath is approximately 455 °C, which is 35 °C above the zinc melting point. The formation of zinc coating is not as simple as it may first appear. There are several different stages that occur in the coating formation. It can be seen from the iron-zinc phase diagram (figure 1.13), that there are a number of iron-zinc phases that form, from the eta (η) phase that is pure zinc through to the gamma (Γ) phase, which is the phase with the largest percentage of iron. Each of the phases has slightly different compositions to one another, which are shown in table 1.1. To avoid the formation of these different phases, aluminium is always present in the zinc bath so that it forms a thin Fe_2Al_5 intermetallic layer on the steel surface known as the inhibition layer. For galvanising products, the aluminium content of the bath is about 0.18 weight %. The inhibition layer is a very thin layer that is usually between 20-300 nm in thickness (Schumacher *et al.* 2000). This layer also contains a small amount of zinc, typically less than 15 weight %, which forms in the intermetallic. The intermetallic layer then prevents further alloying, which would normally grow uncontrollably until it became very brittle, thus affecting the formability. It must be stated that the bath temperature and aluminium content are

directly related, because a change in temperature will change the optimum amount of aluminium that should be present and vice versa. If the immersion time in the bath was increased significantly, then further alloying would occur with an increasing possibility of forming a range of iron-zinc alloys. A schematic diagram showing the typical galvanised coating can be seen in figure 1.14.

Once the steel has been dipped in the zinc, it leaves the bath and passes through gas knives in order for the coating thickness to be controlled to the desired level. The knives blow the gas, which can be either air or nitrogen onto the steel to give a good uniform coating thickness. The thickness of the coating can be quantified by the following empirical equation:

$$th = 2/3\ (V\eta/\rho g)$$

[equation 1.14]

where V = gas velocity, ρ = melt density, η = dynamic viscosity, g = acceleration due to gravity and th = emerging thickness.

Equation 1.14 indicates that if certain line parameters and zinc properties are known, the coating thickness can be controlled.

The final stages of the galvanising line involve cooling the strip by air and water followed by temper rolling and tension levelling. The temper mill is used to eliminate the discontinuous yielding effect that occurs in steels that have interstitial elements present in solid solution. It is also used for roughness and shape control. For non-automotive applications, the steel is post treated with a chromate film to minimise staining, whereas automotive steels are oiled or kept dry before being passed through the exit accumulator and then sheared at the point where the weld was made.

1.5.4 Zinc Bath Conditions

1.5.4.1 Effective Aluminium

As stated previously, aluminium is added to the zinc bath so that the inhibition layer can be formed on the surface of the steel substrate. The percentage of aluminium present in the bath will have a direct bearing on the rate of formation and the thickness of the inhibition layer. The level of aluminium is also directly related to the amount of intermetallic compounds formed in the bath. The percentage aluminium measured is known as the effective aluminium and corresponds to the amount of aluminium that is actually in solution in the bath and not the total amount, shown in equation 1.15.

$$\text{Effective Al} = \text{total Al in bath} - \text{total Fe in bath} \qquad \text{[equation 1.15]}$$

This method for calculating effective aluminium is known as the NSC method and is named after the Nippon Steel Corporation (NSC) system of calculation. However, there is another method that involves a complex computer software package developed by the Cominco Corporation known as DEAL, (Determining Effective Aluminium). The NSC is most commonly used due to its simplicity, but it does not take into account a variation in temperature, whereas the DEAL method does (Tang *et al.* 1998).

1.5.4.2 Dross

In the bath, intermetallic compounds known as dross are present, these intermetallics contain aluminium, zinc and iron. The formation of intermetallic compounds (dross) in the zinc bath can be classified into two groups; top dross and bottom dross. Top dross is found to float at the top of the zinc bath and is made up of an iron/aluminium intermetallic and bottom dross is formed at the bottom of the zinc bath and consists of an iron/zinc compound. Top to bottom dross ratio is determined by the amount of aluminium and iron present in the bath. The effective aluminium in the galvanising

bath was stated previously as being approximately 0.18 %, which yields more top dross. To obtain a higher proportion of bottom dross the effective aluminium content would have to be below approximately 0.1 %. However, the problem of changing the aluminium content to suite the type of dross formed is not a viable option because the aluminium content is directly related to the inhibition layer formation, which is of primary importance. Dross can cause a very poor coating adherence to the surface of the coated steel. However, it is preferable to have a greater proportion of top dross because this can be skimmed from the top of the zinc bath whereas bottom dross is more difficult to remove. Bottom dross is usually removed by increasing the effective aluminium in the bath, causing a bottom to top dross transition, the top dross is then skimmed away (Jestin 2003).

1.5.4.3 Spelter Temperature

The temperature at which the zinc bath is held is a very important factor in influencing the coating that is produced. The aim temperature for many zinc spelters is 455 °C. This is roughly the standard temperature of most galvanising lines. An increase in bath temperature will cause the formation of a thicker inhibition layer and a degree of alloying usually associated with galvanneal (Jordan *et al.* 1995).

1.5.5 Steel Chemistry Effect on Coating Quality

Elements present in the steel can affect the coating quality primarily through wetting issues caused by surface oxides. The substrate chemistry can also play a role in reaction kinetics of iron and zinc.

1.5.5.1 Silicon

The presence of too much silicon in the steel has been known to cause problems in obtaining a good galvanising coating, that is known as de-wetting. This is because of the preferential surface silicon oxide that forms, which prevents the zinc from

adhering to the surface (Okada *et al.* 1996). It may therefore seem obvious to limit the amount of silicon in the steel but, since it is a strengthening agent, both parameters must be satisfied.

1.5.5.2 Manganese

Manganese acts in a similar way to silicon when the effect on galvanising is considered. It forms a surface oxide that causes de-wetting, which gives poor surface finish. Zhang *et al.* (1995) reported that 'bare spots' were found in the coating, which they attributed to the large percentage (1.62 weight %) of manganese present. However, this phenomenon was observed with interstitial free steel where Zhang *et al.* (1995) stated that lower carbon levels present in ferrite would increase the activity of manganese, thus making manganese easier to oxidise. The manganese oxide formed in the annealing furnace at a temperature that was thought to be acceptable, but the reaction took place at a lower temperature because of the part played by carbon in changing the thermodynamics. This highlights that manganese can cause problems but the part played by other variables only proves that it is not possible to attribute the problem to manganese without discounting the other variables.

1.5.5.3 Chromium

Chromium is another element that can cause dewetting due to the fact that it forms an oxide layer on the surface (Goodwin 1997). In most cases, the addition of chromium is not used specifically for strengthening purposes and could be limited significantly without having any adverse affect on the properties. However, dual phase steels often contain chromium in order to obtain the desired metallurgical properties. Again, the fine balance between satisfying substrate and coating properties is identified.

1.5.6 Annealing Furnace Conditions

Several authors (CRM 1998, Hertveldt *et al.* 1998 & Lamberigts 1999) have targeted the annealing furnace conditions as a possible area to manipulate in order to obtain a superior quality galvanised coating. A number of the factors that have been discussed include the furnace atmosphere, temperature, heating rates, cooling rates and the dew point.

1.5.6.1 Furnace Atmosphere

A typical galvanising line would have a furnace atmosphere made up of 95% nitrogen and 5% hydrogen. These are the conditions used in the ZODIAC galvanising line at Corus (Llanwern), but some other galvanising lines use different ratios of nitrogen and hydrogen. The conditions are set so that reduction of any oxides that may still be present, takes place in the furnace as well as the annealing.

The dew point in the annealing furnace is a factor that has been investigated a great deal recently (CRM 1998, Hertveldt *et al.* 1998 & Lamberigts 1999). Many annealing furnaces currently operate at a dew point of –30 °C (Jenkins *et al.* 1992). It is best described as the temperature at which a vapour mixture first begins to condense. An increase in dew point from –30 °C to +10 °C has been proposed by Lamberigts (1998) to counter the effect of problems associated with galvanising high strength steels. Problems that have arisen with the use of the current dew point include bare spots and other surface defects caused by de-wetting. Hertveldt *et al.* (1998) investigated the effects of changing the dew point from –30 °C to +10 °C for manganese strengthened interstitial free steel. They found that after annealing at a dew point of –30 °C, there was a significant amount of manganese oxide on the surface that would cause de-wetting. On the other hand, they found that after annealing using a dew point of +10 °C, there was a massive improvement on the surface, with only a few manganese oxide particles present. Hertveldt *et al.* (1998) also investigated the effect of the changing dew point on inhibition layer formation and found that there appeared to be no undesirable effects from using the higher dew point. This evidence suggests that the adoption of the higher dew point would be advantageous in order to limit the

amount of surface oxides that form when using high manganese steels. This can be explained from the fact that the higher dew point (+10 °C) causes internal oxidation as opposed to external oxidation that occurs with the lower dew point (-30 °C).

1.5.6.2 Furnace Temperature

Annealing temperature is a factor that influences the amount and rate of recrystallisation that takes place in the steel following cold rolling. It is worth noting the amount of previous cold reduction also affects the amount and rate of recrystallisation during annealing. Clearly, the higher the temperature the greater the amount of recrystallisation that occurs. The temperature at which annealing takes place can be lower than the A_3 when multi-phase steels are not produced, i.e., recrystallisation of the ferrite will still take place even at these lower temperatures. However, multi-phased steels require a higher annealing temperature because the two-phase region (austenite & ferrite) must be reached, which involves crossing the A_3 line (figure 1.1). The A_3 line can be depressed or raised by the presence of certain elements, therefore this must be accounted for when deciding the annealing temperature. Lamberigts (1998) reports that high amounts of manganese and boron in the steel would depress the A_3 line, which was also discussed in section 1.4.

1.5.7 Other Factors Affecting Coating Quality

Zinc quenching is a process that has been investigated as a mode of achieving rapid cooling rates on galvanising lines that do not have high cooling rate capabilities. This process involves using the lower temperature of the molten zinc as a method of cooling the steel, which would be at a temperature close to the annealing temperature. The strip entry temperature (SET) associated with this process can vary, but for quenching to occur SET must be in the region of 550-750 °C. An elevated SET modifies the galvanising kinetics such that a very thick δ phase and ζ free coating forms due to an increase in iron dissolution time (Le Jeune *et al.* 1999). A thick δ layer in the coating would result in a coating that would be more susceptible to flaking and/or powdering, i.e., the forming behaviour would be poorer than a regular

galvanised coating. The difficulty in controlling the galvanising kinetics at high SET means that it would be very challenging to produce commercial zinc quenched steels.

1.6 GALVANISED HIGH STRENGTH STEEL

Zinc coated product quality has improved significantly in recent times because of better processing conditions and a greater understanding of process variables. Nevertheless, the new challenge facing the industry is in production of coated high strength steels for the automotive market. As well as issues concerning coating quality, the heating and cooling capabilities of existing galvanising lines must be addressed. Most industrial lines were built without the requirement for rapid cooling sections but, with an ever-increasing demand for high strength steel, these issues are of greater significance in current times. Without considerable capital investment, older galvanising lines would not be suitable for the production of certain grades.

1.6.1 Commercial Industrial Galvanising Lines

Apart from galvanising lines built very recently, most are unsuitable for HSS galvanised products. Line configurations in most cases could be adjusted at a cost to accommodate the new products. Many galvanising lines were designed with overageing sections for IF products, but this would make DP products very difficult to produce because they require a rapid cooling section prior to and after dipping.

1.6.2 Current Commercial Products

1.6.2.1 Galvanised High Strength Steels

Production of commercial DP steels is at an early stage at present, with only a few steel makers producing galvanised DP steels. The three largest and most advanced markets in the world are North America, Europe and Japan. With developments in each market driven by domestic issues, it is useful to consider each one individually. Dual phase steels are usually characterised by the abbreviation DP followed by the minimum tensile strength, i.e., DP600 refers to a grade with a minimum tensile strength of 600 MPa. The same classification method is true for TRIP steels.

Several North American steel companies have supplied the market with DP600 and DP800 grades produced with 1 and 2 mm gauges respectively. American steel makers Ispat Inland Inc. and United States Steel (USS) Corporation have produced coated DP grades; galvanised, galvannealed and electroplated zinc. Ispat Inland currently produces elctrogalvanised DP550, DP700 and DP965 grades and is working on the development of galvanised types of these grades (www.ispat.com). However, USS have produced DP600, DP800, TRIP600 and TRIP800 grades with galvanised DP600 supplied to Honda and Nissan, which have been used in the (Honda) Civic and (Nissan) Altima models (www.uss.com).

In Europe, companies including Arcelor, SSAB, Thyssen Krupp Stahl (TKS), Voest-Alpine Stahl, have produced DP grades. Most of these grades have been supplied as uncoated products; whereas TKS have produced galvanised DP grades. A product range of galvanised DP500, DP600, TRIP600 and TRIP700 as well as uncoated TRIP800 are currently offered by TKS (www.thyssen-krupp-stahl.com).

Japanese steel makers have focussed their attention on TRIP grades more than DP steels. Indeed, Nippon Steel Corporation (NSC) is at an advanced stage of developing HSS grades in the Japanese market. With Kobe Steel also claiming to be the first company in the world to produce grades with tensile strengths of 980, 1180 and 1470 MPa, it shows that the Japanese steel makers appear to be leading the way.

1.6.2.2 High Quality Galvanised Products

Many steel makers do not supply exposed galvanised steel products. In fact, Canadian steel maker Dofasco Inc. is the only steel producer in North America that currently supplies the product. They offer HSLA exposed material, which is marketed as Extragal^{TM}, with a view to replace existing electrogalvanised products. However, most suppliers continue to provide galvannealed or electrogalvanised products as they attempt to develop exposed galvanised panels. The development of exposed galvanised panels is a more pressing issue than galvanised HSS in some cases, which only reiterates the importance placed on the product.

1.7 LITERATURE REVIEW CONCLUSIONS

The threat posed by non-ferrous materials, particularly aluminium, has driven the development of high strength steels for automotive applications. Even though the aluminium spaceframe body structure has been successfully manufactured, the high strength steel body in white does offer a better value alternative. With question marks raised over aluminium properties and plastics not currently offering a genuine alternative, for the immediate future, steel will remain the principal material for automotive production.

A range of high strength steels was highlighted for use in the body in white structure, which were chosen specifically for certain components. Where highly formed components were required, grades like High Strength Low Alloy, High Strength Interstitial Free and Solid Solution Strengthened were recommended. Likewise, when higher strength components were needed, grades such as Dual Phase, Transformation Induced Plasticity and Martensitic steels were suggested. With Dual Phase and Transformation Induced Plasticity steels generally offering the best strength to formability values, these grades were used for the most part in the ULSAB projects, which implies that significant research should be and has been focussed on these grades.

The need for galvanising high strength steels has raised many issues, not least the wetting behaviour of highly alloyed steels. Bare spots or de-wetting has been an issue emphasised over many years in galvanised products. To overcome these problems, varying several process parameters have been suggested, which include spelter conditions, furnace conditions and steel chemistry.

One of the major factors to consider with commercially produced galvanised high-strength steel is current line setting. Given that many commercial galvanising lines were not built with a view to producing high strength steels, substantial capital investment would be required to produce these grades. There are a select few steel makers that have the facilities to galvanise high strength steel and these companies have taken advantage of their situation to be the leaders in this market.

Table 1.1: Iron zinc intermetallic phases that form during galvanising and galvannealing reactions.

Phase	Symbol	Composition	Weight % Iron
Eta	η	Pure zinc	0
Zeta	ζ	$FeZn_{13}$	5.75 – 6.25
Delta	δ	$FeZn_7$	7.4 – 11
Gamma	Γ	Fe_5Zn_{21}	16 - 28

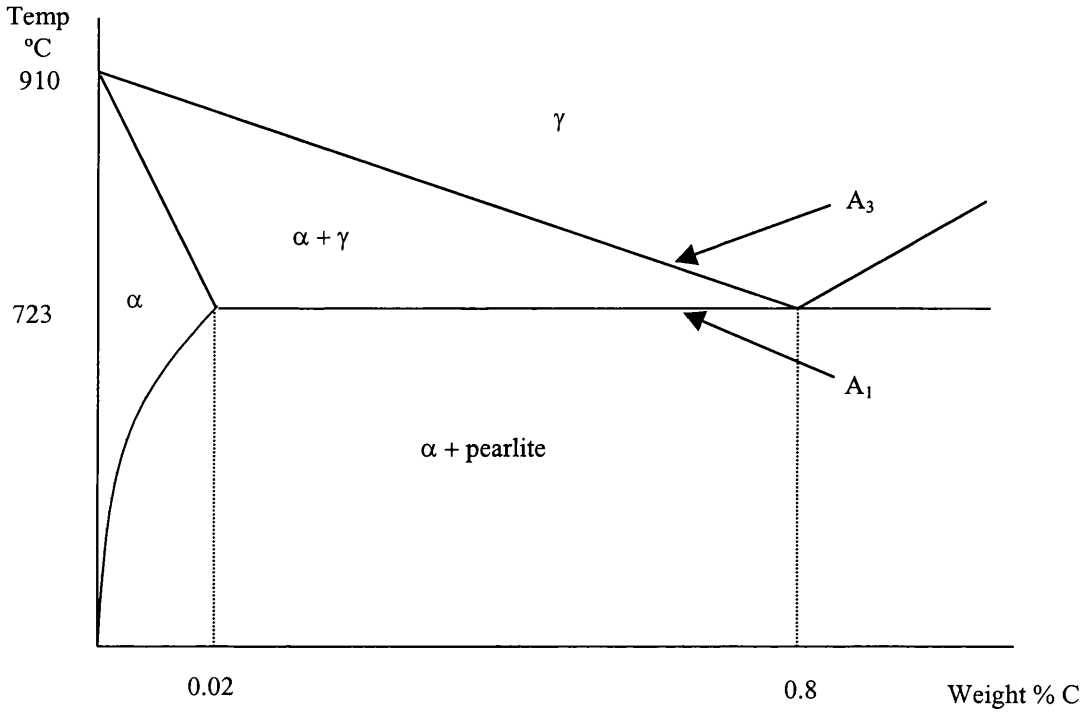

Figure 1.1: A schematic diagram showing the iron-rich end of the iron – carbon phase diagram.

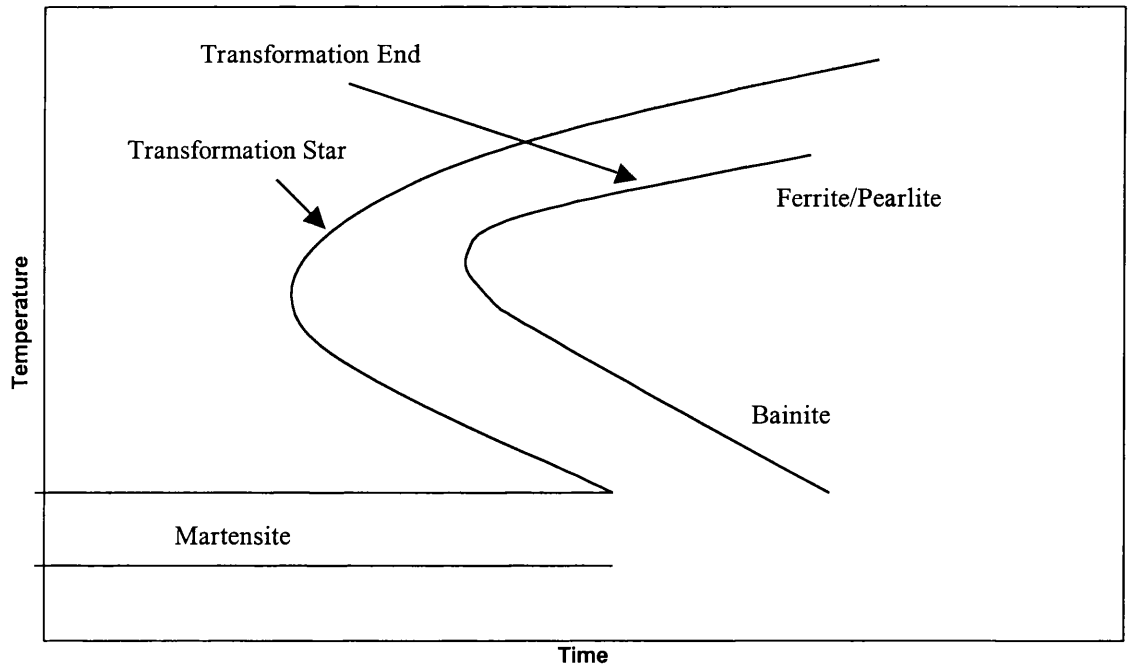

Figure 1.2: A schematic diagram illustrating the time temperature transformation (TTT) diagram for austenite transformation.

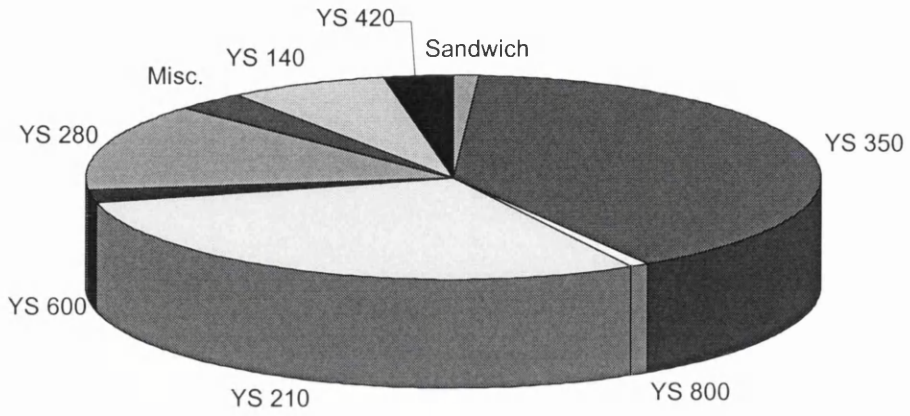

Figure 1.3: A pie chart illustrating the materials used in the ULSAB project.

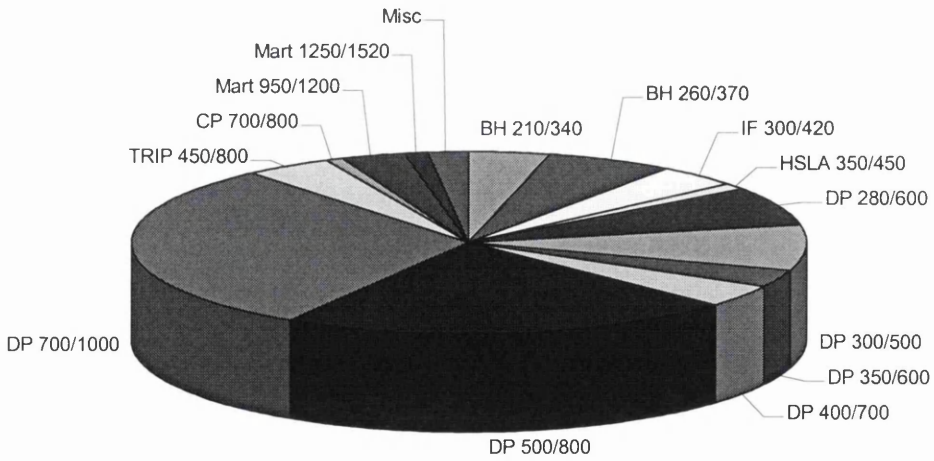

Figure 1.4: A pie chart showing the materials used in the ULSAB-AVC project (data labels show - steel grade / yield strength / tensile strength).

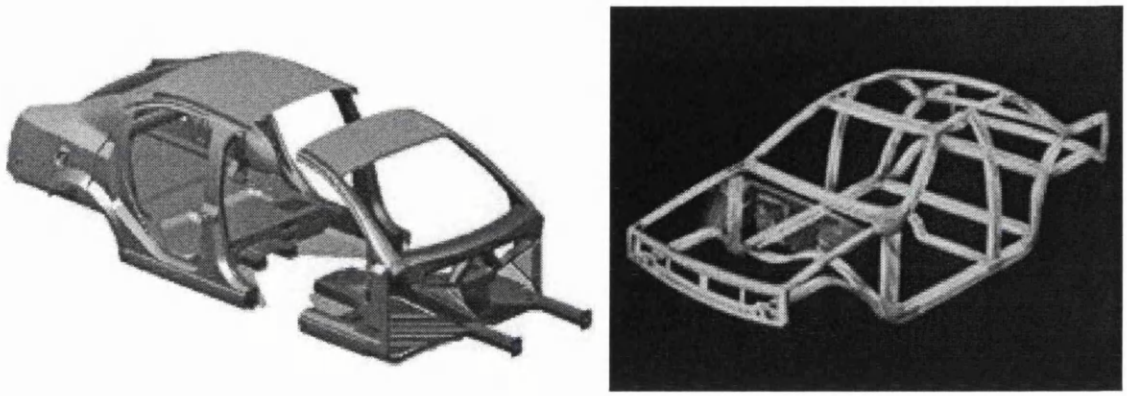

Figure 1.5: The steel body in white structure (left) and aluminium spaceframe structure (right).

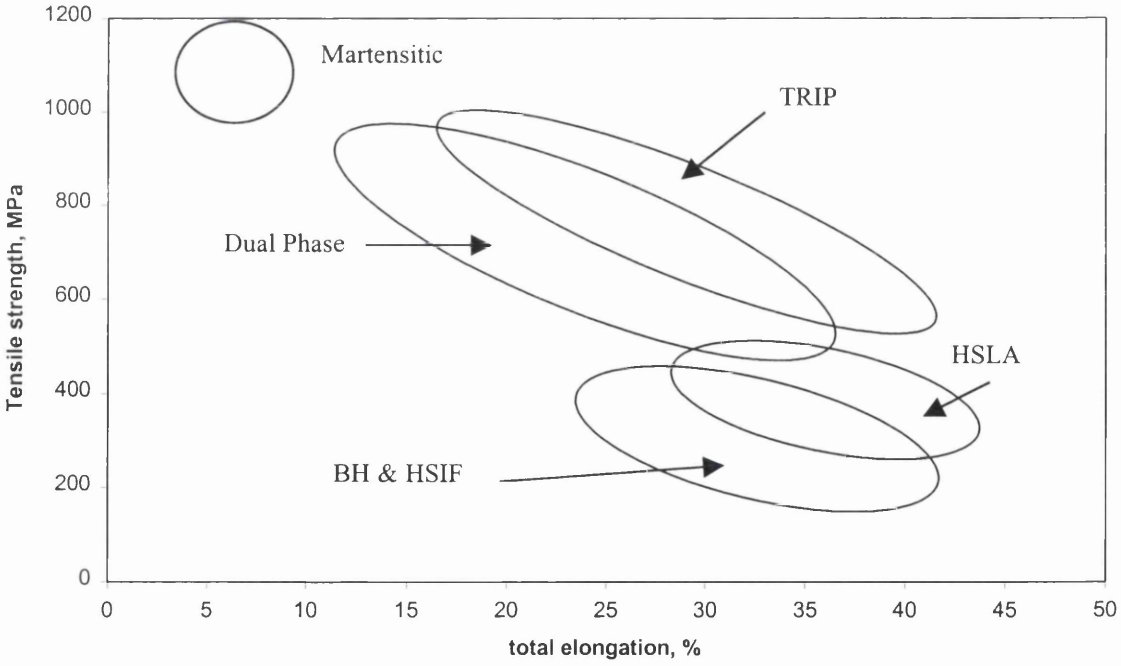

Figure 1.6: Tensile strength plotted against total elongation represented schematically for a selection of high strength steels.

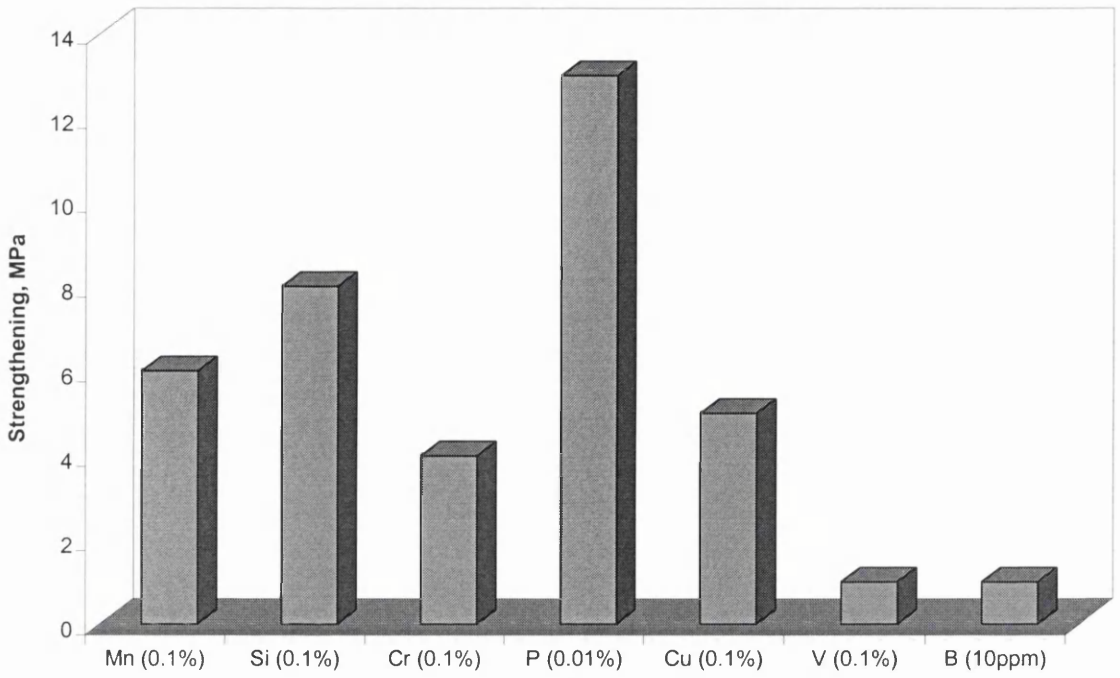

Figure 1.7: Solid solution strengthening associated with several commonly used strengthening elements.

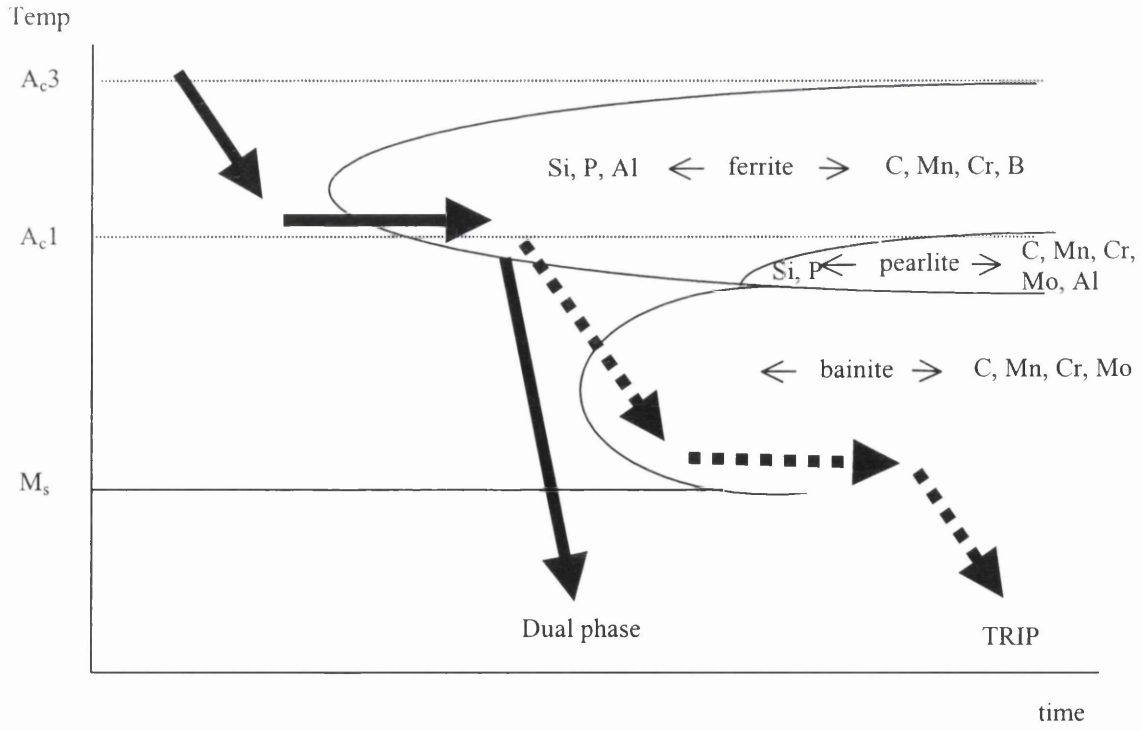

Figure 1.8: Steel chemistry influences on transformation kinetics, the presence of selected additions are shown to promote or delay reaction time.

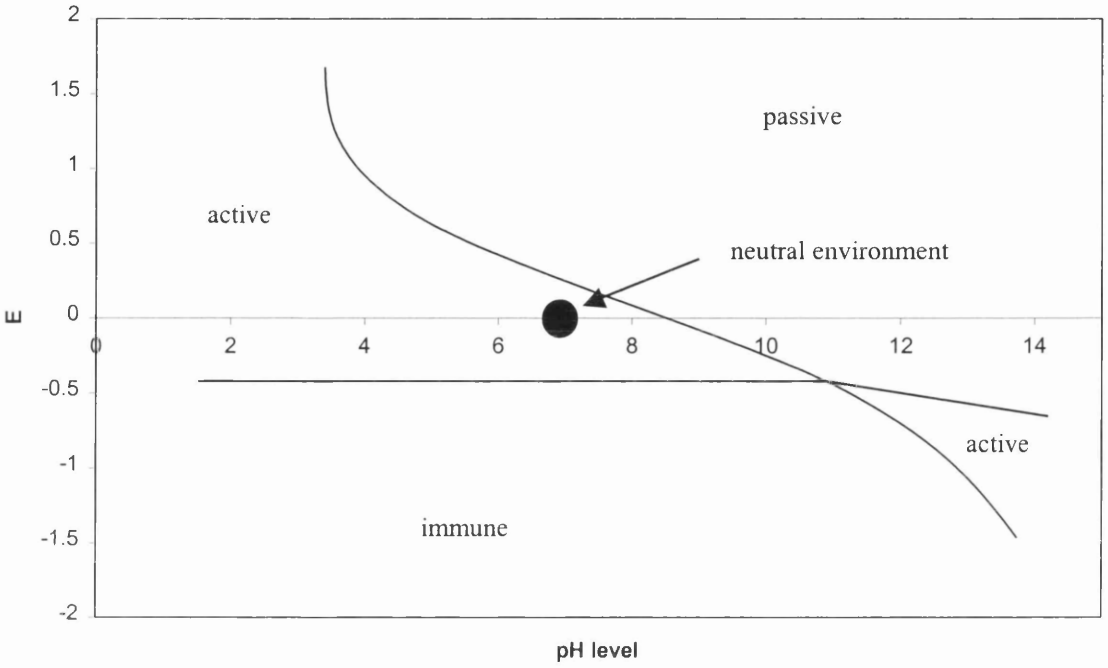

Figure 1.9: The Pourbaix diagram for iron.

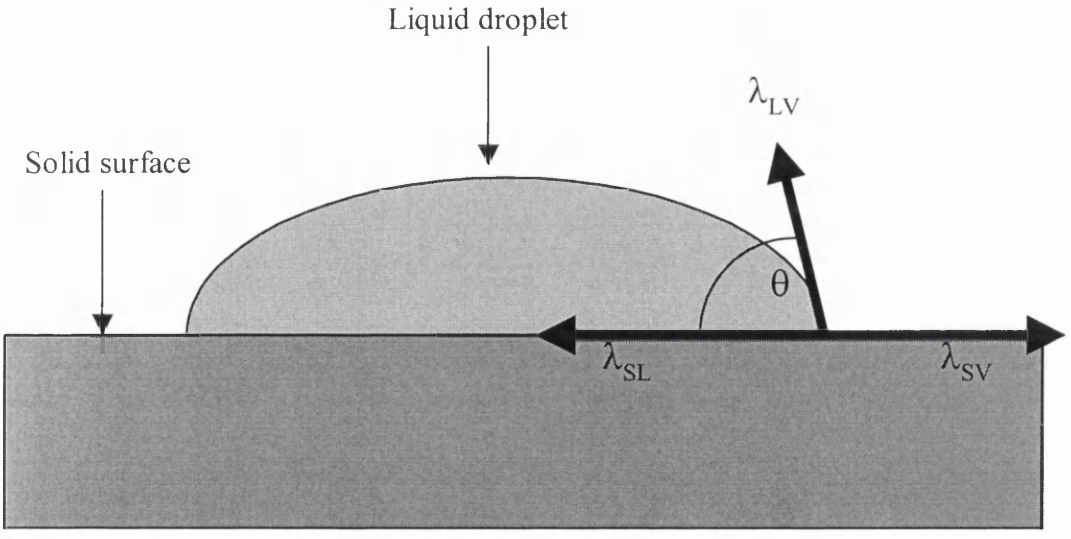

Figure 1.10: The interfacial tensions acting on a liquid droplet in equilibrium on a solid surface.

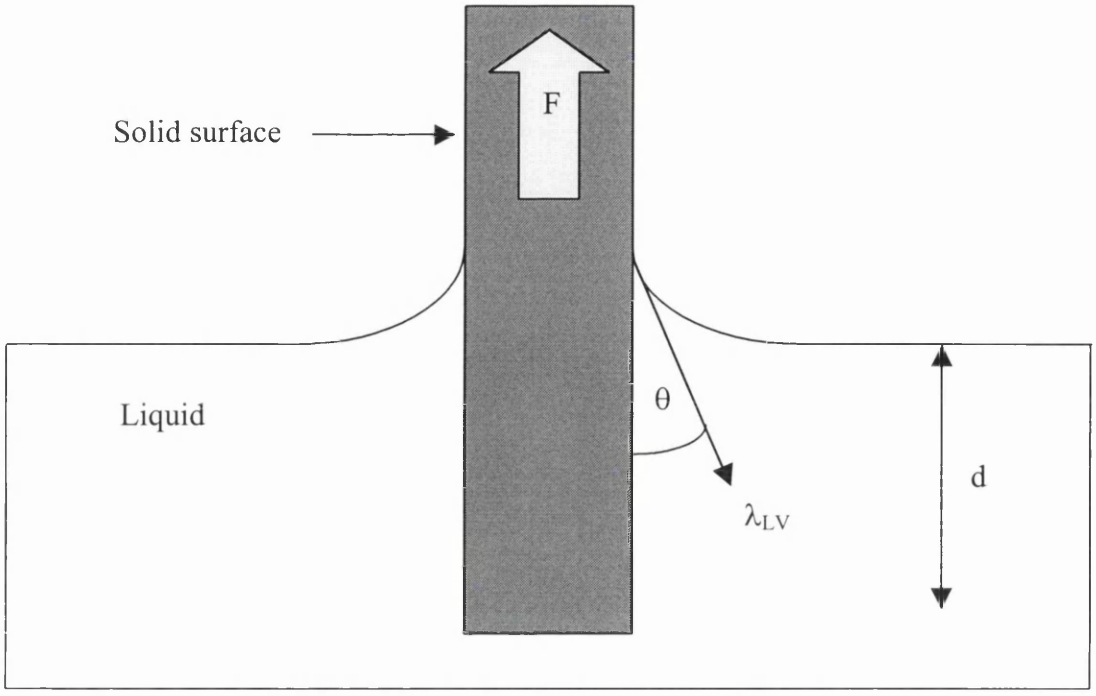

Figure 1.11: The tensiometric method of surface tension represented schematically.

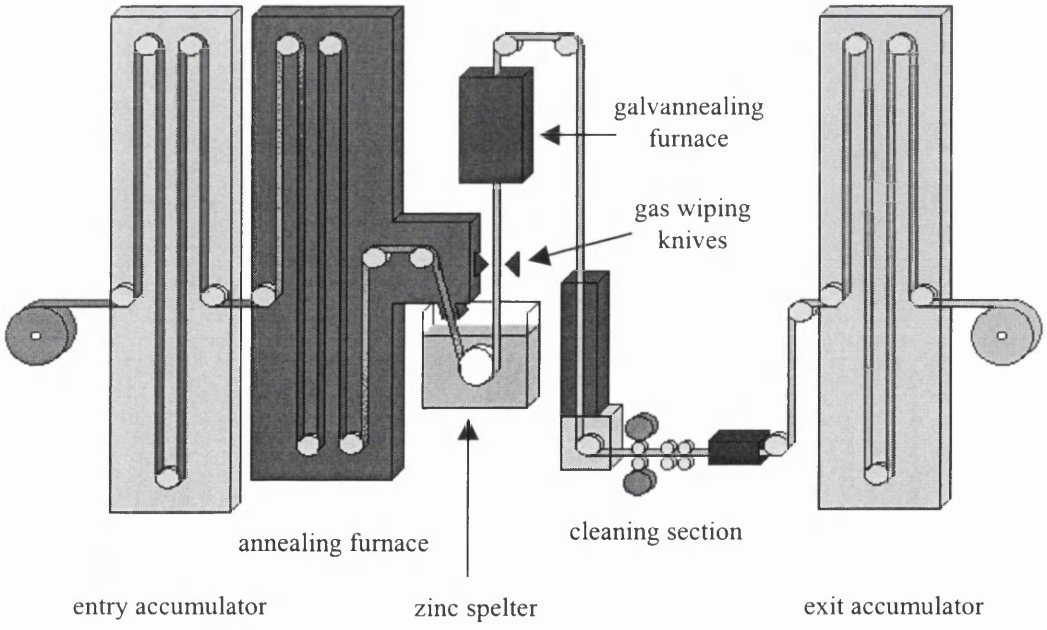

Figure 1.12: A schematic diagram of an industrial galvanising line.

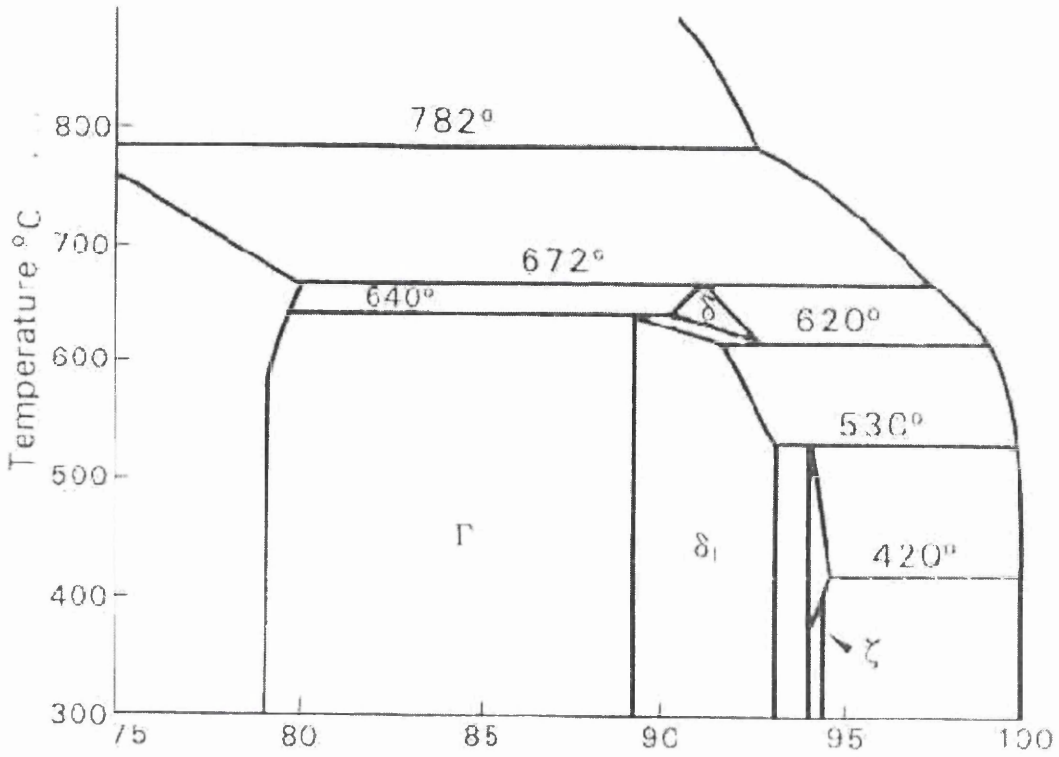

Figure 1.13: The zinc end of the iron – zinc phase diagram.

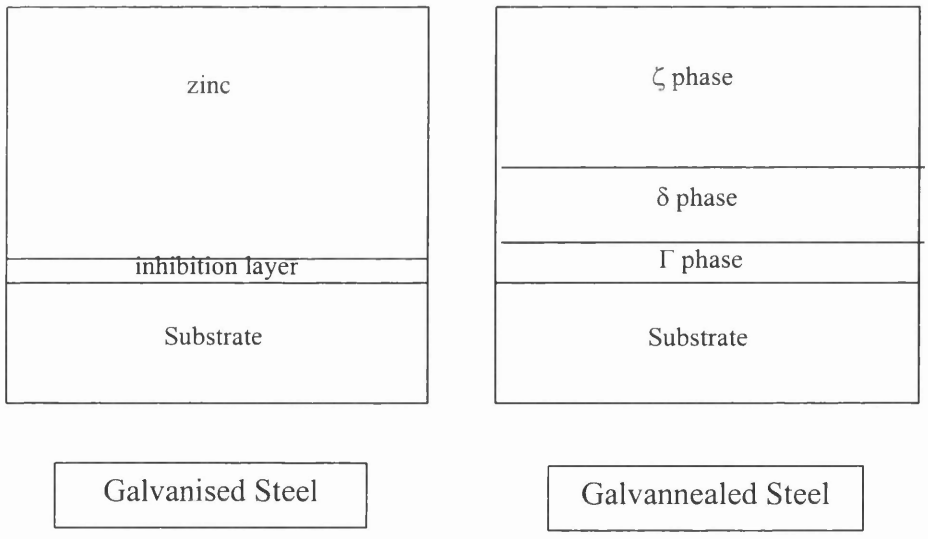

Figure 1.14: A schematic illustration of a typical galvanised coating.

2.0 AIMS OF PROGRAMME

The literature review described the current drive towards producing galvanised high strength steel, which is exemplified by the ULSAB project. Particular attention was placed on galvanised dual phase steels. Hence, by taking these findings into account, this investigation will focus on the production of galvanised dual phase steels. The following points describe the principal objectives of the project, defined from the findings of the literature review. Ultimately, they will outline the steps needed to successfully produce hot dip galvanised dual phase steels.

- To identify suitability of dual phase steel production from a selection of steels with various chemistries. All steels will be based on C-Mn grades with varying levels of additions such as silicon, niobium, chromium, molybdenum and vanadium.

- To assess the suitability of current industrial annealing/galvanising lines for dual phase steel production, by focussing particular attention on the effect of a varying cooling rate (from the intercritical region) on steel microstructures and mechanical properties. The cooling rates utilised will be kept within the limits of current industrial practice, i.e., cooling rates that cannot be recreated industrially will not be used.

- To compare the mechanical properties achieved with products demanded by the market and current available high strength steel grades. In other words, determine whether the mechanical properties would conform to the requirements set out by automotive manufacturers for high strength steel standards.

- To assess the galvanised coating quality of the highly alloyed steels selected for dual phase steel production. Given that the steels will require a set level of alloying to obtain the mechanical properties, an adverse effect on coating

quality may be experienced. This will be achieved by analysing the wetting of the zinc to the various substrates.

- To investigate the effect of variations in furnace and bath conditions in order to establish best practice for optimum galvanised coating quality. This will be achieved by varying conditions that include annealing time and temperature, annealing atmosphere and zinc spelter conditions. This is a pre-emptive step due to the anticipated coating quality problems.

3.0 EXPERIMENTAL PROCEDURES & TEST APPARATUS

The aims of the programme in chapter 2 described the objectives of the investigation. However, this section describes the test procedures and the equipment employed for the experimental programme, which is described in the next chapter. As well as describing the procedures carried out during the investigation, equipment limitations are also stated.

3.1 LABORATORY CAST STEELS

Experimental grades of steel were cast at the Corus Swinden Technology Centre into 1000x170x40 mm 60 kg ingots. Casts were received in ingot form and were subsequently cut into blocks for hot rolling.

3.1.1 Hot Rolling

The hot rolling operation was carried out at the Chemistry laboratories at Corus-Llanwern using the two-high, laboratory reversing hot rolling mill. Samples were in block form with a width of 170 mm due to roll width limitations. It was possible to have widths up to 200 mm, but narrower widths were favoured. The samples were initially placed in a Carbolite furnace set at 1250 °C where they were soaked for at least an hour in an argon atmosphere to prevent decarburisation. On removal from the furnace, the steel samples were struck repeatedly onto a steel plate to remove any surface scale that had formed during heating.

A reversing mill was utilised for hot rolling, with seven passes required to reduce the steel from a 40 mm gauge to a 3.5 mm plate, each pass achieving the following reduction, 40-27-18-12-8-6-4.7-3.5 mm. After each pass, the mill was reversed and lowered to the next desired gauge. The roll gap, which indicated the approximate gauge, was measured using the Solatron 110 mm stroke 'Mach 1' linear displacement transducer and displayed on a Solatron C53 digital unit.

Hot-rolled steel plates were placed into a Wild Barfield furnace to maintain the heating pattern associated with industrial hot-rolled sheet steel, thus simulating the coiling temperature. For both the finishing temperature and coiling temperature, a hand held Minolta Cyclops pyrometer was used to obtain the temperature at the required times. The finishing temperature was taken as soon as the steel had exited the seventh pass, whereas the coiling temperature was recorded prior to the steel plate being placed in the coiling furnace.

3.1.2 Pickling

Samples were pickled prior to cold rolling (section 3.1.3) to remove scale present on the surface as a result of hot rolling. The pickling procedure involved immersion of the steel in 10 % hydrochloric acid at room temperature for about half an hour. This was followed by immersion in an aqueous soda lime solution to neutralise any remaining acid. The final stage involved dipping the samples into a hot water bath and drying under the hot drier to assist water evaporation. Pickling was also utilised on some occasions to remove light corrosion from steels that had been stored over a long period of time.

3.1.3 Cold Rolling

Cold reduction of the steel plates was carried out using the two-high cold reducing 50 tonne Hille-100 mill based at the Chemistry laboratories at Corus-Llanwern. The steel samples were reduced from a 3.5 mm gauge down to approximately 1.2 mm with five passes. Unlike the hot mill, the cold mill was not a reversing mill, so, the steel was passed in the same direction after the upper rolls had been lowered to the required roll gap. Sample widths were limited to 200 mm, because the roll width was only slightly wider.

3.1.4 Jominy End Quench Test

The hardenabilities of the laboratory cast steels were determined using a Rockwell Hardness Machine and the Jominy End Quench Test. The Jominy test was carried out initially to create the variable hardenability in the specimen, which was measured using the Rockwell tester.

The Jominy test procedure involved the use of a steel block machined to the required dimensions of 100 mm in length and 25 mm diameter, which was heated up to an intercritical temperature in a non-oxidising, non-carburising and non-decarburising atmosphere. The test piece was then removed and subjected to water quenching at one end within five seconds of removal from the furnace. Two diametrically opposed flats were ground out of the test pieces, which were machined along the length of the sample, that were 0.4-0.5 mm in depth. This was performed in preparation for the hardness testing. The Jominy test is shown schematically in figure 3.1(a).

In order to measure the hardenability of the steel, the hardness needed to be determined using a Rockwell Hardness Machine, using a 100 kg load. The hardness was measured sequentially along the ground part of the specimen and the operation was repeated on the opposite side to obtain an average reading. Because the greatest variation in hardness was expected to be at the quenched end of the specimen, more tests were carried out in that region. The hardness was measured at points 1.5 mm, 3 mm, 5 mm, 7 mm, 9 mm, 11 mm, 13 mm, 15 mm and every 5 mm thereafter up to and including 95 mm away from the quenched end, which is shown in figure 3.1(b).

3.1.5 Dilatometry

The experimentally cast steels were subjected to a dilatometric test to determine the A_1, A_3, M_s and M_f values. Volume changes associated with a phase transition during heating, cooling or an isothermal hold forms the basis of dilatometry. Start and finish temperatures were recorded over a range of cooling rates in order to construct a Continuous Cooling Transformation (CCT) diagram, which gave the relevant information. The A_1 and A_3 temperatures were measured during slow heating from

room temperature to the austenite region, while the M_s and M_f temperatures were recorded during the rapid cooling from the austenitic region.

3.2 COMMERCIALLY PRODUCED STEELS

Steel sheets that had been cold rolled were obtained from the Corus Port Talbot and Llanwern steel making sites. The commercial material was subjected to the specific rolling regimes associated with each mill; so the process conditions could not be controlled exclusively for the project.

3.2.1 Hot & Cold Rolling

The hot rolling configuration at Port Talbot and Llanwern are generally comparable, apart from certain features that would have a minimal affect on steel quality. Both mills utilised a seven stand rolling section leading to a run out table before being coiled. However, the main difference was the roughing section prior to rolling. At Llanwern, a five-stand tandem roughing mill was used, whereas Port Talbot has a reversing roughing mill. A five-stand cold reduction mill achieved the final steel thickness, the configuration being the same at the Llanwern and Port Talbot sites.

3.3 ANNEALING SIMULATIONS

Annealing work on the steel substrates was carried out using a Resistance Heating Annealing Simulator (RHAS). The apparatus was used to simulate the industrial continuous annealing cycles, but, the RHAS was capable of mirroring only the heating, holding and cooling paths. A non-oxidising atmosphere was not possible, so, only mechanical properties could be determined with no scope for surface topography analysis. A photograph of the RHAS apparatus is shown in figure 3.2. The RHAS consists of three sections, (i) a sealed operations cabinet in which the annealing is performed, (ii) a controller that is linked to a computer, where the annealing cycle is programmed and (iii) a separate computer for data logging of temperature-time plots.

3.3.1 Heating & Cooling Capabilities

The RHAS operates from a 3 phase, 415V power supply, which is channelled to a 30A thyristor via a 70A transformer. Heating rates of up to 3000 °C/s can be achieved, which is significantly higher than any industrial practice. The RHAS cooling system can utilise both air and water, with cooling rates using water being as high as 800 °C/s compared with up to 150 °C/s with air. Both heating and cooling rates attained are somewhat lower when thicker gauged material samples were used. The ERAS operation unit is shown in figure 3.3.

3.3.2 Annealing Cycle Control

A series of links between the RHAS, thermocouples and a computer using dedicated software supplied by Eurotherm Control controlled the annealing cycle. Three thermocouples were spot welded to the steel panel, two of the thermocouples measured temperature that was fed back to the RHAS in order to control electrical input and cooling control. The third thermocouple acts as the contact between the RHAS and the control computer, which ensured the selected annealing cycle was followed accurately.

3.3.3 Material Requirements

The steel panels used for the RHAS were typically 260x50 mm^2, a schematic diagram highlighting the panel dimensions and sample use is shown in figure 3.4. The panels were clamped into a pair of moveable jaws via a series of screws. The panels can have larger dimensions if required, but the non-uniform nature of the temperature distribution does mean a greater degree of inaccuracy. In order to maintain consistency, the thermocouples were spot welded to the same selected area each time.

Thermal variation across the steel sample was an issue with this test apparatus. However, by only using the area that was highlighted in figure 3.4, the amount of

thermal variation was minimised. Indeed, work carried out by Le Jeune (2000) showed that only a 5 °C variation was found in the area selected for testing.

3.4 TENSILE TESTING

The mechanical properties of the steels were measured using a Zwick Z010/TN2A mini tensile machine with a 10kN load cell. The apparatus operates with a twin screw, two column electro-mechanical machine. Strain was measured by an EXA 10-8A axial extensometer over a gauge length of 10-mm. Tensile specimen dimensions, which were machined to the desired dimensions, were 90 mm by 15 mm with tested area dimensions being 10 mm parallel gauge length and 5 mm gauge width. The width and gauge of the tensile specimen was measured using a Mitutoya micrometer, an average reading taken from three different gauge and width measurements was used each time. Data was recorded onto a control computer and a print out of every test was taken. Any burrs present as a result of the machining process were removed before proceeding with the tensile test.

For a greater degree of accuracy, three samples were tested for each selected variable, the average properties where then presented in the results. In most cases, the results from the three tests were relatively close, i.e., within 20 MPa for strength and within 4 % for total elongation.

3.5 LABORATORY GALVANISING

The galvanising work was carried out on the Rhesca Hot Dip Simulator (HDS) based at the Corus Welsh Technology Centre. The HDS was used to simulate the industrial continuous annealed hot dip coating of strip steel which, in this project, was zinc coated. Both galvanised and galvannealed coatings could be produced but, for the purposes of this study, only galvanised products were used. A software package supplied by Faulk Systems, in which desired processing conditions were entered, allowed the process to be controlled by the main computer unit. Figure 3.5 shows a photograph of the HDS set-up.

At the start of each day or session of work, control panels were processed in order to determine whether the apparatus was ready for use in the investigation, i.e., once the control panels produced a satisfying coating, experimental work could begin. Control panels were prepared from commercial IF steel sheets on every occasion, because of the relatively low level of additions in the steel.

3.5.1 Material Preparation

Samples required for the HDS were cut into panels of 195x120 mm^2 using the Morgan-Rushworth shears. A 30-ton Hi-ton hydraulic press was used to form 3-mm rigidising beads down the side of the panel in order to make the panel more rigid for HDS use. This feature was required for any material with gauges below 1.5 mm. A schematic diagram of the panel is shown in figure 3.6. The panels were cleaned with acetone to remove any oil or dirt that may have been present on the surface. A mark was scribed on the same spot for each panel to determine the location of the thermocouple attachment, which was carried out by using a wooden template. The thermocouple was attached using a spot welder prior to attaching to the HDS.

3.5.2 HDS Processing Route

The panel was placed into the holder in the upper section of the HDS, which included the attachment of the thermocouple from the panel to the HDS. Setting up the required cycle followed this on the computer in order to run the cycle. The sample was moved into the infra-red furnace by a drive rod that was attached to the sample holder. Heating, holding and cooling rates entered via the computer were replicated in the furnace. Furnace atmosphere was also controlled, a non-oxidising atmosphere of nitrogen was used and a reducing HN_X atmosphere. Following the annealing cycle, the steel was dipped into the zinc bath. Prior to dipping, the manual de-drossing scissors were used to clear the surface in order to avoid dross pick up on the panel. The zinc spelter was usually held at a temperature of 460 °C ± 5 °C, which was controlled by the main computer unit. On exiting the zinc bath, the excess zinc was blown away with gas wiping knives. This ensured that coating thickness was 8 μm ±

2 μm, which is consistent with industrial practice. Finally, the panel was returned to the upper chamber for cooling.

The laboratory galvanising simulator is a test apparatus with relatively good repeatability. Temperature control of annealing conditions and zinc spelter was within ± 2 °C. However, the manual de-drossing stage of the process was the most critical stage with regards to obtaining repeatability, because the quality of the panels could vary significantly if de-drossing was not carried out effectively. Indeed, there were occasions when panels were rejected solely because of dross pick up that could be attributed to poor de-drossing practice.

3.6 METALLOGRAPHY

Metallurgical examination was performed on annealed samples following RHAS use. In order to maintain consistency, the metallography samples were taken from the same area each time, i.e. just below the point the thermocouple was attached as shown in figure 3.4.

3.6.1 Mounting Specimens

For substrate analysis, the method of mounting the specimen required the Struers Predopress Hot Mounting method. This technique relies on the basis of forming the mounting medium by applying heat and pressure to polyvinylec powder (Formvar). The substrate sample was placed on the lower ram, which was then filled with the polyvinylec powder. The next stage involved pushing the top ram down on to the mounting medium, ensuring that it was fixed in tightly. Each sample took 40 minutes to complete, which involved a pre-heat, application of pressure followed by cooling.

Cold mounting was used for coating analysis because hot mounting was not appropriate due to the pressure that would be applied to the coating. The cold mounting process involved the use of a resin and hardener mixed together to form a hard material suitable for grinding and polishing. An Epofix resin and hardener was

used, which is a cold setting resin based on two epoxy components. Fifteen parts Epofix resin was mixed with two parts hardener and stirred, then placed into a Struers Epovac to remove any air bubbles that may have been present. On removal from the vacuum, the resin was poured over the samples held by Struers Multi-Clips that are used for cross-sectional analysis. Finally, the moulds were left to set, this took between 1 and 5 hours.

3.6.2 Grinding & Polishing

A series of grinding wheels on the Struers Rotopol was utilised to remove the unnecessary top layers of the samples. Coarse grinding using 120-grit silicon carbide paper was the first step, which took approximately 2 minutes under a load of 20 N. Samples were held in the rotating Struers Pedmat holder and spun anti-clockwise against the direction of the rotating grit. A constant water supply was present to remove debris and keep the samples cool. Samples were washed in Teepol and rinsed using isopropanol, then dried by a hot air drier to ensure no debris was carried to the next stage. The same method was used for the 320 grit silicon carbide grinding, as well as to the fine grinding using the 500 and 1000 grit silicon carbide papers.

Samples were polished on a Struers Labopol polishing wheel using a 6 μm diamond suspension for rough polishing and a 1 μm diamond suspension for final polishing.

3.6.3 Etching

A 2 % nital etchant was used for grain structure analysis of the steel microstructures. Samples were etched for 10 seconds, although further etching was required with some under-etched samples. The etchant was washed off with methanol to prevent over etching.

3.7 SAMPLE ANALYSIS

Microstructural and coating evaluation was carried out using both light optical and scanning electron microscopes. A deltascope was also utilised to measure the coating thickness.

3.7.1 Fischer Deltascope

Coating thickness was measured with a MP30 Deltascope, which was used as soon as the samples were produced. The Deltascope utilises the magnetic induction method of measurement to determine the thickness of non-ferrous coatings on a steel substrate. The thickness was measured across the whole panel; a grid that was effectively split into nine sectors (3 x 3) was used with an average value from five measurements taken.

3.7.2 Optical Microscopy

The examination of the etched samples was carried out using a Reichart Polyvar optical microscope, which was connected to an image acquisition system. Samples were placed under the microscope and the image capture software captured the images. It was possible to obtain images with a magnification of 2000 times. The optical microscope also contained the KS300 software for image analysis.

Ferrite grain size measurements were carried out by counting number of ferrite grains along a 50 μm part of the microstructure. The grain diameter was therefore determined by dividing number of grains by the measured length. This was carried out across the length and width of the microstructure and was measured on numerous parts of the microstructure to obtain a representative measurement.

3.7.3 Scanning Electron Microscope (SEM)

Higher magnification analysis was carried out using a JEOL 840A Scanning Electron Microscope (SEM). The analysis was carried out with the use of the ISIS EDS software and images were stored using the SEMAFORE software. Both mounted and flat samples were analysed. Flat samples were 20 by 20 mm and allowed surface analysis of the coating. Mounted samples for cross-sectional evaluation were sputtered with silver to ensure that the polymeric mount material would become conductive.

The Energy Dispersive X-ray Spectroscopy (EDS) facility available on the SEM was also used. Chemical analysis of the steel substrate and coating defects was carried out with EDS. During EDS, electron bombardment of the sample causes X-rays to be emitted from the sample, which are collected and measured by an energy dispersive spectrometer. The results are corrected by the ZAF software and are presented as a series of marked peaks and/or a table highlighting the volume fraction of the elements present.

3.7.4 X-Ray Diffraction (XRD)

Analysis with a Siemens D5000 diffractometer for X-ray diffraction (XRD) was used to detect any retained austenite in the steel and whether any iron-zinc alloys (often associated with galvannealed products) was present. The intensity peaks from the diffraction patterns are unique. Therefore, the iron-zinc phases in the galvanised coating could be distinguished and any retained austenite in the steel substrate could be detected. It should be noted that the operating procedure for retained austenite and iron-zinc alloys was slightly different, i.e., equipment set-up was different resulting in different operating procedures for the two kinds of analysis.

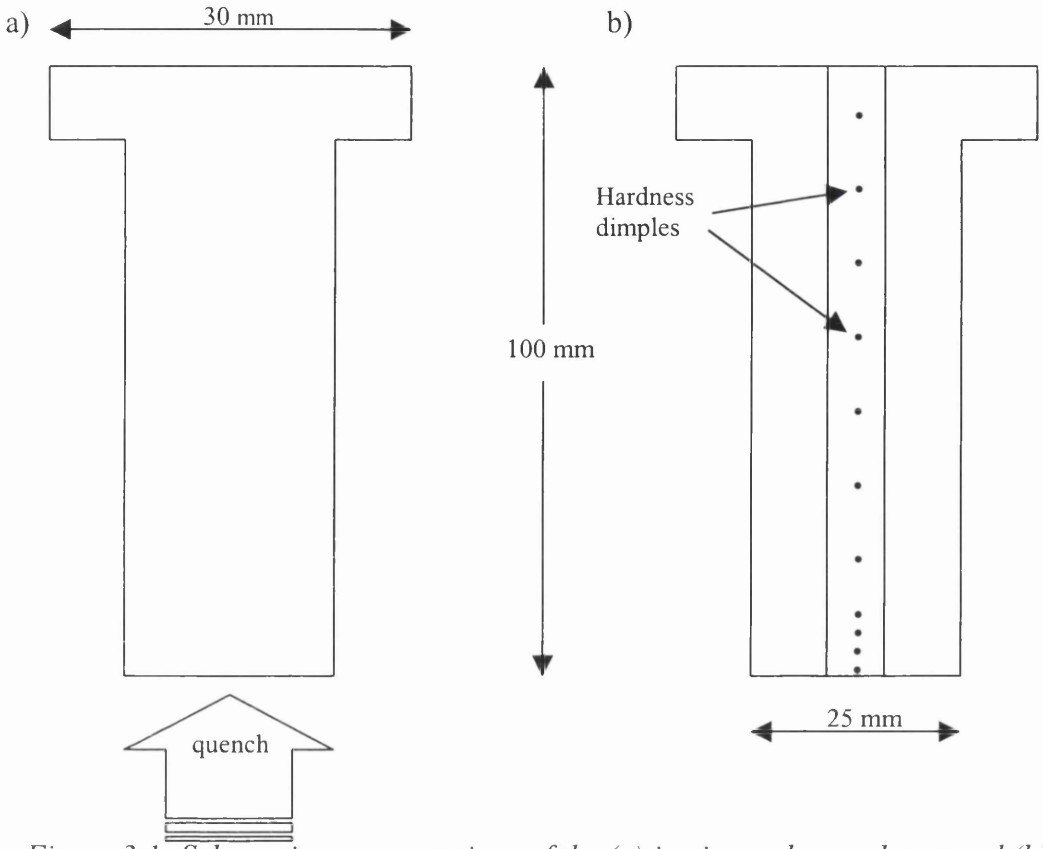

Figure 3.1: Schematic representations of the (a) jominy end quench test and (b) the following hardenability determination across the sample.

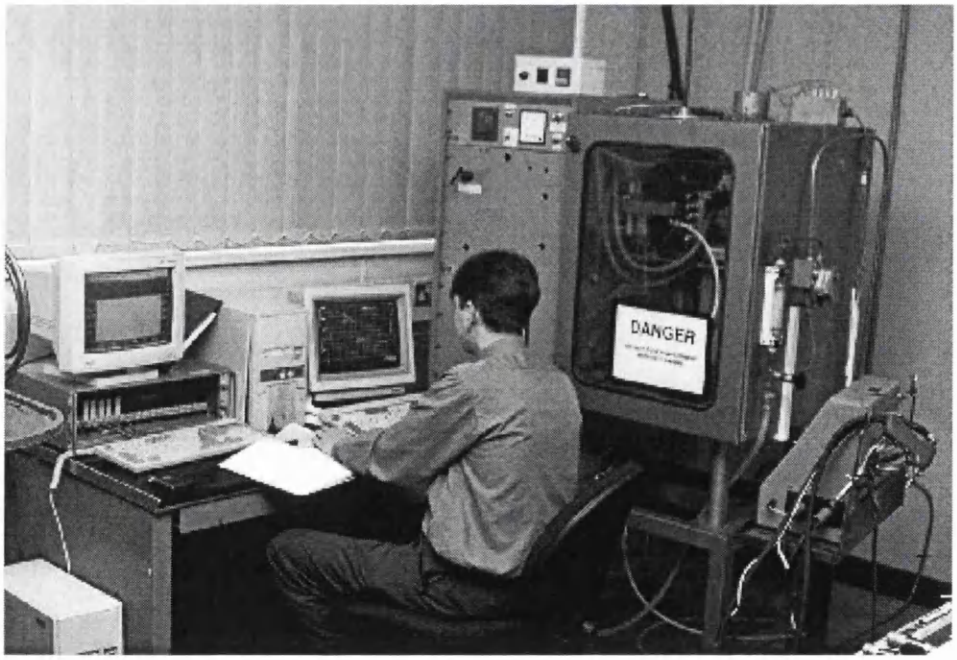

Figure 3.2: A photograph of the Resistance Heating Annealing Simulator (RHAS) showing the control computer (left), data logging computer (middle) and the operations unit (right).

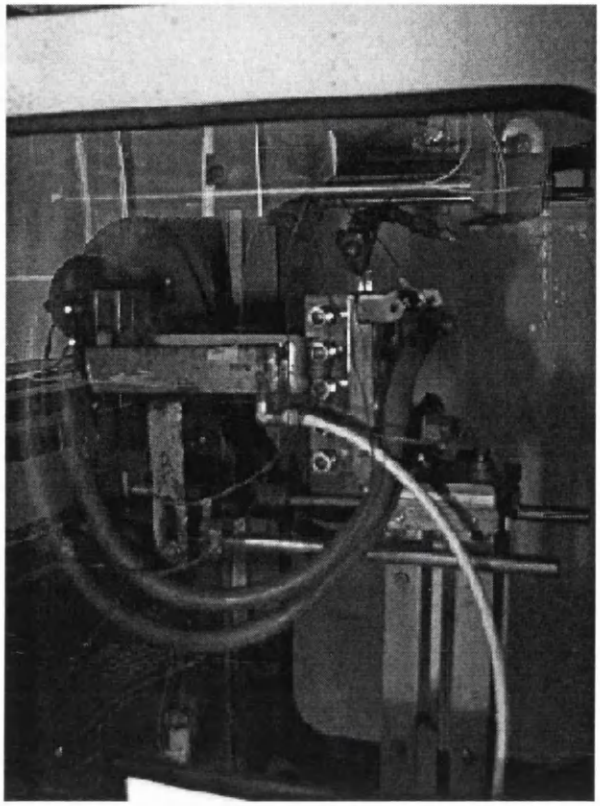

Figure 3.3: A photograph of the Resistance Heating Annealing Simulator (RHAS) operation unit.

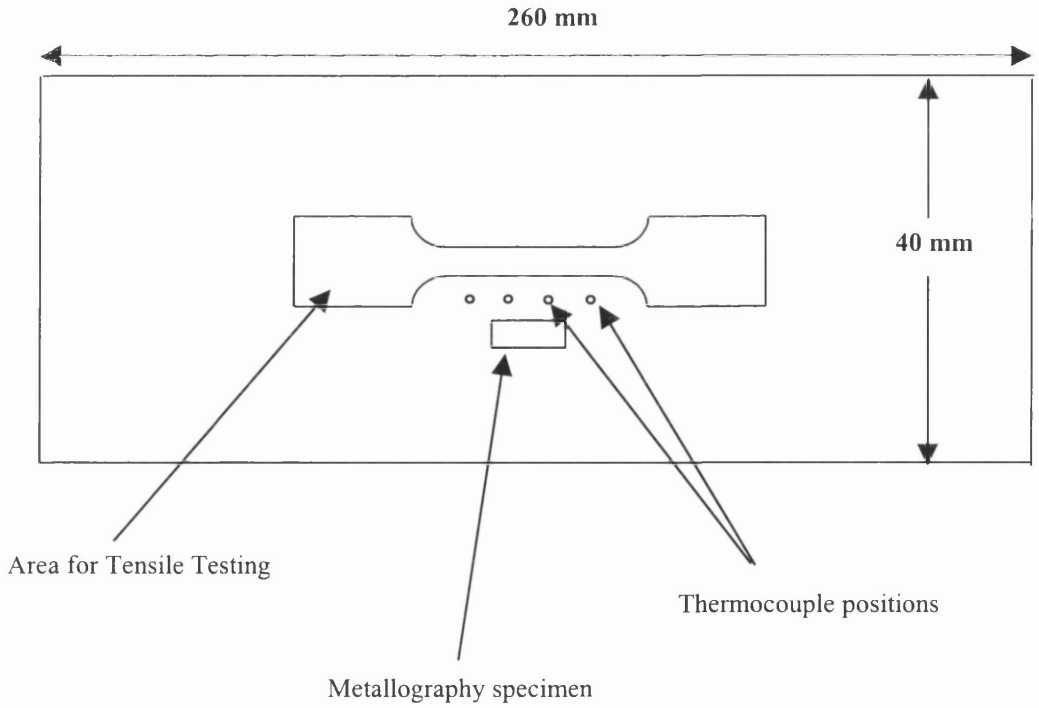

Figure 3.4: A schematic diagram showing a typical sample used for the annealing simulations.

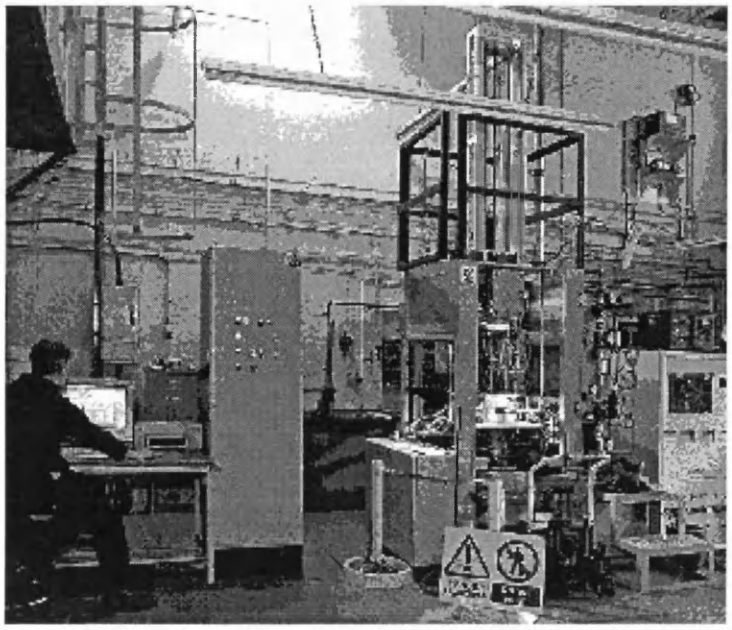

Figure 3.5: A photograph of the HDS showing the process control unit (left), HDS (centre) and gas control unit (right).

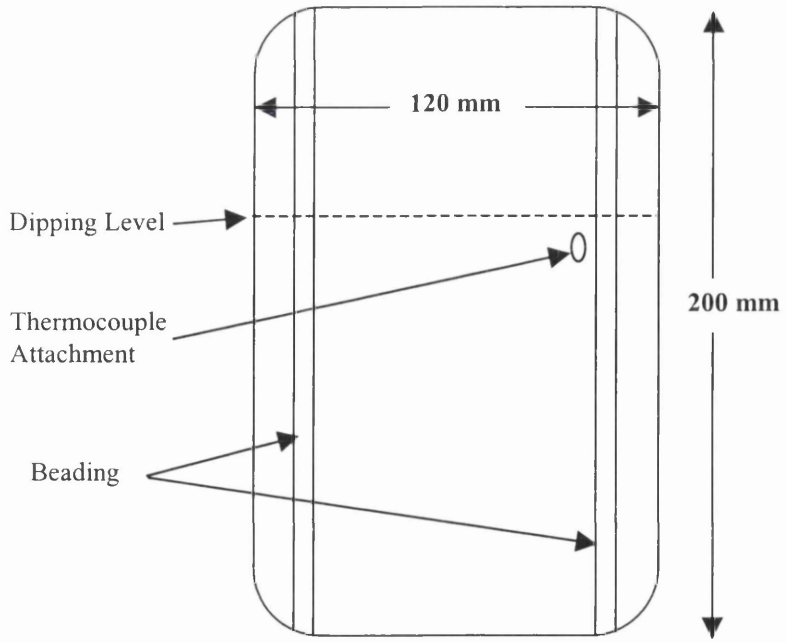

Figure 3.6: A schematic diagram illustrating the HDS panel dimensions.

4.0 EXPERIMENTAL PROGRAMME

This section brings together the aims of the programme (chapter 2) and experimental procedures (chapter 3) into a defined work programme, which will be split into three investigations. In other words, stating the test apparatus required to carry out the project objectives. An overview of the steels chosen for the project will also be given.

All materials utilised during the project were based on C-Mn steels with subtle differences in chemistry distinguishing each grade. The composition of the steels differed so that a range of high strength steels were produced, varying from basic C-Mn steels to dual phase grades. Seven steels were selected in total, as listed in Table 4.1. Four steels were laboratory cast, with commercially produced steels accounting for the remaining three grades.

4.1 STEEL CHARACTERISATION

The laboratory-cast steels, labelled A, C, D and E, were produced in 60 kg ingots that were subsequently hot and cold rolled (method described in the procedures). The hot rolled product was reduced to a gauge of 3.5 mm, which was consequently cold reduced to approximately 1.2 mm gauge. Cold rolled sheets of the commercially produced steels were obtained from Corus Strip Product sites at Llanwern and Port Talbot. The steels had been hot and cold rolled and were supplied with gauges of approximately 1.2 mm. The steels supplied were Corus grades that are defined as steels B, F and G throughout this programme.

Steel chemistries are listed in table 4.1, demonstrating the slight differences from steel to steel. The reference steel was steel B because it contained the least amount of alloying additions, i.e., steel B was a useful C-Mn steel that formed the basis of all the other steels apart from a variation in specific key additions. The main difference between the reference grade and steel A was the higher volume fraction of silicon, which was true for steel C except for even higher silicon levels. A higher niobium level was the primary difference associated with steel D and carbon levels in steel E

were doubled. Steel F was produced with higher molybdenum and vanadium levels, neither of which was as significant as certain additions to other steels. Finally, higher chromium was the major difference associated with steel G.

4.2 INVESTIGATION 1 – PRODUCTION OF CAST STEEL AND SUBSEQUENT PROCESSES

The main objective of this part of the project was to ensure all experimentally produced steels were in the required condition for annealing work to be carried out. Hence, this section of work was predominantly viewed as a preliminary step in the research, which involved rolling the as-received casts into thin gauge material for the main body of the practical work.

Initially, the empirical equations (1.1-1.7) shown in the literature review were used to calculate the predicted transformation temperatures and cooling rates for the steel used in this study. These calculated values were used to compare with actual recorded values to establish the validity of the equations. This investigation also dealt with the results from both Jominy end quench tests and dilatometry (for steels C, D and E), which were described in section 3.1. These results, coupled with the predicted transformation temperatures, acted as a very useful foundation for investigations 2 and 3.

The largest section of work carried out in investigation 1, was to prepare the laboratory casts (steels C, D and E) for the main aim of the project, i.e., investigations 2 and 3. The laboratory hot and cold rolling facilities, which were described in section 3.1, were utilised to achieve this objective.

4.3 INVESTIGATION 2 – THE PRODUCTION OF HIGH STRENGTH STEELS

This section of the experimental programme set out to establish whether high strength steels could be produced with the materials selected for the project. This was

achieved by analysing the microstructural and mechanical properties of the steels after the annealing process was carried out. Several annealing cycles were selected, based on current galvanising line capabilities employed within the Corus Group. Therefore, the properties achieved would indicate the feasibility of producing the high strength steels on Corus owned galvanising lines.

The annealing simulator (RHAS) described in section 3.3 was used to subject all steels (grades A-G) to five annealing cycles that were based on industrial annealing cycles. Specifically, these cycles are used typically on the plants known as the continuous annealing processing line (CAPL) at Port Talbot and the continuous galvanising line known as Zodiac at Llanwern. The other annealing cycles are employed on the process sections of two continuous galvanising lines known as DVL and Galtech 2 at the Corus IJmuiden plant in the Netherlands. Additionally, a modified Zodiac cycle based on the current cycle with a rapid cooling section was used. The annealing cycles are shown in figures 4.1-4.5, with the detailed information regarding heating rates, cooling rates, hold time and hold temperature defined in table 4.2.

The annealed steels were subjected to a comprehensive metallographic evaluation to determine the microstructures of the steel. Samples were prepared using the metallographic procedure described in section 3.5 and analysed with an optical microscope discussed in section 3.7. The volume fraction of ferrite and non-ferritic phases was recorded with particular attention placed on volume fraction of martensite. The technique used to identify the phases present was a 100 point count method that utilised a grid placed over the image of the steel. The amount of each phase present was calculated by identifying the phase present beneath each point. For example, the number of points crossing ferrite grains determined volume fraction of ferrite. This was repeated five times, which meant that an average value was taken from the total of 500 measurements. An image of each sample was also recorded to establish a catalogue of the images produced from the matrix of the seven different grades of steel coupled with the five annealing cycles. These samples were also subjected to XRD testing (described in section 3.7) to determine whether retained austenite had been produced.

Tensile tests were carried out (described in section 3.4) on all steels to establish whether the properties obtained were in line with current or future grades of high strength steel. The results from this investigation were compared closely with grades highlighted in the ULSAB project for HSS. Given that grades shown in the ULSAB project stated HSS properties required, linking the two seems reasonable. Yield and tensile strengths were observed in particular detail, as well as total elongation while properties such as n values and yield to tensile ratios were also considered.

4.4 INVESTIGATION 3 – THE PRODUCTION OF GALVANISED HIGH STRENGTH STEEL

All steels (A-G) were subjected to a galvanising programme on the Hot Dip Simulator (HDS), which was described in section 3.5. The initial work focussed on standard conditions. Process parameters within the HDS were adapted thereafter to optimise coating appearance. Analysis of the coating quality was carried out after each HDS study, using both visual and microscopic inspection.

The initial and largest galvanising study was carried out on all steels utilising standard conditions on the HDS, which are specified in table 4.3. Conditions considered most significant were the dew point, strip entry temperature and effective aluminium in the zinc spelter. The annealing cycle used during this part of the investigation is shown in figure 4.6. Following the initial comprehensive study, several smaller investigations were completed. An investigation utilising the standard conditions, but with changing atmospheric dew point, was carried out with dew points at -40 °C, -15 °C and 5 °C. A study with varying strip entry temperature, with all other condition set to standard, was also carried out at temperatures of 460 °C, 490 °C, 520 °C and 550°C. Finally, the effect of varying the effective aluminium in the zinc spelter was investigated, at compositions of 0.13 %, 0.15 % and 0.18 %. Investigations to establish the effect of varying annealing cycle was also performed, but this was only for steel B due to a lack of material. All of the variations utilised are shown in table 4.4.

The coating thickness for the galvanised panels was measured with a Deltascope, described in section 3.7. The panels were split into nine distinct areas, based on 3 by

3 grid, where 10 readings per square were measured producing the average coating thickness for each square. A cross sectional measurement under the optical microscope was also utilised. Galvanised panels produced in the HDS were analysed by both visual and microscopic methods. The bare-spot detection across the whole panel was calculated as a percentage of uncoated area using a 100-point count technique. That is, bare spots falling below the 100 point grid was classified as uncoated area, which gave overall percentage coverage. More detailed analysis of the bare spots was carried out on the SEM, again described in section 3.7. Images and elemental analysis of the defects were taken. The SEM was utilised in order to determine the type of defect and more often than not the cause. This was achieved by utilising the EDS to obtain the chemical make up of any defects within the coating. A sample from all steels and various conditions was taken. The XRD analysis was also carried out for iron-zinc alloy identification (described in section 3.7).

Table 4.1: Steel chemistries for all seven materials used in the investigation.

		Chemistry (weight %)						
Steel	Type	C	Mn	Si	P	Al	Nb	Other
A	Lab	0.16	1.51	0.38	0.012	0.038	0.001	
B	Com	0.13	1.28	0.05	0.015	0.040	0.005	
C	Lab	0.10	1.31	1.28	0.050	0.048	0.005	
D	Lab	0.10	1.50	0.10	0.005	0.048	0.011	
E	Lab	0.20	1.51	0.10	0.009	0.005	0.005	
F	Com	0.09	1.49	0.14	0.017	0.045	0.002	Mo0.01 V 0.01
G	Com	0.07	1.51	0.06	0.016	0.048	0.005	Cr 0.45

NB: *Lab* refers to laboratory-produced steels and *Com* refers to commercially produced material.

Table 4.2 Annealing conditions for the 4 annealing cycles used.

Process Condition	DVL	Zod	GT2	CAPL
Heating rate, °C/s	19	35	35	9
Holding time, seconds	102	73	40	120
Annealing temperature, °C	830	800	830	800
Initial cooling rate, °C/s	2	10	-	10
Pre-dipping cooling rate, °C/s	7	25	18	60

Table 4.3: Preliminary processing conditions for the galvanising study.

Process Parameter	Value
Ramp up time, seconds	60
Dew point, °C	-40
Annealing time, seconds	60
Annealing temperature, °C	800
Cooling rate, °C/s	30
Strip entry temperature, °C	460
Spelter temperature, °C	455
Dipping time, seconds	3
Effective aluminum, %	0.18

Table 4.4: Variation in process parameters from preliminary study.

Process Parameters	Variation			
Annealing cycle *	DVL	Zod	Gal	Zod-rev
Dew point, °C	-40	-15	0	10
Strip entry temperature, °C	460	490	520	550
Effective aluminium, %	0.12	0.13	0.15	0.18

* - Annealing cycle variation was only carried out with steel B.

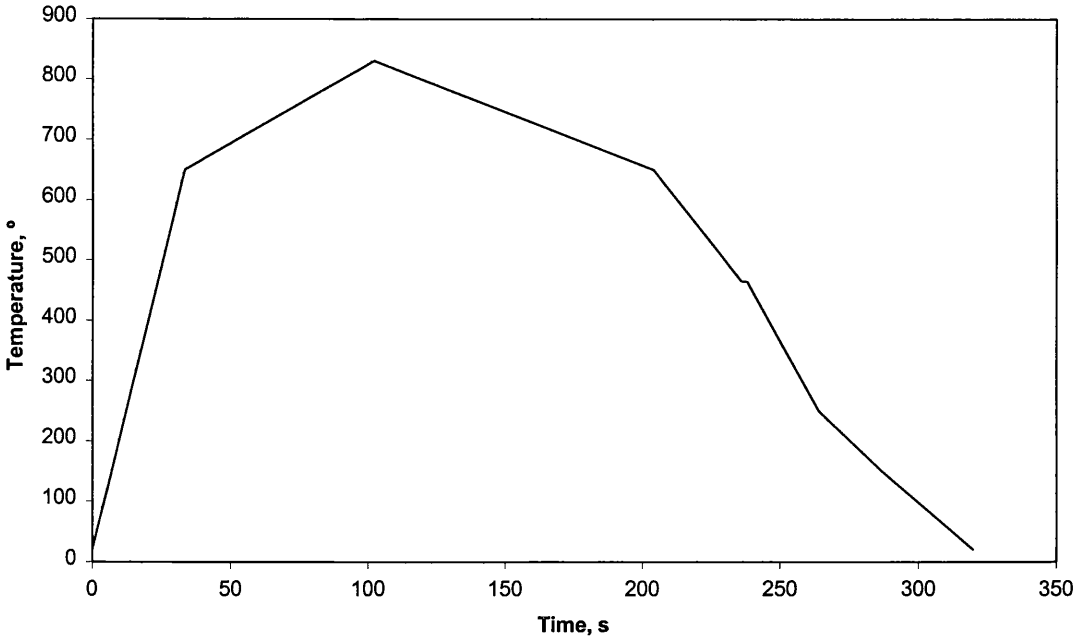

Figure 4.1: A schematic representation of the annealing cycle based on the DVL cycle.

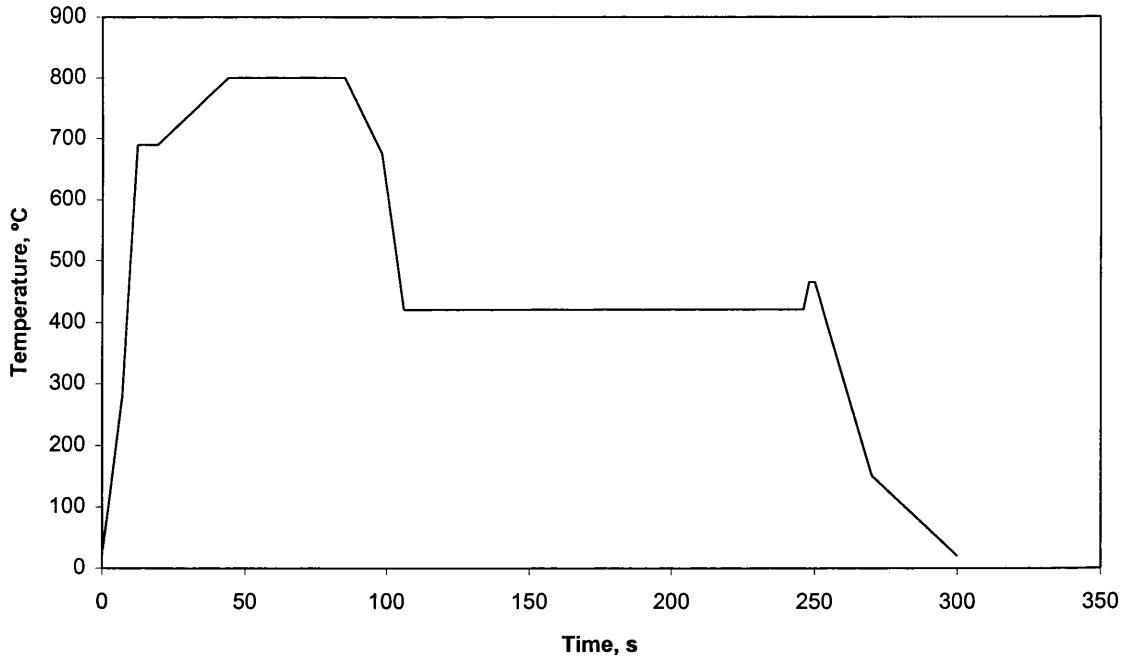

Figure 4.2: A schematic representation of the annealing cycle based on the Zodiac cycle.

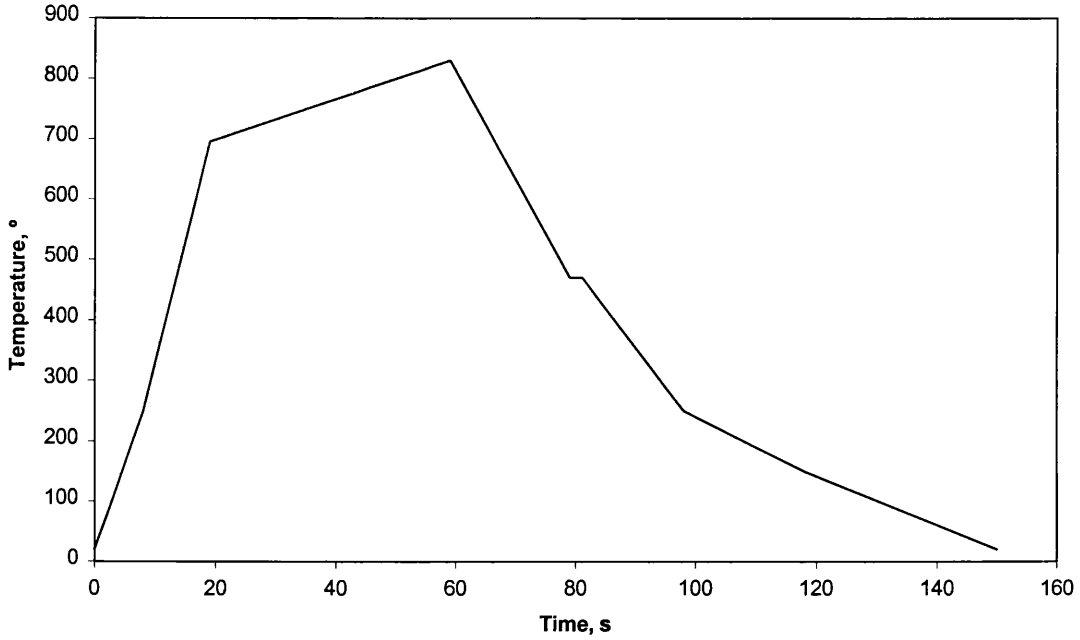

Figure 4.3: A schematic representation of the annealing cycle based on the Galtech 2 cycle.

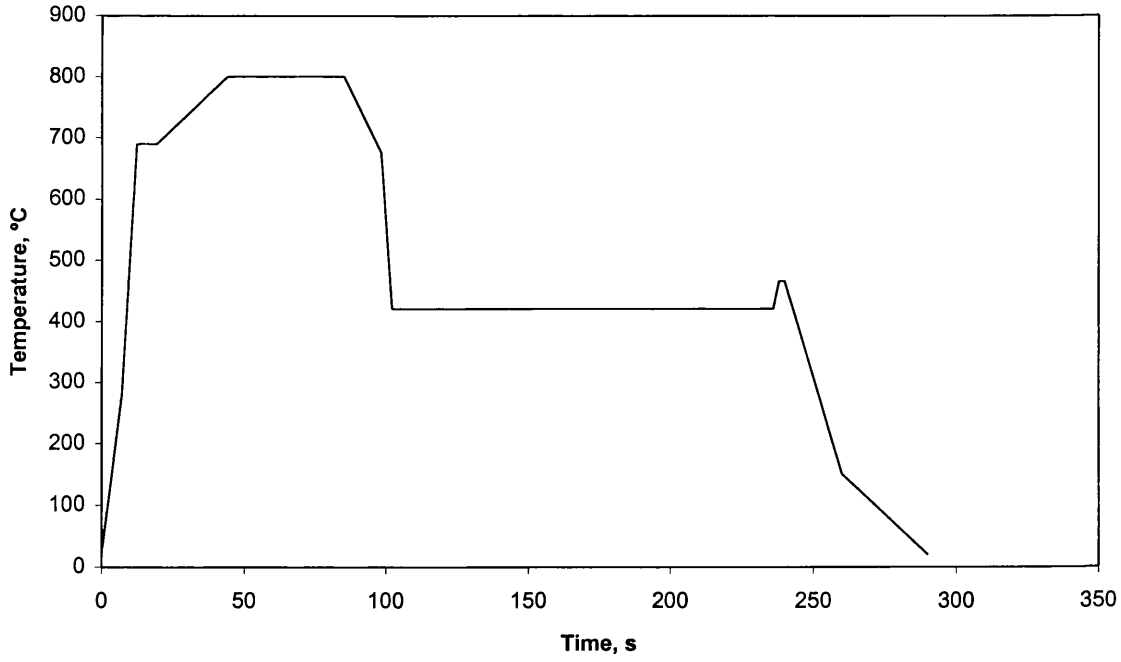

Figure 4.4: A schematic representation of the annealing cycle based on the revised ZODIAC cycle with rapid cooling.

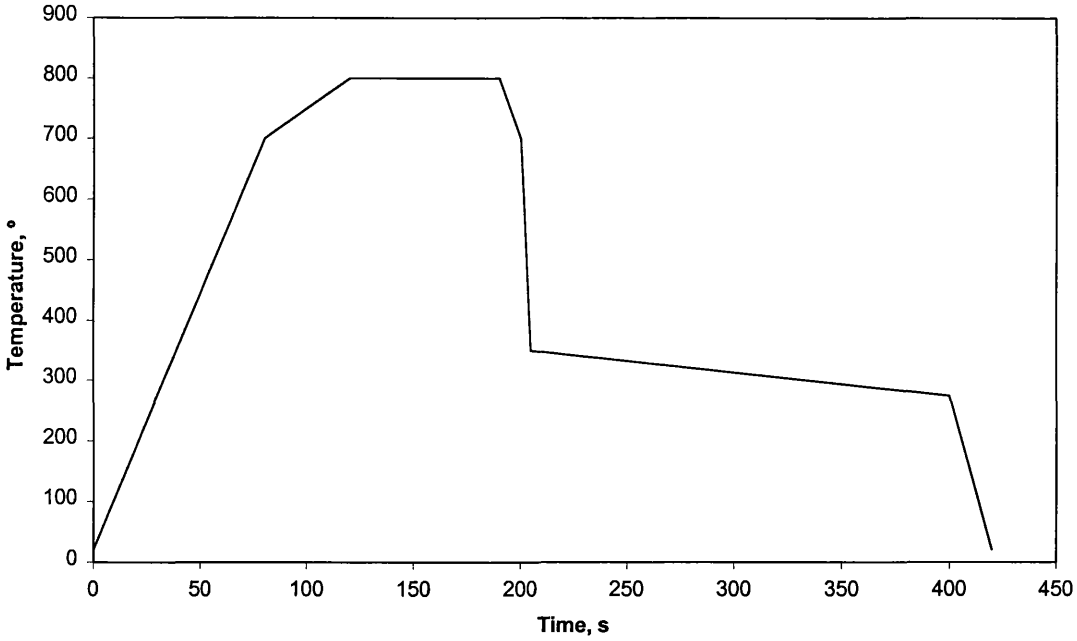

Figure 4.5: A schematic representation of the annealing cycle based on the CAPL cycle.

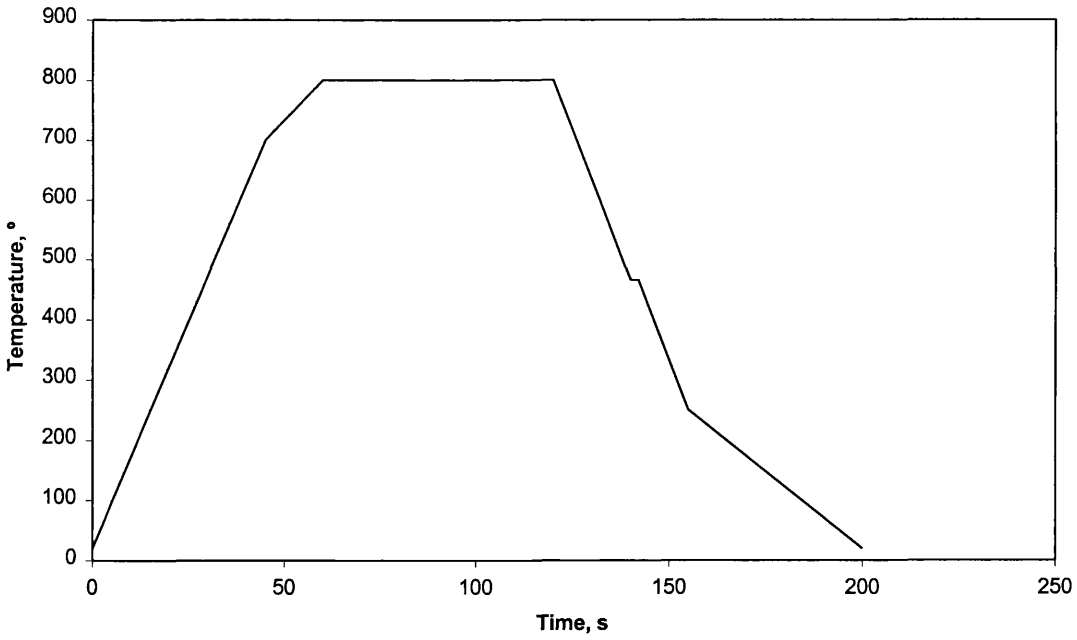

Figure 4.6: A schematic representation of the standard annealing cycle utilised for the Hot Dip Simulator.

5.0 INVESTIGATION 1 - PRODUCTION OF CAST STEEL AND SUBSEQUENT PROCESSES

As described in section 4.1, this section of work dealt primarily with preliminary aspects of the project as well as assessing theoretical transformation equations suggested by numerous authors. The theoretical and practical results will be discussed in addition to comparing the findings of both sets of results to establish whether the theoretical and actual results are similar.

5.1 THEORETICAL TRANSFORMATION TEMPERATURES

The transformation temperatures predicted from the empirical equations shown in equations 1.1-1.7 (excluding equation 1.2) were calculated for the seven steels used in the investigation. It must be appreciated that several equations for the same transformation have been suggested and that those described in this work are commonly used equations, which does not necessarily mean the most accurate.

5.1.1 Austenite/Ferrite Transformation Equations

Transformation temperatures taken from the Andrews empirical equations (equations 1.1 and 1.2) for estimating A_1 and A_3 temperatures are shown in table 5.1. The A_3 temperature, which relates to the boundary between the austenite and ferrite plus austenite region, ranged between 824 and 903 °C, with five of the steels being between 840 and 860 °C. Steels C and E were the two extremes, steel C relating to the highest temperature and steel E relating to the lowest temperature. The A_1, which refers to the end of austenite formation, ranged between 671 and 699 °C. These values were much closer to one another when compared with A_3 temperatures, steel C exhibited the lowest temperature and steel G had the highest temperature. Indeed, steel C had the largest range in values between A_1 and A_3 temperatures, i.e. it displayed the highest A_1 and lowest A_3.

The highest A_3 transformation temperatures were consistently with the steels containing the greatest fractions of ferrite formers. Indeed, the highest of all was attributed to the steel containing very high silicon levels, i.e., steel C. Steels F and G, which contained molybdenum-vanadium and chromium respectively, had the next highest A_3 transformation temperature. Likewise, all the other steels apart from steel E contain ferrite-forming additions, i.e., steel A contained higher than average amount of silicon and steel D contained slightly higher niobium. Conversely, the steel with the lowest A_3 temperature (steel E) had the lowest levels of ferrite formers and, also had double the carbon levels of the other steels. In fact, the significantly higher carbon would account for the lower transformation temperature, this is because carbon is an austenite stabiliser, i.e., expands the austenite temperature range.

5.1.2 Bainite Transformation Equations

The austenite to bainite transformation is difficult to achieve in low carbon steels unless additions such as boron and molybdenum are present that shorten the time for the reaction to occur. In most cases, continuous cooling would not produce bainite because of the nose of the TTT diagram, which was discussed in the literature review, i.e., continuous cooling would usually produce ferrite-pearlite or martensite. Even an isothermal hold is not entirely effective in the production of a bainite structure. Nevertheless, the bainite transformation temperatures are required in order to make a distinction with ferrite-pearlite formation temperatures.

Bainite start and finish temperatures obtained from equations 1.4 and 1.5, which are shown in table 5.1, reveal that start temperatures ranged from 569 to 623 °C and that finish temperatures ranged from 449 to 503 °C. The equations show that bainite finish temperature is obtained by simply subtracting 120 °C from the bainite start temperature. Therefore, given that the step between the temperatures would always be the same, it would seem obvious to consider only one temperature, i.e., the bainite start temperature. Steel E exhibited the lowest transformation temperatures. In fact, bainite transformation temperature for steel E was significantly lower than the other steels. The only other significant point was steel A, which had a transformation temperature that was between the temperature for steel E and the other steels.

It can clearly be seen from the equations that, carbon has the greatest influence on bainite transformation temperatures. As stated earlier, with the austenite to ferrite transformation, carbon is the major austenite stabiliser, i.e., the carbon retards the reaction kinetics. Therefore, it is not surprising that steel E had the lowest transformation temperatures, given that steel E had more than double the carbon levels when compared with most other steels. Steel A had the next lowest transformation temperatures, which again is attributed to the higher than average carbon levels in this grade. All the other steels had transformation temperatures that were relatively close, which can be attributed to the very similar carbon levels for these grades.

5.1.3 Martensite Transformation Equations

Martensite transformation temperatures calculated from equations 1.6 and 1.7, which can be seen in table 5.1, showed martensite start temperatures ranging between 407 and 462 °C. As with bainite, the transformation temperature for martensite finish is basically 215 °C below start temperature, therefore, only the martensite start will be considered. As with the bainite transformation temperatures, steel E exhibited the lowest transformation temperature of 407 °C. Again, apart from steel A (M_s = 421 °C), all other grades had similar values, which were all very close at about 450 °C.

Reasons for the lower transformation temperatures associated with steels A and E (in particular steel E) are the same as those stated in the previous sections, specifically and most significantly, due to the carbon levels. At the same time, nearly all additions to the steel will also lower the transformation temperatures, which accounts for the relatively close values for the other steels.

5.1.4 Cooling Rate Against Volume Martensite Equations

Table 5.2 displays the recommended cooling rates required to produce 5 % volume fraction martensite based on steel chemistry according to two authors. The two authors, Tanaka *et al.* (1979) and Rigsbee *et al.* (1979), have attempted to quantify

this with empirical equations, namely equations 1.10 and 1.11. Both authors attempted to relate the kinetics of the austenite transformation to the steel chemistry. Neither equation takes factors such as holding time and temperature into account, which would have an influence on final properties. Therefore, the results must be treated with caution.

Yet, while results obtained from the two equations generally differ; there are reasonably similar trends that appear on a few occasions. Both equations highlight that steels A, C and E do not require particularly rapid cooling and that steels B and D require a higher cooling rate to achieve 5 % martensite. However, steels F and G appear to show contradicting results, with Tanaka *et al.* suggesting that a relatively low cooling rate would be required whereas Rigsbee *et al.* proposes the opposite to be true.

On several occasions, the results of both equations show very different values, which can be related back to the variables used in the actual equations. Rigsbee used only manganese, silicon and carbon as variables, whereas Tanaka used manganese, silicon, phosphorous, chromium and molybdenum. It may appear that, because Tanaka had introduced more variables than Rigsbee, this equation would be more accurate and representative of actual results. However, Tanaka failed to introduce carbon to the equation, which is of paramount importance in relation to the hardenability. It can only be assumed that the equation devised by Tanaka was proposed for steels with carbon levels fitting a set value.

Clearly the equations are only a useful tool in assisting with selecting steel chemistry for dual phase steel. The degree of accuracy achieved must be questioned in view of the fact that all factors apart from chemistry are ignored.

5.2 STEEL HARDENABILITY RESULTS

The Continuous Cooling Transformation (CCT) curves and hardenability plots obtained from the dilatometry and Jominy tests are key factors when considering dual phase or multi phase steels. This is because they give valuable information regarding

processing conditions required for producing these grades of steel. As stated in the experimental programme, only steels C, D and E were subjected to these tests due to a lack of appropriately sized material.

5.2.1 Dilatometry – Microstructural Evaluation

Continuous Cooling Transformation (CCT) results obtained from dilatometric tests carried out on steels C, D and E are shown in figures 5.1-5.3 with more detailed descriptions of the microstructures shown in table 5.3.

5.2.1.1 Steel C

The most distinctive feature of the transformation curve for steel C (figure 5.1) was that initial transformation had taken place before the dilatometer recording had begun. Specifically, the initial transformation had taken place before the holding period of 800 °C, which meant that the volume change associated with the transformation, could not be measured. The silicon levels in this particular grade of steel can explain the high transformation temperature, because it is known that silicon is a ferrite former, i.e., austenite transformation takes place at higher temperatures. Even though there were several austenite stabilising additions present, the existence of significant silicon levels meant that transformation temperatures were above 800 °C.

Initial transformation from austenite can only be given as equal to or greater than 800 °C from the CCT graph. Completion of transformation ranged from 600 °C to 320 °C at cooling rates of 1 °C/s and 50 °C/s respectively. A ferrite-pearlite structure was observed when the cooling rate was approximately 1 °C/s, whereas a martensite-ferrite structure was formed when the cooling rate was 50 °C/s. Bainite formation started when cooling rate was 3 °C/s and martensite formation started at around 6°C/s. The relatively low cooling rates required for martensite formation can be explained by the highly alloyed nature of the steel, which was high in both silicon and manganese. Therefore, the CCT graph (and results from empirical equations) confirms that steel C had a chemistry that could potentially produce dual phase steel.

5.2.1.2 Steel D

The CCT curve for steel D (figure 5.2) shows that the start of austenite transformation ranged between 730 and 570 °C for cooling rates of 1 and 50 °C/s, whereas transformation was completed at 480 and 290 °C with the same cooling rates. The differentials between start and finish temperatures remained reasonably constant at approximately 250 °C with all cooling rates. A ferrite-pearlite structure was identified with the slowest cooling rate (1 °C/s) and a bainite-martensite structure was observed with the fastest cooling rate (50 °C/s). The first sign of bainite formation was when cooling rate was about 1.5 °C/s, with martensite formation beginning at 30 °C/s. Again, the CCT curve suggests that steel D had a chemistry capable of producing dual phase steel, but with a higher cooling rate than steel C.

5.2.1.3 Steel E

The CCT curve for steel E (figure 5.3) shows transformation start times at 690 and 440 °C with finish temperatures in the range of 510 and 190 °C at cooling rates of 1 and 50 °C/s respectively. A distinctive feature noted with this curve was that around 10 °C/s both transformation temperatures were lowered significantly. This feature seems to coincide with the beginning of martensite formation along with pearlite-ferrite formation ending, which occurs simultaneously. Ferrite, pearlite and bainite were seen with the slowest cooling rate (1 °C/s) whereas bainite and martensite was identified at 50 °C/s. The onset of martensite formation was at 10 °C/s and by 50 °C/s a totally martensitic structure was achieved. The transformation curve shows that the chemistry of steel E was in fact suitable for dual phase steel.

5.2.1.4 Overall Trends

When comparing the CCT curves for steels C, D and E, it is apparent that steel D requires the most rapid cooling rates to achieve martensitic formation. This can be attributed to the lower silicon (compared to steel C) and lower carbon (compared to steel E) levels, which both increase hardenability and promote martensite formation.

It is also clear that the transformation temperatures for steel E appear to be lower than the other two steels, which can again be explained by the higher carbon levels that lower the transformation temperatures. The one noticeable similarity with the three steels is that they all exhibit CCT curves that would be suitable for dual phase steels.

5.2.2 Dilatometry – Hardness Measurements

Figure 5.4 represents the hardness values plotted against cooling rate for the dilatometry samples. It shows, that for all steels, there is a steady increase in hardness up to about 15 °C/s, which is the point at which martensite formation occurs for all steels. Steels C and D continue to rise steadily, whereas steel E exhibits a marked rise in hardness values for the subsequent cooling rates. The sudden increase in hardness values for steel E can be explained by the volume of martensite present. Even though all steels begin to form martensite at similar times, steel E produces a much higher volume fractions of martensite. This can be attributed to the higher carbon levels in steel E that, are almost double the amount of the other steels, which accounts for the higher hardness recorded.

5.2.3 Jominy End Quench Test

Hardness values recorded from the end quench test for steels C, D and E are displayed in figure 5.5. The graph shows varying hardness values across the entire length of the samples used, which measures the hardenability of the steel. High hardenability is represented as a flat Jominy curve whereas low hardenability would produce a sharp initial drop in the curve. By relating this to the graph, it shows that steel C has the highest hardenability because it exhibits the flattest curve. Steels D and E show similar lower hardenability with the only difference being the position of the curves. Steel E is consistently about 10 Rockwell hardness units higher at each point, which can be attributed to the higher carbon values (0.2 weight % for E, 0.1 weight % for D).

The results of the Jominy test only confirm what was observed in both the empirical equations and the CCT results. It was shown, that steel C had the highest hardenability because of the substantial levels of manganese and more significant the levels of silicon. Steels D and E had significant alloying additions that explain the relatively high hardenability.

5.3 ASSESSING THEORETICAL AND ACTUAL TRANSFORMATION TEMPERATURES

A comparison of theoretical and actual transformation temperatures should be approached with caution because of the nature of the test. The practical tests are a measure of transformation temperatures with respect to cooling rate or time, whereas the equations refer to equilibrium conditions. Therefore, when comparing the two sets of results, slowest cooling rates should be used for the closest comparisons.

Prior to the dilatometry test commencing, the samples were cooled from 1100 °C at a rate of 3 °C/s. Given that an increase in cooling rate lowers the transformation temperatures, this must be taken into account when comparing actual and predicted transformation temperatures. An assessment of the CCT curves used in this study seems to suggest that a cooling rate of 3 °C/s reduced initial transformation from the austenite region by 30 °C.

The CCT curve for steel C showed that initial transformation from austenite had taken place before the test had started, which was above 800 °C. With reference to the predicted A_3 temperature, it was not surprising that it had occurred because an initial transformation temperature of 903 °C had been predicted. In view of the fact that a cooling rate of 3 °C/s was employed to cool to 800 °C for the test start, it is estimated that actual transformation start temperature was about 870 °C. This equates to a difference of about 60 °C between actual and predicted transformation start temperature. The measured transformation finish temperature at the slowest cooling rate was about 70 °C lower (600 °C) than the predicted A_1 temperature (671 °C). Bainite start temperatures were much more consistent than the austenite transformation value, being the same as the predicted value of 420 °C. However, the

martensite start temperature was about 60 °C higher than the predicted temperature (443 °C).

From the CCT curve for steel D, the transformation start was at 730 °C, which is 120 °C lower than the predicted value. With an initial reduction of about 30 °C in transformation temperature from the predicted value, it is still about 90 °C higher than the actual measured value. The same is true for the transformation finish temperature, with actual value being about 200 °C higher than measured temperature, which equates to 170 °C when accounting for initial cooling rate. It is reasonable to conclude that the empirical equations for austenite transformation were not truly representative of this steel grade. However, bainite transformation temperature predictions were very accurate, both temperatures were within 10 °C of actual values. The martensite transformation temperatures were not as accurate, with actual start being 50 °C lower and actual finish being 50 °C higher than predicted values.

Austenite transformation temperatures for steel E were both well over 100 °C lower than the predicted values, even with an initial reduction of 30 °C. Actual transformation temperatures were 690 and 510 °C, which compare poorly with predicted values of 824 and 691 °C. The range between the actual bainite transformation temperatures was much larger than the predicted values. Predicted temperatures were 60 °C too high for the start temperature and 100 °C too low for the finish temperature. Martensite transformation temperatures matched the predicted values very closely for this steel grade; a difference of less than 10 °C was found for both temperatures.

This exercise has shown that comparing CCT data with empirical equations for transformation temperatures can be used as a guide, providing that only slowest cooling data is used. The Andrews equations in particular showed the greatest degree of inaccuracy, with the initial higher cooling rate being the most likely cause for this. Generally the martensite and bainite transformation equations were more accurate, but even these values showed enough discrepancies to warrant caution when using them.

5.4 HOT ROLLING PROPERTIES

During laboratory hot rolling of steels C, D and E, finishing and coiling temperatures of 850 and 650 °C were aimed for as well as a gauge of 3.5 mm. Actual finishing and coiling temperatures are shown in figures 5.6 and 5.7. The finishing temperatures were generally slightly below the aim, with steel E in particular falling below the desired temperature. The finishing gauge was consistently between 3.3 and 3.7 mm.

The coiling temperature was set at a level that could be considered to be at the top end of possible temperatures. The reasons for the relatively high coiling temperature relate to the following cold reduction process. If the steel was coiled at lower temperatures, then there was the possibility of difficulty in the cold reduction because of the higher strength of steel. Therefore, to avoid possible problems and in view of the fact that the dual phase structure was to be produced during the annealing process, the temperature was set at 650 °C. However, there are disadvantages in utilising a higher coiling temperature that are still prevalent after cold reduction and annealing. A study that looked at the effects of varying coiling temperature on dual phase grade steels, which were subsequently subjected to cold reduction and annealing, found that higher coiling temperatures did not produce the best final mechanical properties (Gavard 2001).

Coiling temperatures for steels C and D were reasonably consistent, but were on average about 50 °C above the aim temperature of 650 °C. However, the steel E coiling temperature was erratic and always lower than the aim temperature, which could be related in part to the consistently lower finishing temperatures. Samples that were closest to the aim temperatures were used in the project, which meant that approximately a quarter of hot rolled samples were not required for the remainder of the project.

Table 5.1: Experimental transformation temperatures (°C) for the A_1 and A_3, bainite and martensite start and finish calculated for all steel chemistries.

	Transformation		Bainite		Martensite	
Steel	A_1	A_3	Start	Finish	Start	Finish
A	685	846	586	466	421	206
B	698	840	610	490	446	231
C	671	903	620	500	443	228
D	691	850	612	492	450	235
E	691	824	569	449	407	192
F	690	856	615	495	452	237
G	699	859	623	503	462	247

Table 5.2: Cooling rates required to produce 5 % martensite from experimental equations suggested by Rigsbee *et al.* (1979) and Tanaka *et al.* (1979).

Steel	Cooling Rate, °C/s	
	Rigsbee	Tanaka
A	8.2	11.5
B	84.0	26.6
C	2.5	6.3
D	45.7	18.7
E	11.4	16.0
F	45.2	11.3
G	73	1.2

Table 5.3: Phase identification for steels C, D and E from the dilatometry samples cooled at rates between 1 and 50 °C/s. Ferrite = α, pearlite = P, bainite = B and martensite = α'.

Cooling Rate, °C/s	Steel		
	C	D	E
1	α + P	α + P + B	P + α + B
1.5	α + P	α + B + P	B + P + α
3	α + P + B + α'	B + α + P	B + P + α
6	α + P + B + α'	B + α + P	B + P + α
10	α + P + B + α'	B + P	B + α'
14	α + B + P + α'	B + P	B + α'
30	B + α	B + α'	α' + B
50	α' + α	B + α'	α' + B

Note. Phases listed in each cell show the greatest volume fraction first and so on.

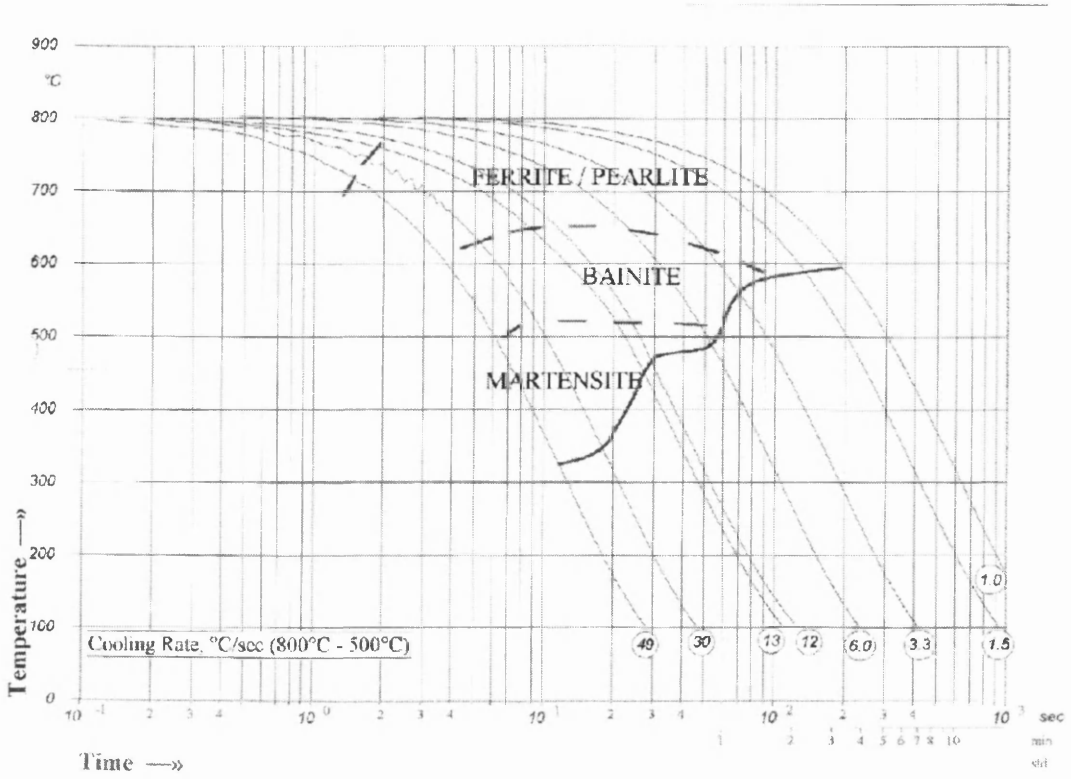

Figure 5.1: The Continuous Cooling Transformation curve (CCT) for steel C obtained from the dilatometry.

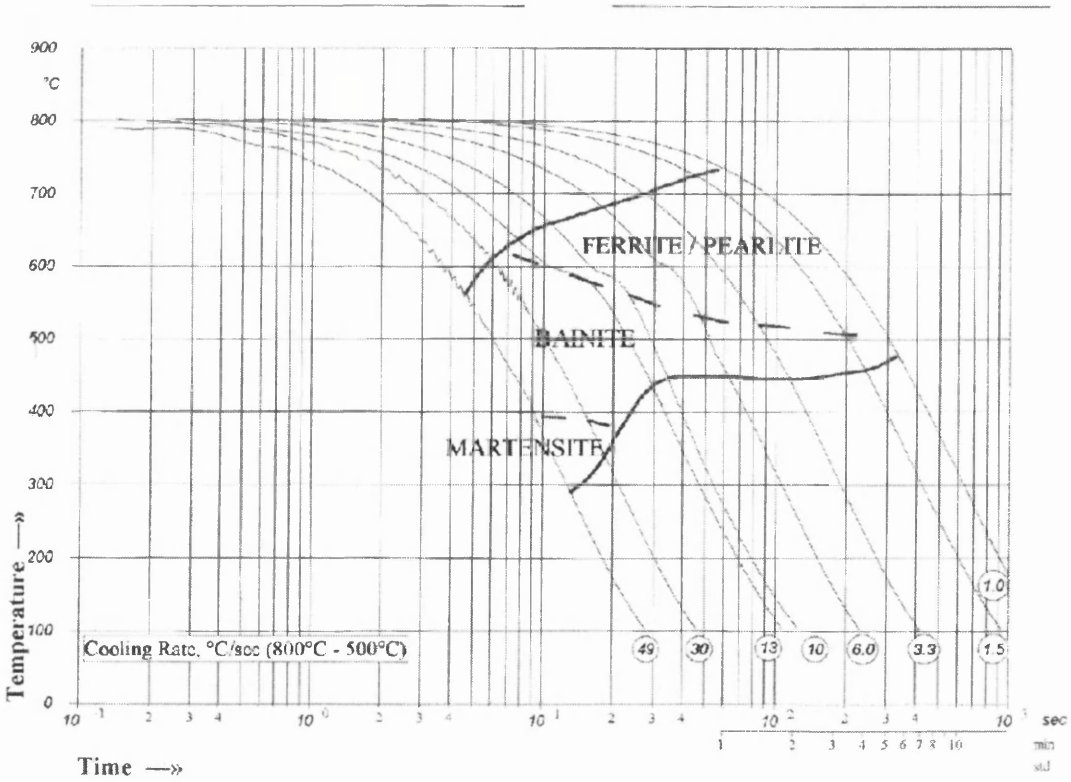

Figure 5.2: The Continuous Cooling Transformation curve (CCT) for steel D obtained from the dilatometry.

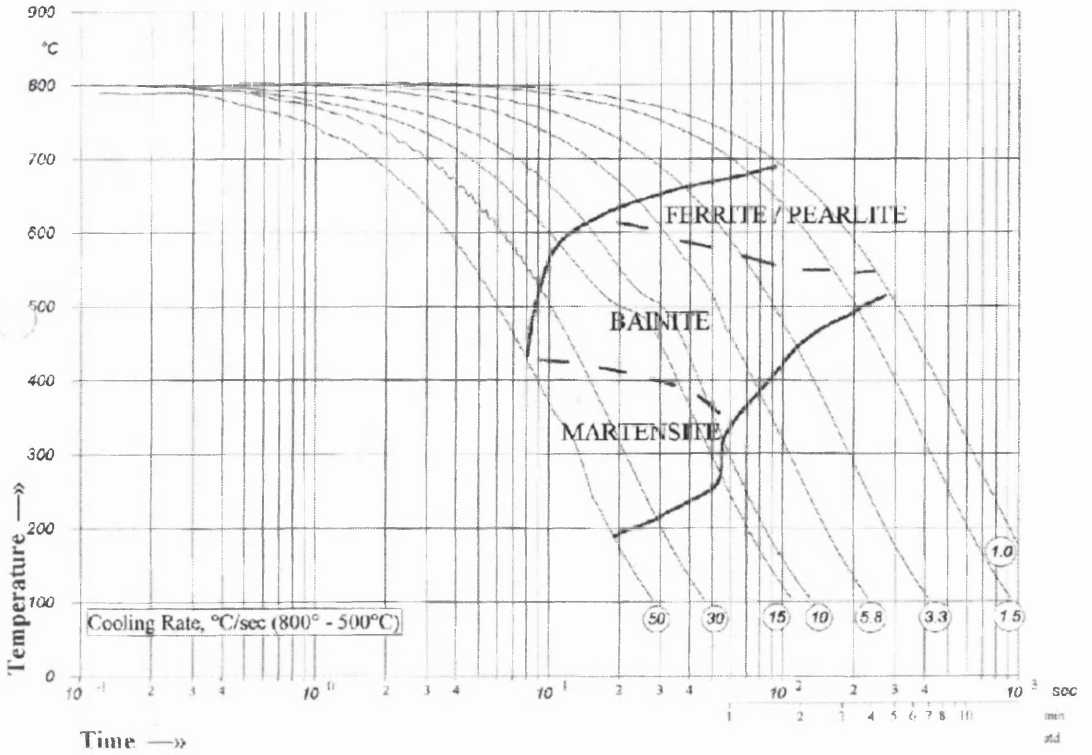

Figure 5.3: The Continuous Cooling Transformation curve (CCT) for steel E obtained from the dilatometry.

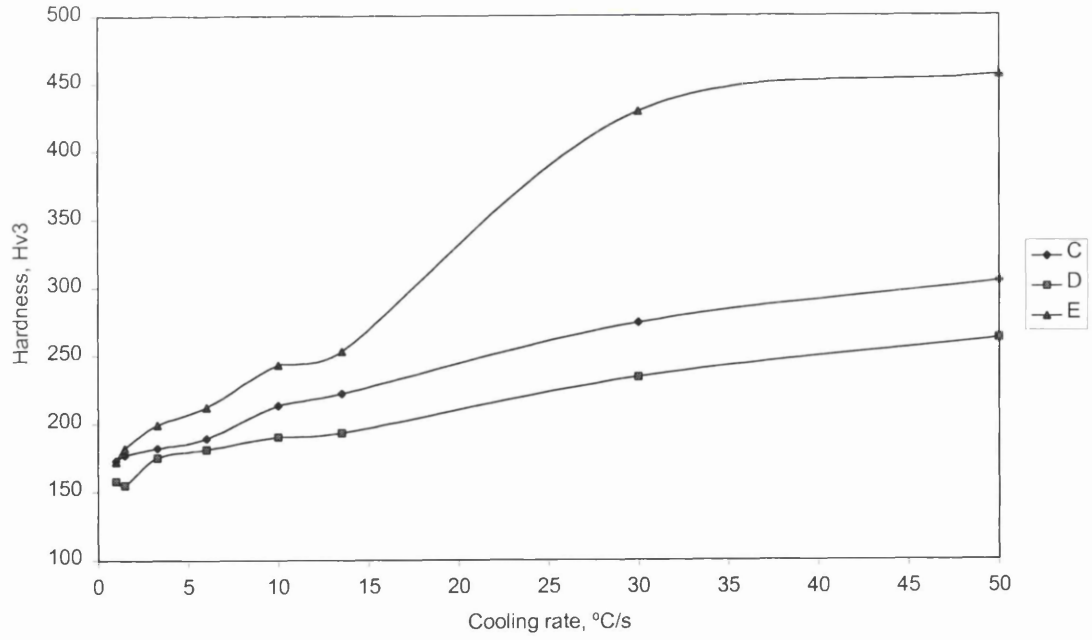

Figure 5.4: Hardness values plotted against cooling rate for steels C, D and E from dilatometry.

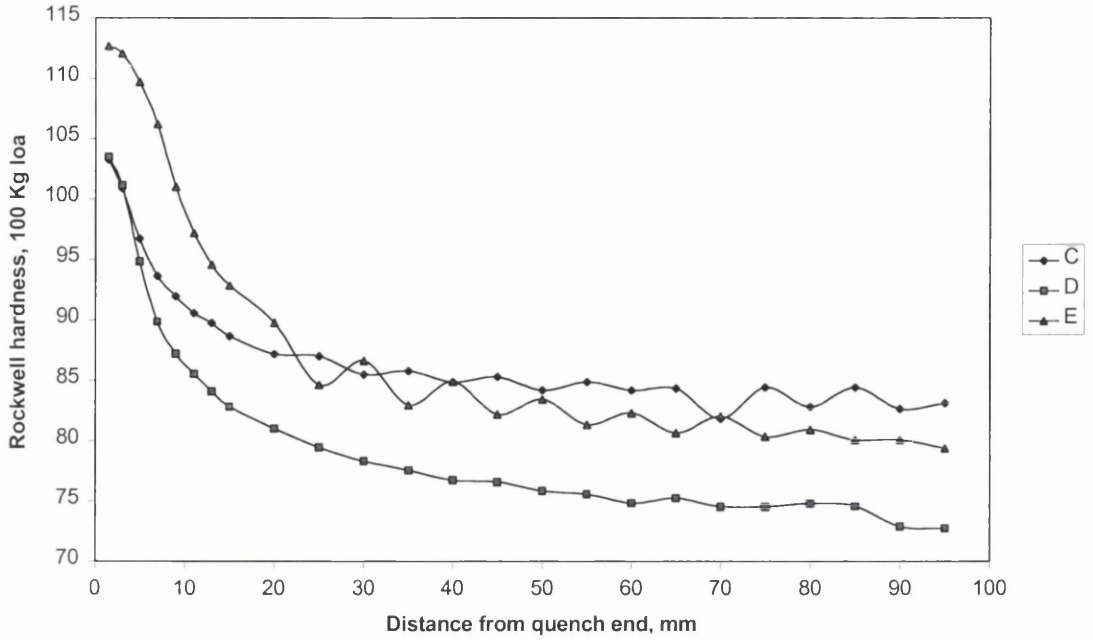

Figure 5.5: Varying hardness measurements of steels C, D and E obtained after the Jominy end quench test.

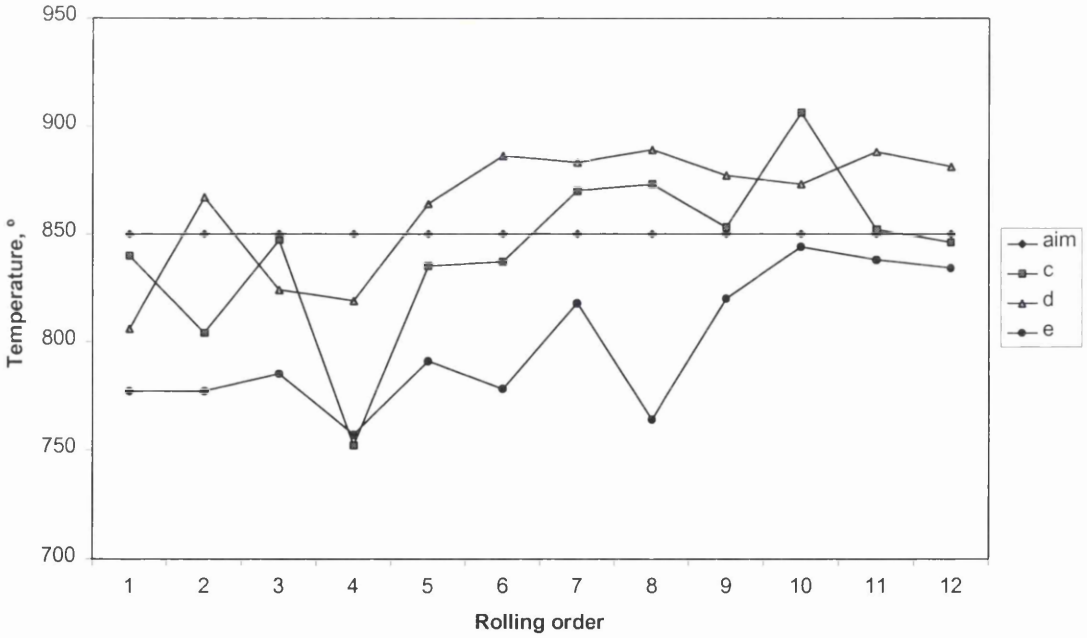

Figure 5.6: Finishing temperatures for steels C, D and E plotted against the sequence in which they were processed. The aim finishing temperature is also included.

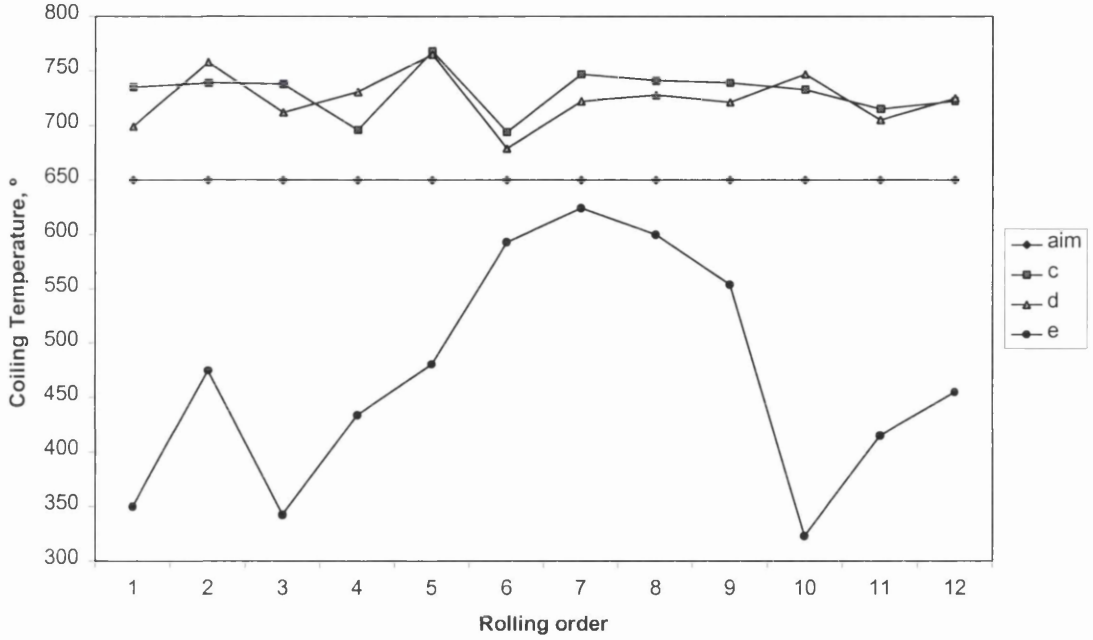

Figure 5.7: Coiling temperatures for steels C, D and E plotted against the sequence in which they were processed. The aim coiling temperature is also included.

6.0 INVESTIGATION 2 – THE PRODUCTION OF HIGH STRENGTH STEEL

As described in section 4.2, this part of the study focussed on steel metallurgy and mechanical properties achieved with the matrix of steels against annealing cycle. The first section involved analysing properties attained with the CAPL line, which was the only line built with high strength steel production in mind. The next section dealt with the cycles for the four galvanising lines, which were not designed to deal with high strength steels. As well as showing the microstructures and tensile results, the interaction between annealing cycle conditions and properties was also investigated and discussed. Once again, steel identification, which was discussed in investigation 1, will be the same for this investigation, i.e., the C-Mn reference material will be referred to as steel B and so on.

6.1 CAPL PROCESSED STEELS

The first step in assessing the feasibility of producing high strength steels was to use the most suitable industrial line. Therefore, initially, the steels were annealed using a CAPL type cycle because of its suitability for dual phase steel production. Indeed, CAPL was the most recently built line from the industrial cycles used, which foresaw high strength steel production during the design stage. However, in view of the fact that CAPL is an annealing line only, galvanised products would not be possible. Nevertheless, this section of work aimed to prove whether the steels chosen were capable of being developed into dual phase steels on an industrially based laboratory investigation.

With all M_s temperatures above 400 °C (calculated in investigation 1), the overageing temperature of 350-250 °C utilised with the CAPL cycle should not be problematic with regard to dual phase production. This coupled with the rapid cooling are the reasons why the CAPL line is most suitable for dual phase steel production.

6.1.1 Ferrite Grain Size

The graph and table representing ferrite grain size are shown in table 6.1 and figure 6.1. With grain sizes varying from 2 to 10 μm and grain shape varying from equiaxed to elongated, there was a certain degree of variation from sample to sample, with specific steels.

Ferrite grain size measurements did not exhibit a large difference for the seven steels utilised. With variation no more than 3 μm, it should be noted that the difference measured from steel to steel could well be as large as the potential error. However, the results can be used as an indicator, provided that no great emphasis is placed upon them. Despite this, by considering steel chemistry as the major factor, it can be seen from figure 6.1 that the ferrite grain size for steels A, B and G were the largest. The same graph shows that steels D, E and F appear to have the finest ferrite grain size, with steel C tending to have the median ferrite grain size. Two of the steels that exhibited the finer grains (D and F) had larger volumes of grain refining elements present. Steel D had niobium levels that were at least double the amount of the other steels and steel F was richer in vanadium than the other steels. With steel E not containing substantial amounts of grain refining elements such as niobium or vanadium, an explanation for the smaller grain sizes cannot be related to chemistry. However, steel E had the lowest coiling temperature of the laboratory cast steels, shown in the results from hot rolling (chapter 5), which could be a reason for the finer ferrite grains.

A comparison of ferrite grain sizes produced with steels B, D and F is a useful tool to prove the reasoning behind the role played by niobium and vanadium. This is because the three steels have very similar chemistries but exhibit a variation in ferrite grain size. The only significant difference in steel chemistry is niobium in steel D and vanadium in steel F. Yet, steels D and F had ferrite grain size measurements approximately 2 μm less than steel B. Given that both niobium and vanadium are well known as grain refining elements, they may well offer the reasons for the difference in grain size. This can be substantiated further by the extensive use of niobium and vanadium in HSLA grades. The results of a study by Abdalla *et al.*

(1999) investigating microalloyed dual phase steels also found that ferrite grain sizes were smaller than those of the reference plain-carbon dual-phase steel. Therefore, in view of the steel chemistries used and other research, it can be assumed that the niobium and vanadium (in steels D and F respectively) caused the ferrite grain refinement in these grades.

6.1.2 Retained Austenite

The results shown in table 6.1 revealed that, of the seven steels utilised, no retained austenite was detected, meaning a transformation induced plasticity (TRIP) effect was not observed. Levels of carbon are lower than those of typical TRIP steels, but manganese and silicon levels are in line with TRIP type chemistry. The chemistry coupled with the annealing cycle, which involved initial rapid cooling from the intercritical temperature as well as a temperature that was similar to an isothermal hold temperature, in theory could have produced a small TRIP effect. However, the overageing temperature used with this cycle (350-250 °C) was too low for the bainitic isothermal hold temperature required for TRIP steels, given that M_s temperatures were all above 400 °C. Also, it is apparent that greater carbon levels would have been required in order for a TRIP steel to be produced. Indeed, the results correspond to findings in studies with similar chemistries carried out by Vrieze *et al.* (2000) and Gallagher *et al.* (2002).

With the possibility of retained austenite transforming to martensite during any deformation, XRD samples were etched to avoid deforming the tested area. Therefore, even though metallography samples were subjected to a certain amount of deformation, there was confidence that the XRD results would have detected retained austenite if it were present. With no retained austenite detected from the XRD, constituents identified as martensite or retained austenite from optical microscopy analysis (next section) could therefore be defined as martensite, i.e., due to the similarity displayed between retained austenite and martensite in light microscopy, any material that could previously have been identified as retained austenite or martensite could therefore be classified distinctively as martensite.

6.1.3 Volume Fraction Measurements

The volume fraction results are displayed in figure 6.2 and are also represented in tabular form (Table 6.1). A range of microstructures consisting of ferrite and various second phase constituents were observed that included pearlite, bainite and martensite. Retained austenite was eliminated as a possible constituent by the XRD analysis, as discussed previously.

6.1.3.1 Steel Identification

Dual phase classification could be attributed to all the steels, apart from steels D and E. Steel D displayed very little martensite, so it would be difficult to class this grade even as a multi phase steel. The microstructure formed is shown in figure 6.3. Conversely, steel E was made up of at least fifty per cent martensite, which would make multi phase classification more plausible. All other grades were either comprised entirely of martensitic second phase or the vast majority of second phase was made up of martensite. The only exception to this statement was steel B, which contained a majority of martensite as second phase, but only about two thirds. Even though dual phase classification would appear to be less stringent in this study, two thirds of the steels were nevertheless classified as multi phase microstructures. In fact, only steels C, F and G had classic dual phase microstructures, composed entirely of ferrite and martensite with no other phases present. The dual phase microstructure for steel G is shown in figure 6.4.

6.1.3.2 Role of Steel Chemistry in Dual Phase

The results have shown that steels B, D and E failed to produce classical dual phase properties, which can be related specifically to the steel chemistry (table 4.1). Steel B was the least alloyed of all materials used in the study and is useful as a C-Mn reference steel that all the other steels can be related to. However, the volume fraction measurements have shown that percentage martensite formed was much less

in steel D and slightly less in steel E. Therefore, the steel chemistry reasoning will be structured so that lowest volume martensite steels are discussed first.

The chemical composition of steel D was very similar to steel B (reference steel), apart from an increase in niobium levels. Given that niobium was added for grain refinement, which it did for this grade (section 6.1.2), its presence should not influence martensite formation. The data from volume fraction measurements appears to confirm this point, as there was no increase in martensite levels. In fact, a similar study by Vrieze *et al.* (2000) found that, when comparing a niobium containing C-Mn steel with a reference C-Mn steel, the niobium had no effect on the volume fraction of martensite.

An increase in carbon was the major change with regard to steel E. Therefore, the results achieved with this steel grade were somewhat surprising. Potentially, a greater volume of martensite would be expected with an increase in carbon level. However, an increase in carbon levels is known to drive the martensite transformation temperatures down to lower levels. Evidence from the calculated values in investigation 1 seems to suggest that the CAPL line cycle would cool to below the M_s temperature. Even though calculated values for steel E were the lowest, transformation was calculated above 400 °C. Nevertheless, given that the presence of other elements that increase hardenability were not abundant, it may be that the carbon levels in this grade did in fact drive the transformation temperatures to below the overageing temperature (350 °C). Indeed, when assessing the steel chemistry, the aluminium level was the only significant difference with regard to chemistry for steel E. Given that aluminium is one of very few additions that does not influence hardenability, the relatively low martensite levels found cannot be attributed to low aluminium levels. As a consequence, bainite and/or pearlite were formed instead. In fact, by examining the chemistry in greater detail, it was clear that composition of the steel was not inherently conducive to either dual phase or TRIP steel production.

Steel A contained higher carbon and silicon levels than the reference steel B. Given that it was found that an increase in carbon failed to influence martensite levels in steel E, it could be assumed that the increase in martensite associated with steel A could be attributed to the slightly higher silicon addition (from 0.05 to 0.38 weight

%). Silicon is known to increase the hardenability of steel, which could help to explain the higher martensite levels recorded. The presence of silicon is known to promote martensite formation because it reduces the nucleation and growth rate for pearlite, i.e., promotes martensite transformation. It appears that this may have been the case with steel A.

The theory behind the role of silicon discussed with steel A would be the same for steel C. The main difference between the steels relates to the total weight % of silicon, which was 0.38 weight % for A and 1.28 weight % for C. The significant increase in silicon levels accounts for the increase in the amount of martensite present, because of the influence it has on hardenability. In fact, the increase in silicon levels would appear to be the primary reason for the production of a dual phase structure for steel C, as opposed to the more multi-phase type structure of steel A.

The chemical composition of steel G was the same as the reference material (steel B) apart from additional chromium. The increase in martensite levels can therefore be attributed to the increase in hardenability associated with chromium. The role played by chromium is similar to that played by manganese but, in fact, has a greater influence on hardenability than manganese. Chromium can essentially be added on to the levels of manganese to emphasise the increase in hardenability that both additions cause.

The key additions in steel F were vanadium and to a lesser degree molybdenum, so significant levels of martensite with this grade are attributed to both vanadium and molybdenum. With regards to hardenability, molybdenum and vanadium are two additions that are recognised as having the most significant influence (Llewellyn *et al.* 1998). Indeed, the presence of both alloying elements can explain the classic dual phase structure that consisted of purely ferrite and martensite. This seems to confirm that molybdenum and vanadium increase the hardenability considerably.

6.1.4 Mechanical Properties

With dual phase steels characterised by continuous yielding, low yield to tensile ratios, high tensile strength, relatively high total elongation values and high work hardening coefficients, it is reasonably straightforward to establish which of the grades displayed the best properties. Given that n value data was not available for all steels and total elongation values remained comparatively consistent, continuous yielding, yield to tensile ratios and tensile strengths were used predominantly to evaluate the dual phase type properties. Nevertheless, care must be taken if tensile strength is used as a measure on its own, because the effects of other strengthening mechanisms would not be considered. Mechanical properties are shown in table 6.2 and figure 6.5 and 6.6.

Results have shown that steels B and D displayed lowest tensile strengths coupled with the highest yield to tensile ratios. Additionally, the tensile curves for these two grades displayed discontinuous yielding. Steel B was chosen as the reference material because it was the least alloyed of all the steel grades used, which can help to explain the lack of dual phase properties. The addition of niobium, which was effectively the difference between steels B and D, failed to improve the mechanical properties with regards to dual phase characteristics.

Dual phase characteristics were observed with steel G, which included a very low yield to tensile ratio, continuous yielding and high total elongation values. However, steel G had a tensile strength that was relatively low at 550 MPa.

Steel E had tensile properties that were among the highest strengths of the steel grades used, while yield to tensile ratios were almost as high as grades B and D. The increase in strength for this grade can be explained by strengthening caused by the increase in carbon and is not attributed to dual phase type properties. Nevertheless, steel E did display continuous yielding behaviour as well as the higher tensile strength, although this was accompanied by low total elongation values.

The properties achieved for steels A and C were very similar, both displaying comparable yield to tensile ratios and tensile strengths. Furthermore, continuous yielding was observed with both grades. The grades were of similar composition, the main difference being a change from moderate to high silicon levels. It therefore seems that the higher silicon levels do not improve dual phase properties, although the corresponding decrease in carbon could account for this outcome.

Based on the characterisation approach above, steels B and D showed very little in the way of dual phase properties. Conversely, the other steels (A, C, E, F and G) did generally exhibit dual phase characteristics in the form of continuous yielding, high tensile strengths and low yield to tensile ratios.

6.1.5 Mechanical Properties Versus ULSAB Requirements

When comparing the steel grades produced in this study with grades set out in the ULSAB literature, there are only two steels that would meet the criteria set out. Steel C meets the DP600 requirements and steel D meets the HSLA450 requirements. In view of the fact that all steels apart from B and D displayed dual phase characteristics, it appears somewhat surprising that only one steel (steel C) met the requirements set out by ULSAB for dual phase properties. With yield and tensile strengths being comparable, it is clear that the total elongation requirements are the reason for the vast majority of the steels failing to reach the required properties. Indeed, if the critical total elongation levels were dropped by up to 5 %, DP600 classification would more than double and a DP700 would also be identified. By comparing the mechanical properties of the steels in this study with data from other similar research projects, it would appear that the recommended ULSAB properties are somewhat optimistic. Projects by Rege *et al.* (2002), Vrieze *et al.* (2000) and Stiaszny *et al.* (2000) to name but a few, all produced dual phase grades that did not achieve properties suggested in the ULSAB literature. However, it must be stated that the properties set out by ULSAB are not industry standards and were meant as a guide to classification rather than a definitive categorisation.

6.1.6 Relationship Between Microstructures & Mechanical Properties

Evaluation of mechanical properties and microstructures in the previous sections revealed the varying properties achieved with the different grades of steel processed using the CAPL cycle. Given that steel microstructures and mechanical properties are fundamentally linked, the following section will attempt to rationalise the results observed for both the microstructures and mechanical properties.

To summarise, steel D did not exhibit any dual phase microstructural or mechanical property characteristics. Steels B and E were two materials that displayed some martensite within the microstructures and were identified as multi-phase microstructures. They also exhibited some typical dual phase mechanical properties. However, steels A, C, F and G showed sufficient dual phase microstructural and mechanical characteristics to justify dual phase identification.

The heating/cooling cycle used played as much of a role as steel chemistry in dual phase production. This study has shown that the CAPL cycle has the capability of producing at least multi phase type steels on all occasions, but dual phase steels were produced with the steels that were more highly alloyed.

It is difficult to relate ferrite grain size to the mechanical properties because of the other factors involved. It is known that ferrite grain size influences yield strength. However, this phenomenon is greatly reduced when factors such as variable second phase make up are considered, which was the case with the selected steels, i.e., this investigation appears to show that no trend relating ferrite grain size to mechanical properties can be seen because of the variety of second phases formed with dual phase and multi phase steels.

Figure 6.7 shows the relationship between volume fraction martensite and both yield and tensile strengths. As the volume fraction martensite increased up to 25 %, the yield decreased and tensile strength increased. This point is shown more clearly when the yield to tensile ratio was plotted against volume fraction martensite (figure 6.8). As expected, the ratio decreased as martensite volume increased. This agrees with the

findings of the literature review and also parallels several studies that included work by Hashimoto *et al.* (1986). The increase in tensile strength can be attributed to the greater volume of martensite because the martensite compared with bainite and/or pearlite, so the strength of martensite obviously impacts on the overall strength of the steel.

The decrease in yield strength in relation to the volume fraction of martensite was because of the gradual elimination of yield point to give continuous yielding. This study showed that this was evident at about 10 % volume fraction martensite. The yield strength does not continue to decrease as volume martensite increases, as shown in numerous investigations that included Rege *et al.* (2002). Their study showed that, once the volume fraction reached around 20 %, the yield strength increased at a similar rate to the increase in tensile strength. With volume fractions of martensite limited to 20 % in this study, observing this type of trend was not possible because it fell short of the range needed. Had greater martensite volumes been produced, the total elongation would have been expected to decrease significantly. Hence, this investigation has shown that elongation values remained reasonably constant regardless of martensite levels but, for the reasons described above, more than 20 % martensite would be expected to significantly decrease total elongation values.

6.2 GALVANISING LINE PROCESSED STEELS

The evaluation of steel properties achieved with CAPL processed steels, described in the previous section (6.1), generally showed that the steels chosen for this study could produce ferrite-martensite dual phase properties. However, in view of the fact that the purpose of the project was to produce galvanised dual phase steels, the annealing cycles of four galvanising lines were also utilised. As with the CAPL processed steels, microstructures and mechanical properties were assessed to determine the success of dual phase production. The four galvanising cycles used (DVL, Galtech, Zodiac and Zodiac revised) were not designed specifically for production of dual phase steels. Therefore, the final properties obtained would not be expected to be the same as those obtained with the CAPL materials, i.e., lower strength multi-phase steel would be the more likely. For this reason, as well as assessing the effect of steel

chemistry and galvanising cycle used, a comparison with the CAPL processed steel was also carried out. Although CAPL processed steels were discussed previously, reference is again made in this section but with greater emphasis placed upon the galvanising line produced steels.

It is apparent from the martensite transformation temperatures calculated in chapter 5, that the overageing section currently utilised by the Zodiac line cycle could be problematic with regard to dual phase steel production. The M_s values ranged from around 400 to 460 °C, which is very close to the overage temperature that was set at 420 °C. Therefore, with some steel grades there may well be instances when the martensite start temperature is not reached prior to overageing, thus preventing dual phase steel formation.

6.2.1 Ferrite Grain Size

The influence of steel chemistry was described in section 6.1 for these steels but, the annealing cycle used will also influence the ferrite grain size. Variables in the annealing process that would influence the ferrite grain size include holding time and temperature, parent austenite grain size and shape, deformation relating to the cold rolling process and cooling rate (Ouchi 1985). With processing prior to annealing kept as constant as possible, the prior cold reduction and austenite grain size effects can be overlooked.

6.2.1.1 Effect of Annealing Cycle

Ferrite grain sizes for samples annealed using the DVL cycle appeared to be larger than the values obtained from the other cycles (tables 6.3-6.7). Indeed, the ferrite grain sizes determined for the DVL processed steels was generally 1 or 2 μm greater than average, typically around 7.5 μm. Both Zodiac cycles appeared to produce the finest grains, typical grain diameters being about 5 μm, while ferrite grain sizes for samples processed with the Galtech cycles were typically around 6 μm. For

reference, the CAPL processed steels had ferrite grain sizes on a par with Galtech produced material.

When the heating/holding/cooling sequence for each of the cycles is studied, it is apparent that holding time and temperature are factors that would have a significant impact on eventual ferrite grain size. An increased hold time and temperature allow more time for recrystallisation to occur. This extra time allows a larger volume of austenite grains to form at the intercritical temperature. The volume of austenite formed will also depend on hold time and temperature. Thus, it would be expected that the differing annealing temperatures employed in this investigation would affect the ferrite grain sizes. The finest grain sizes were generally attributed to the Zodiac produced steels, which had the lowest annealing temperature. The results seem to suggest that a lower annealing temperature equates to finer grain sizes.

Grains were very rarely equiaxed as evident from figure 6.9. Data points on the left hand side of the graph are longitudinal measurements, whereas data points on the right hand side of the graph are width measurements. The graph clearly shows that grain size measurements were generally about 3 μm more in the longitudinal direction. In some cases, the grains were extremely elongated, for example, the grain sizes for steels E and F annealed using the Galtech cycle were 10 by 2.5 μm. The elongated grain structure can be explained by the microstructure of the previous cold rolled process not being recrystallised sufficiently to produce the 'new' structure. Steel with the highest grain size aspect ratio was produced using the Galtech cycle, which had the shortest hold time of all cycles used. Even though the annealing temperature was higher than average with the Galtech cycle, it is evident that either a higher annealing temperature or longer soak time would be required to overcome this issue. However, with the intercritical annealing temperature close to the maximum possible, the hold time would be the most feasible parameter to change.

6.2.1.2 Effect of Steel Grades

It can be seen from figure 6.10 that the ferrite grain size for steels A and B were consistently the largest. The same graph shows that steels D and F appear to have the

finest ferrite grain size, with steels C, E and G tending to have intermediate ferrite grain sizes.

There are numerous factors that could have an influence on the ferrite grain size, which include the annealing time and temperature, parent austenite dimensions, the amount of cold reduction and cooling rate. The influence of the annealing conditions and cooling rate was described in the previous sub-section, and can be overlooked in this instance because steels processed with exactly the same annealing and cooling conditions will be compared. Therefore, apart from cold reduction and parent austenite dimensions, the only other variable relates to steel chemistry. Given that the cold rolling process varied for the steels, i.e., some were laboratory rolled and others were commercially rolled, the effects of this factor cannot be fully investigated. Nevertheless, an attempt to keep a consistent level of cold reduction was made, this was because the laboratory cold rolling system was modelled on the commercial process. Therefore, given that all factors apart from austenite grain dimensions and chemistry were kept reasonably constant, the variation in grain size could be attributed to these factors. With steel chemistry having a direct bearing on austenite grain dimensions, these factors are inherently linked. Indeed, by evaluating the steel chemistry used, the steels that had the finest ferrite grain sizes were those that contained grain refiners such as niobium and vanadium. Even though it may be expected that the cold reduction and annealing process would have an adverse effect on grain refinement during initial austenisation, a correlation between hot rolled and cold rolled/annealed products has been proposed by Bordignon *et al.* (1984).

6.2.2 Retained Austenite

None of the steels exhibited retained austenite when processed using the annealing cycles adopted with the galvanising lines. The lack of a TRIP effect can be attributed to the low carbon levels, which were described in the previous section (6.1). In fact, considering the higher overageing temperature associated with the Zodiac cycles (420 °C) compared to CAPL (350 to 250 °C), retained austenite production would seem to be more feasible with the Zodiac cycles.

It was found that varying the annealing cycle did not produce retained austenite. Even though the cycles used had the possibility of being used for TRIP steels, it seems that the steel was not sufficiently alloyed. This was established by two studies that successfully produced TRIP steels using cycles similar to those utilised in this investigation. The studies were carried out by Gallagher *et al.* (2002) and Traint *et al.* (2002), using steels containing 0.15 % carbon, 1.5 % manganese and 1.6 % silicon and 0.2 % carbon, 1.5 % manganese and 1.5 % silicon respectively, i.e., both steels were produced with critical additions above those in this investigation. These studies also utilised a higher isothermal temperature, which would have been higher than M_s temperature. On this basis, the annealing cycles chosen for this investigation appear capable of producing TRIP steels, if the chemistries and/or the isothermal holding temperature were changed.

6.2.3 Volume fraction Measurements

A selection of the micrographs is shown in this section, illustrating the various constituents of the high strength steels. These results are backed up with graphs displaying key factors regarding volume fraction measurements, which are also represented in tabular form (Tables 6.3-6.6). A range of microstructures consisting of ferrite and various second phase constituents were observed that included pearlite, bainite and martensite.

6.2.3.1 Steel Identification

Metallurgical classification of steel grades processed using the galvanising line cycles was split into three categories, namely non-martensitic grades, multi-phase and dual phase. With a certain degree of irregularity across the various cycles, classification was less specific than those described for the CAPL steels.

Steels that failed to produce any or very little martensite included grades B, D and E. A micrograph of steel containing no martensite, (in fact, for steel B processed by the DVL line), is shown in figure 6.11. Volume fraction measurements for steel B, which

are shown in figure 6.12, revealed that none of the galvanising cycles produced significant quantities of martensite. With the volume fraction of martensite being less than 3 % and the remainder made up from bainite and/or pearlite, it would be difficult to classify these steels as multi-phase. The volume fraction measurements for steel D displayed very low martensite levels, evident from figure 6.13. Martensite levels did not rise above 2 % of the total volume, which equates to no more than 9 % of the total second phase. In view of the fact that martensite levels were consistently low, it was not possible to observe any trend relating to the annealing cycle used, although DVL (slowest cooling rate) displayed no martensite at all. Phase identification of steel E revealed trace amounts or no martensite for all galvanising cycles (figure 6.14). With the volume fraction of martensite less than 2 %, these steels cannot be classed as dual phase.

Multi-phase microstructures were produced with steels A and G, which displayed significant martensite as well as bainite and/or pearlite. The micrograph of steel A annealed with the Zodiac cycle is illustrated in figure 6.15, which indicates the presence of ferrite, martensite and bainite/pearlite. Figure 6.16 revealed a general increase in the volume fraction of martensite as the cooling rate from the intercritical hold was increased for steel A. Indeed, steel A displayed only 1 % martensite when the DVL cycle was used, which contrasts with the 18 % observed with the CAPL cycle. The other cycles resulted in an approximately equal split between martensite and other second phase constituents. Therefore, multi-phase microstructures were produced when utilising the Galtech, Zodiac and Zodiac revised cycles, which differed from the more dual phase type microstructure obtained with the CAPL cycle. A slight increase in martensite was observed as the cooling rate was increased for steel G, which is shown in figure 6.17. All steels displayed a certain volume of martensite, but not sufficient to warrant dual phase classification.

Dual phase microstructures were identified on two occasions for the galvanising line processed steels, namely, steels C and F. A dual phase microstructure is shown in figure 6.18, which was produced when steel C was processed via the Galtech cycle. The galvanising cycles produced steel microstructures with large volume fractions of martensite for steel C (figure 6.19). The volume fraction of martensite ranged from 36 to 80 % of total second phase, with the microstructure produced by the DVL cycle

being the only one that failed to achieve a minimum of two-thirds martensite. As a result, DVL processed steel can be classed as a multi-phase grade. On the other hand, the microstructures resulting from the other three cycles could all be classed as dual phase, because no more than 3.5 % bainite and/or pearlite was seen with these samples. The formation of martensite was significant in steel F, which can be seen in figure 6.20, i.e., the martensite volume fraction was more than three quarters of total second phase present, which can be classified as dual phase. However, on one occasion, this was not the case because the Galtech processed steel displayed no martensite and also displayed the elongated grain structure associated with cold rolled steel. The presence of this microstructure can explain why no martensite was formed, i.e., insufficient time for recovery, recrystallisation and grain growth resulting in a predominantly cold rolled structure being observed.

As discussed with regard to the CAPL processed steels, the steel chemistry played a vital role in final steel microstructure, i.e., those materials that contained elements that increased hardenability were more likely to give dual phase microstructures. Steels C and F were described previously for the higher levels of silicon (steel C) and molybdenum and vanadium (steel F) and again appeared to have the greatest impact on the successfulness of dual phase formation. Steels A and G, with slightly less additions required to increase hardenability, help to explain the tendency for multi-phase microstructures. Steels B, D and E had lower additions of molybdenum, vanadium, chromium and silicon which, if present, would have produced greater volumes of martensite.

6.2.3.2 Annealing Cycle Effects

As explained previously, the cooling rate from the intercritical annealing temperature had greater significance than the hold time and temperature. As a result, the following discussion does not totally disregard hold conditions but, instead, places greater emphasis on cooling rate.

Results from the volume fraction measurements have shown that, regardless of steel chemistry, the DVL cycle did not have a sufficiently fast cooling rate to allow the

austenite to martensite transformation. The cooling rate can be pinpointed as the reason, ahead of hold temperature and time, because of the similar hold time associated with the CAPL cycle. In fact, this reason is vindicated because, with the exception of steel D, the CAPL cycle (with its rapid cooling section) was capable of producing a dual phase or multi-phase microstructure, with mainly martensite being the dominant second phase with all chemistries tested.

The Galtech and Zodiac cycles had the capability of producing dual phase steels with the most highly alloyed steels. However, in most cases, multi-phase structures were observed with some dual phase structures produced.

The most significant aspect of these results was that the revised Zodiac cycle, which incorporated a more rapid cooling rate, failed to produce martensite-rich microstructures. In fact, the volume fraction of martensite was slightly less on some occasions with the 'improved' revised cycle. This suggests that the overageing temperature, which was the same for both Zodiac cycles, is significant in determining final microstructures. The overageing factor is noteworthy because an increase in cooling rate from 25 to 50 °C/s does not have any significant influence on final volume fraction microstructure. With the overageing temperature set at 420 °C for these cycles, it is close to the expected martensite start temperature for these steels. If the martensite start temperature were not reached, then the formation of bainite would occur during the overageing period. The CCT diagrams for steels C, D and E, discussed in section 5.1.2, show that the martensite start temperature is slightly lower than the empirical values, i.e., closer to 400 °C. An important point to note from the CCT diagrams was that, at the 50 °C/s cooling rate, the martensite transformation temperatures were about 50 °C lower than those for a cooling rate at 25 °C/s. This trend would be the same for all steels, which shows that the rapid cooling cycle should have utilised a lower overageing temperature. Ideally, a cycle with no overageing would overcome this problem but, in order to replicate the industrial practice, this is a factor that cannot be removed.

6.2.4 Mechanical Properties

Properties distinctive to dual phase steels were very rarely achieved with the materials processed through the galvanising line type cycles. Reasons for this were identified primarily because of the nature of cycles used. Factors such as cooling rate from the intercritical region, overageing sections and the time step for galvanising were identified as possible problem areas.

When evaluating the tensile properties of the seven steels processed via the galvanising line annealing cycles (tables 6.7-6.10), it showed that those processed using the Galtech and the two Zodiac cycles displayed very similar mechanical properties. The DVL processed steels tended to show different properties, usually lower strength characteristics.

6.2.4.1 Mechanical Property Evaluation

The steels were categorised into two broad groups, which were steels that exhibited dual phase mechanical properties and those that did not. Characteristics specific to dual phase steels include continuous yielding, low yield to tensile ratio, relatively high tensile strength and high rate of work hardening. With the variation in galvanising line conditions producing steels with varying properties, the general trends for the steel grades were described. Again, as with the volume fraction section (section 6.2.3), a detailed account of reasons for the varying properties was described with the CAPL processed steels.

Four of the steel grades did not show any dual phase characteristics from the tensile data, which were steels B, D, E and G. As with the CAPL results, steels B and D generally displayed the lowest tensile strengths, coupled with the highest yield to tensile ratios. However, for the galvanising line produced materials, the mechanical properties for steel G had similar characteristics to B and D, which was not the case under CAPL conditions. Additionally, all tensile curves for these three grades showed discontinuous yielding. Steel E again showed tensile properties that were among the highest of the steel grades used. However, as with the CAPL processed

steel, yield to tensile ratios were as high as the grades that did not exhibit dual phase properties. Steel E did not display continuous yielding from tensile data for the galvanising line cycles, which was also the case under CAPL conditions.

Three of the grades did exhibit dual phase mechanical properties from the steels annealed via the galvanising cycles. The steels, A, C and F, displayed these characteristics from at least two of the four cycles used. The properties achieved for steels A and C were similar, both had comparable yield to tensile ratios and tensile strengths, furthermore continuous yielding was observed with both grades. Although steel F exhibited dual phase characteristics, lower tensile strengths and higher yield to tensile ratios were experienced.

Based on the characterisation approach above, steels B, D, E and G showed very little in the way of dual phase properties. On the other hand, steels A, C and F did exhibit dual phase characteristics in the form of continuous yielding, high tensile strengths and low yield to tensile ratios on occasions. This follows the general observations made with the CAPL processed material, the main difference being that steels E and G went from exhibiting dual phase properties under CAPL conditions to not exhibiting dual phase properties under the galvanising line processing conditions.

6.2.4.2 Effects of Annealing Cycle

As described above, very few of the steels exhibited dual phase properties from the annealing cycles used on the galvanising lines. In fact, the Zodiac standard cycle did not produce any steels with dual phase mechanical properties. The DVL cycle produced dual phase type mechanical properties on one occasion, the Zodiac revised did twice and Galtech on three occasions.

Because the galvanising cycles are not ideal for dual phase production, the fact that dual phase steels were produced is welcoming, so the study has shown that the potential for galvanising high strength steels on industrial galvanising lines is possible. The degree of success varied from cycle to cycle, with the results suggesting that the Galtech process would be the most suitable. Even with the rapid

cooling added to the Zodiac cycle, it does not seem to increase the likelihood of dual phase production. It therefore appears that the overageing section should be significantly lowered or removed completely in order to overcome this problem. This study has also proved that, unless highly alloyed steels are used, DVL and Zodiac do not have the relevant cycle. The cooling rate in the DVL cycle and the overageing section in Zodiac appear to be the main problem for dual phase production. The overageing issue seems to be stated further by the failure of the revised Zodiac cycle to achieve properties akin to CAPL processed steel.

6.2.4.3 Mechanical Properties Versus ULSAB Requirements

The vast majority of mechanical properties for the galvanising cycle processed steels did not display the required dual phase properties. In fact, most classifications would identify HSLA450 as the grades produced. The over stringent ULSAB requirements, coupled with the inferior mechanical properties for these steel grades, explain why dual phase classification was not achieved. However, it should be noted that the properties achieved are within the scope of high strengths and would be possibilities as potential future grades.

6.2.5 Relationship Between Microstructures & Mechanical Properties

Evaluation of mechanical properties and microstructures in the previous sections revealed the varying properties achieved with the different grades of steel and annealing cycles utilised. In essence, a total of 28 different steels were produced if the seven grades and four cycles were considered. As was the case with CAPL processed steels, the relationship between metallurgical findings and mechanical properties was carried out for the galvanising line steels.

6.2.5.1 Specific Microstructural & Mechanical Properties

To summarise the inferences made in sections 6.2.3 and 6.2.4, in general, steels B, D and E did not exhibit dual phase microstructures or mechanical properties. Steel G was identified as a multi-phase microstructure, without exhibiting dual phase mechanical properties, whereas steel A was also identified as multi-phase steel from the microstructure but did display dual phase mechanical properties. Conversely, steels C and F showed sufficient dual phase microstructural and mechanical characteristics to justify dual phase grade identification. This shows that there appeared to be more grey area when classifying these steels compared with the CAPL processed materials.

6.2.5.2 Variable Points

There were a number of points from the matrix of results that did not appear to fit the other material properties. Indeed, if these points were removed from certain sets of data, the trends would appear to be distinctly clearer.

The most significant anomaly was steel F produced by the Galtech cycle, which displayed an elongated ferrite grain structure, extremely low elongation values, very high strength, low yield to tensile ratio and no martensite. Metallurgical evaluation clearly showed that very little if any recrystallisation had taken place, which would account for the elongated grains. Reasons for this microstructure cannot easily be identified because it was not observed for this steel or cycle on other occasions. The structure of the cold rolling process also explained the very high tensile strength and poor elongation. Furthermore, continuous yielding was observed, which is a characteristic of cold worked steel. With the same characteristic found in dual phase steels, it would be easy to assume that dual phase characteristics were being seen. However, the lack of martensite and low elongation discounts the prospect of a dual phase structure being a possibility.

6.2.5.3 General Trends for Microstructures v Mechanical Properties

The general trends relating steel microstructure and mechanical properties are shown in figures 6.21 to 6.23. The relationship between ferrite grain size and mechanical properties plotted in figure 6.21 shows that, as ferrite grain size increased the yield and tensile strengths decreased. Even though there is considerable scatter on the graph, a suggestion of a downward trend can be seen, which is consistent with the Hall – Petch effect (equation 1.3). With many other factors influencing mechanical properties, this study shows that the ferrite grain size appears to play an almost negligible part in relation to mechanical properties. Figure 6.22 shows the effects that the volume fraction of martensite had on yield and tensile strengths. As volume fraction martensite increased up to 25 %, the yield decreased and tensile strength increased. This point is justified when the yield to tensile ratio was plotted against volume fraction martensite (figure 6.23). As expected the ratio decreased as martensite volume increased.

Table 6.1: Microstructural evaluation of steels A to G after processing through the CAPL cycle.

	Ferrite grain size, μm			Retained	Volume fraction measurements, %			
Steel	length	width	average	austenite, %	ferrite	martensite	NM 2^{nd} phase	Martensite /NM
A	7.6	4.6	6.1	0	76.5	17.8	5.7	75.7
B	7.6	5.2	6.4	0	79.5	14.0	6.5	68.3
C	6.3	4.9	5.6	0	84.5	14.0	1.5	90.3
D	5.2	3.9	4.6	0	81.0	1.3	17.7	6.8
E	5.5	4.3	4.9	0	77.5	11.5	11.0	51.1
F	6.0	4.0	5.0	0	85.0	15.0	0.0	100
G	7.6	5.3	6.5	0	76.5	23.5	0.0	100

Table 6.2: Mechanical properties of steels A to G processed through the CAPL cycle.

	Yield strength (MPa)	Proof(0.2) strength (MPa)	Tensile strength (MPa)	Total elongation (%)	Yield/tensile ratio
A	-	393	750	10	0.52
B	433	-	564	24	0.77
C	-	350	664	25	0.53
D	394	-	521	16	0.76
E	-	492	743	12	0.66
F	-	290	642	18	0.45
G	-	250	551	25	0.45

Table 6.3: Microstructural evaluation of steels A to G after processing through the DVL cycle.

	Ferrite grain size, μm			Retained	Volume fraction measurements, %			
Steel	length	width	average	austenite, %	ferrite	martensite	NM 2^{nd} phase	Martensite /NM
A	8.9	8.1	8.5	0	84.0	1.0	15.0	6.3
B	6.3	7.8	7.1	0	80.0	0.0	20.0	0.0
C	7.3	5.2	6.3	0	87.5	4.5	8.0	36.0
D	7.6	7.6	7.6	0	85.3	0.0	14.7	0.0
E	8.5	6.3	7.4	0	84.0	0.0	16.0	0.0
F	8.1	6.4	7.3	0	88.0	9.0	3.0	75.0
G	8.2	5.4	6.8	0	83.5	1.0	15.5	6.1

Table 6.4: Microstructural evaluation of steels A to G after processing through the Galtech cycle.

	Ferrite grain size, μm			Retained	Volume fraction measurements, %			
Steel	length	width	average	austenite, %	ferrite	martensite	NM 2^{nd} phase	Martensite /NM
A	6.9	5.4	6.2	0	76.3	13.5	10.3	56.8
B	7.3	4.9	6.1	0	79.3	1.7	19.0	8.2
C	7.0	5.0	6.0	0	88.0	8.5	3.5	70.8
D	5.0	5.2	5.1	0	85.0	0.7	14.3	4.7
E	9.0	3.0	6.0	0	83.0	0.0	17.0	0.0
F	10.0	2.5	6.2	0	85.0	0.0	15.0	0.0
G	7.9	5.2	6.6	0	81.0	2.5	16.5	13.2

Table 6.5: Microstructural evaluation of steels A to G after processing through the Zodiac cycle.

	Ferrite grain size, μm			Retained	Volume fraction measurements, %			
Steel	length	width	average	austenite, %	ferrite	martensite	NM 2^{nd} phase	Martensite /NM
A	6.9	4.1	5.5	0	79.0	7.0	14.0	33.3
B	6.5	4.9	5.7	0	76.6	3.0	20.4	12.8
C	7.4	4.9	6.2	0	85.5	11.5	3.0	79.3
D	5.4	4.5	5.0	0	84.3	0.7	15.0	4.5
E	8.0	4.0	6.0	0	84.0	1.5	14.5	9.4
F	5.1	3.9	4.5	0	85.5	12.0	2.5	82.8
G	5.4	4.9	5.2	0	81.0	6.0	13.0	31.6

Table 6.6: Microstructural evaluation of steels A to G after processing through the Zodiac revised cycle.

	Ferrite grain size, μm			Retained	Volume fraction measurements, %			
Steel	length	width	average	austenite, %	ferrite	martensite	NM 2^{nd} phase	Martensite /NM
A	6.3	5.0	5.7	0	73.4	7.8	18.8	29.3
B	7.3	5.9	6.1	0	72.0	1.7	26.3	6.1
C	6.7	5.0	6.4	0	85.5	12.0	2.5	82.8
D	5.9	4.5	5.2	0	80.3	1.7	18.0	8.6
E	6.3	4.6	5.6	0	79.5	1.3	19.2	6.3
F	5.6	3.6	4.6	0	87.0	11.5	1.5	88.5
G	6.3	5.1	5.7	0	81.0	5.0	14.0	26.3

Table 6.7: Mechanical properties of steels A to G processed through the DVL cycle.

	Yield strength (MPa)	Proof(0.2) strength (MPa)	Tensile strength (MPa)	Total elongation (%)	Yield/tensile ratio
A	385	-	575	24.0	0.67
B	382	-	529	27	0.72
C	415	-	606	25.4	0.68
D	366	-	480	26	0.76
E	422	-	564	23	0.75
F	-	299	553	25	0.54
G	338	-	462	26	0.73

Table 6.8: Mechanical properties of steels A to G processed through the Galtech cycle.

	Yield strength (MPa)	Proof(0.2) strength (MPa)	Tensile strength (MPa)	Total elongation (%)	Yield/tensile ratio
A	317	-	624	22.0	0.51
B	418	-	558	17.3	0.75
C	395	-	636	27.8	0.62
D	424	-	530	23.3	0.80
E	448	-	592	22	0.76
F	-	301	690	7	0.44
G	360	-	477	25	0.75

Table 6.9: Mechanical properties of steels A to G processed through the Zodiac cycle.

	Yield strength (MPa)	Proof(0.2) strength (MPa)	Tensile strength (MPa)	Total elongation (%)	Yield/tensile ratio
A	426	-	611	23.7	0.70
B	430	-	551	21.3	0.78
C	416	-	632	28.2	0.66
D	394	-	510	22.7	0.77
E	444	-	576	23	0.77
F	416	-	557	24	0.75
G	363	-	474	28	0.77

Table 6.10: Mechanical properties of steels A to G processed through the Zodiac revised cycle.

	Yield strength (MPa)	Proof(0.2) strength (MPa)	Tensile strength (MPa)	Total elongation (%)	Yield/tensile ratio
A	-	340	620	21.4	0.55
B	423	-	558	21.8	0.76
C	406	-	623	29.3	0.65
D	416	-	526	24.7	0.79
E	486	-	606	21	0.80
F	369	-	540	17	0.68
G	402	-	473	20	0.85

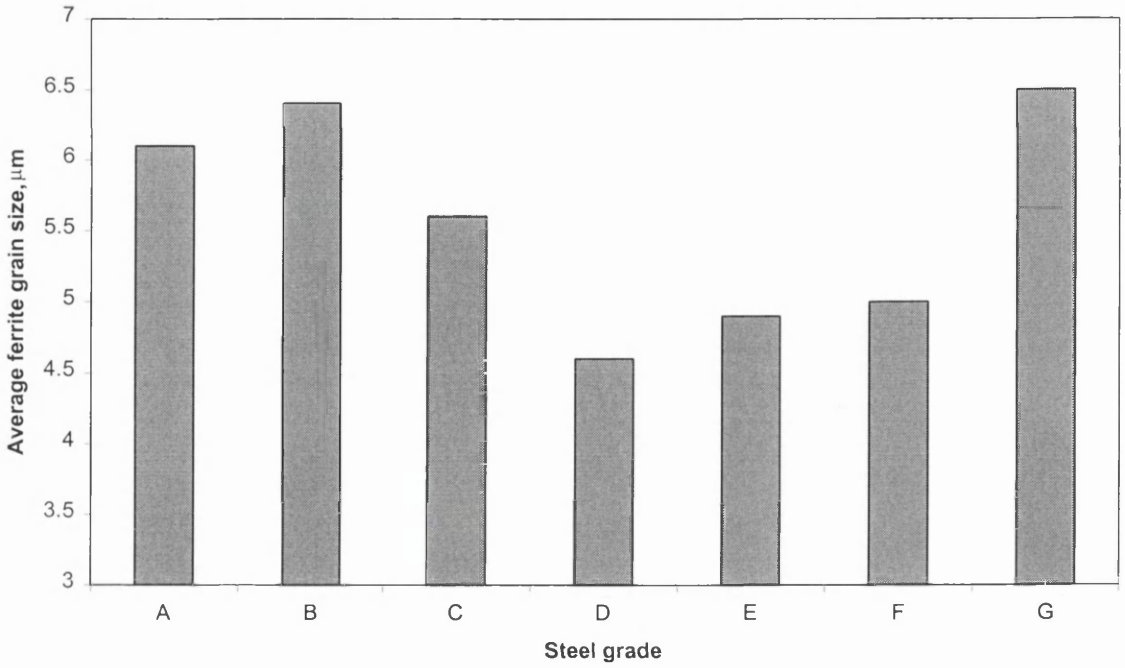

Figure 6.1: Average ferrite grain size measurements for the CAPL processed steels.

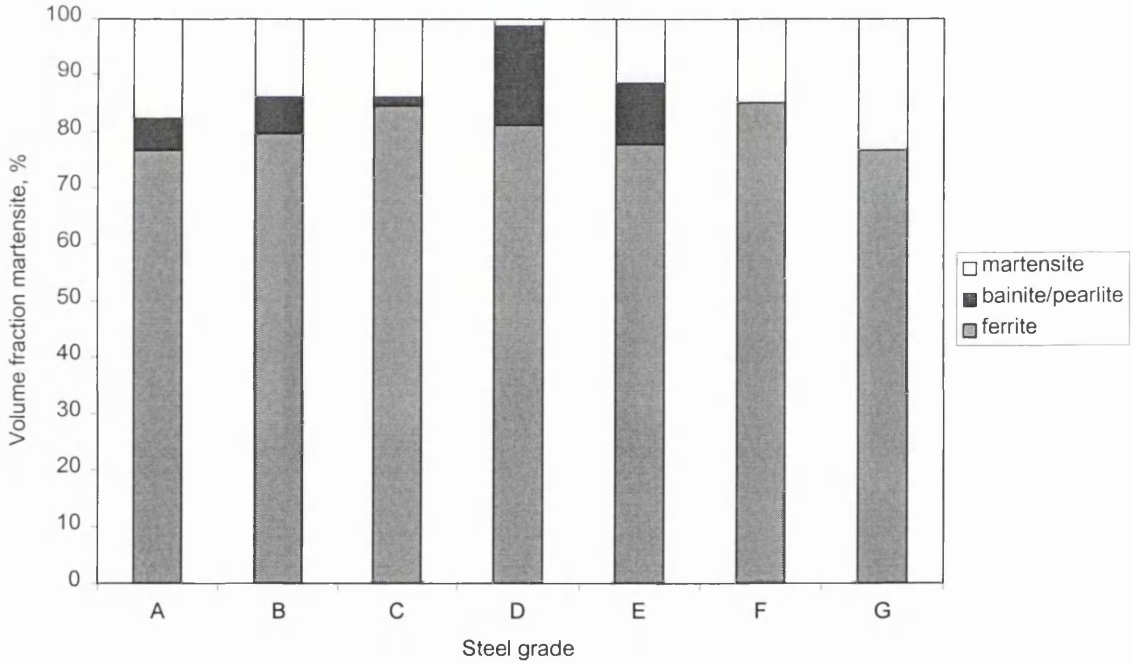

Figure 6.2: Volume fraction measurements for the CAPL processed steels.

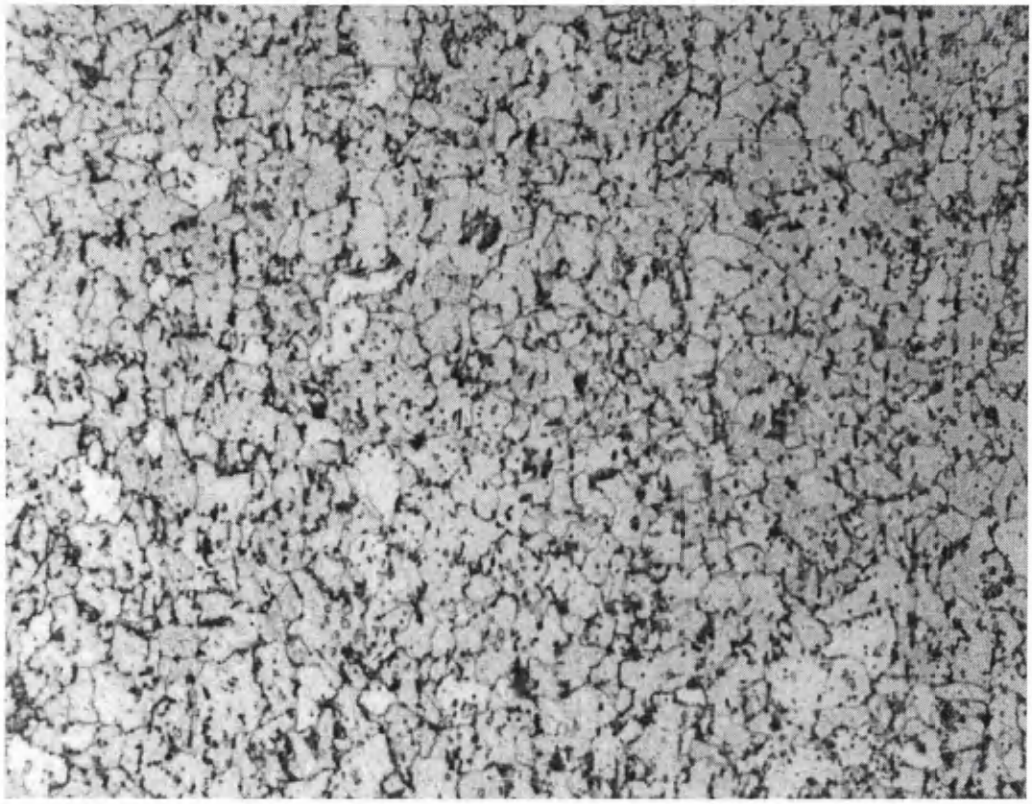

Figure 6.3: Non-martensitic microstructure of steel D processed with the CAPL cycle (x1000).

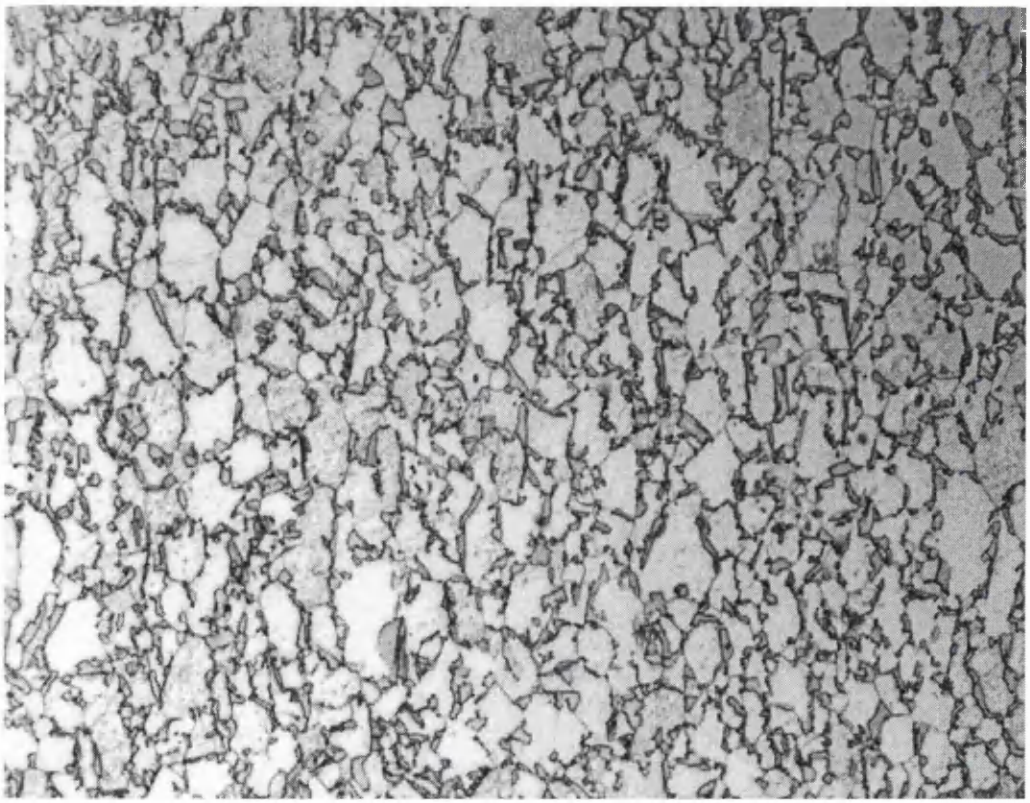

Figure 6.4: Dual phase microstructure of steel G processed with the CAPL cycle (x1000).

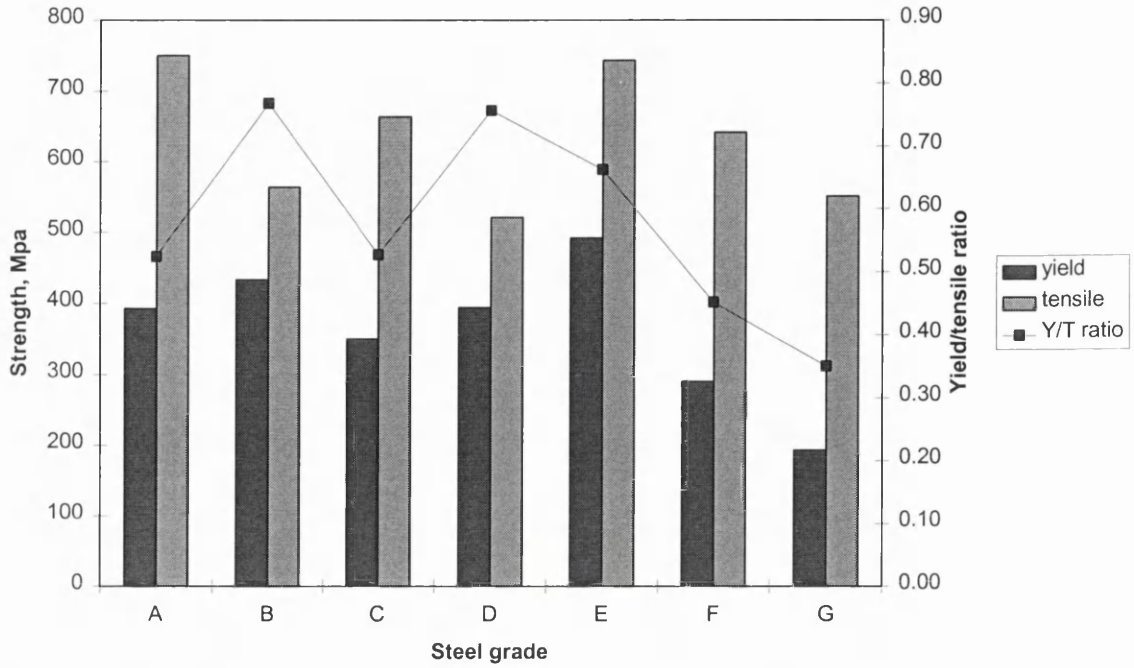

Figure 6.5: Yield and tensile strengths for all steels processed on CAPL cycle.

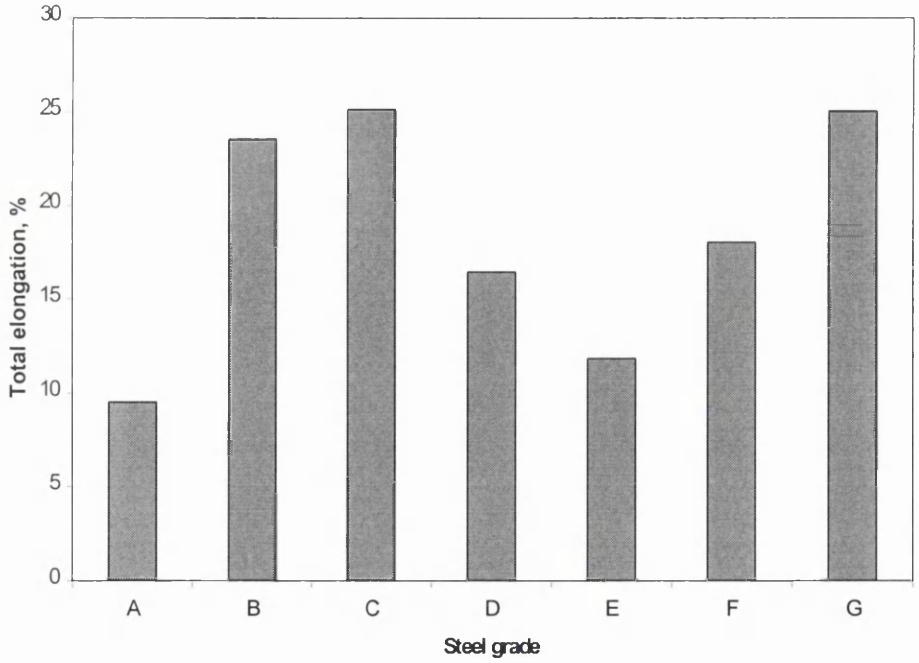

Figure 6.6: Total elongation values for the steels processed with the CAPL cycle.

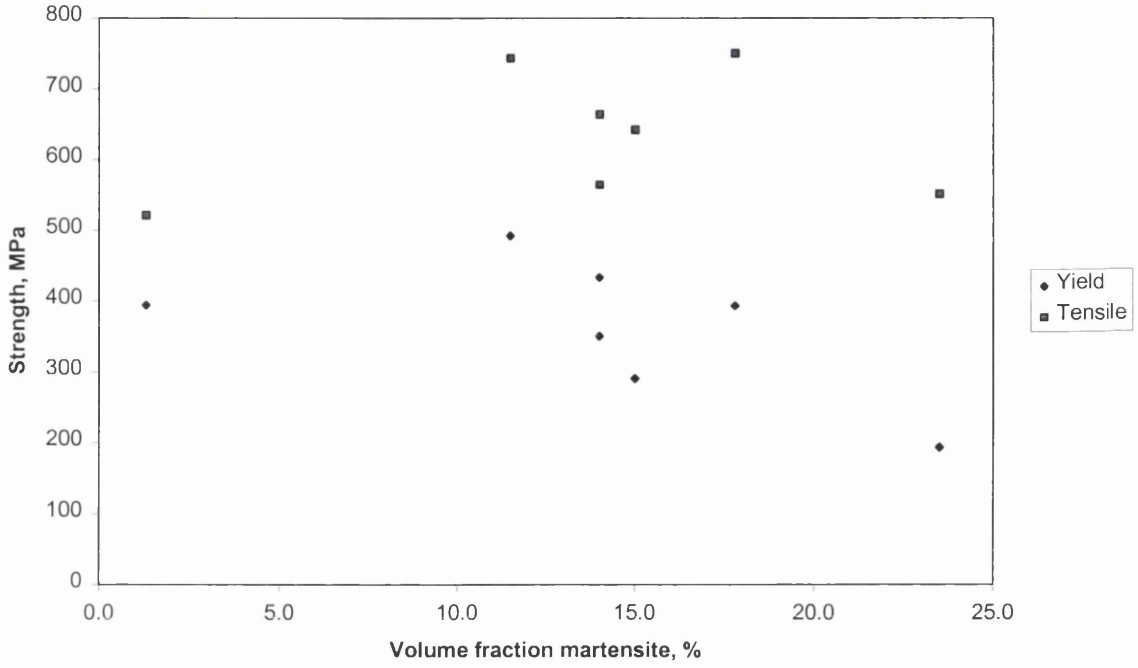

Figure 6.7: Yield and tensile strengths plotted against volume fraction martensite for the CAPL processed steels.

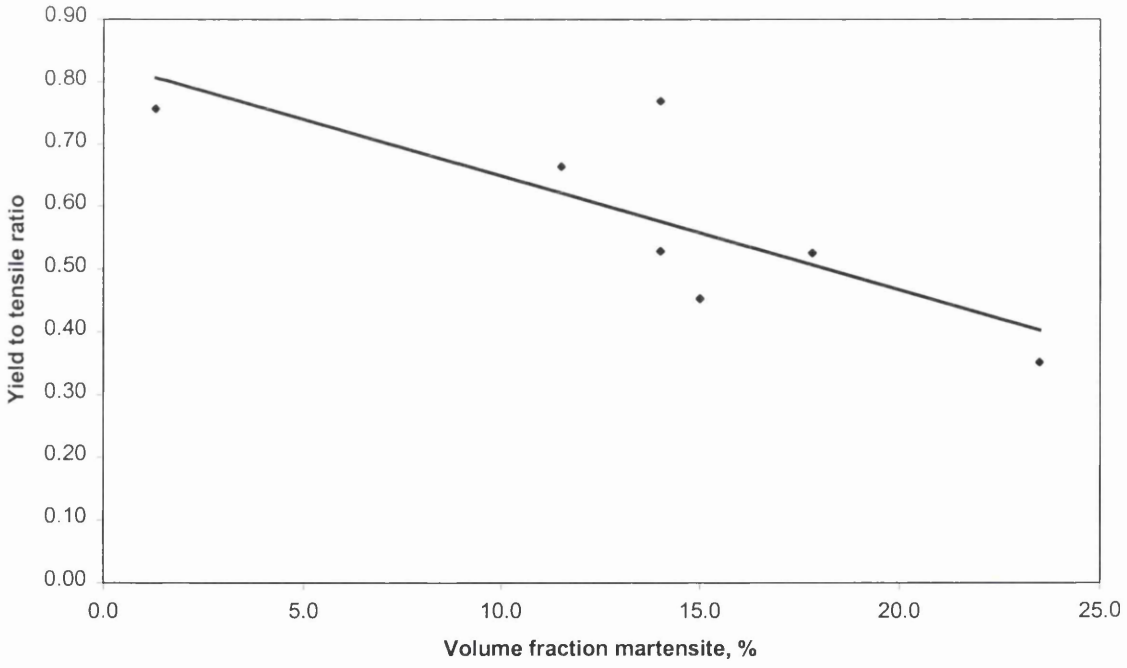

Figure 6.8: Yield to tensile ratio plotted against volume fraction martensite for the CAPL processed steels.

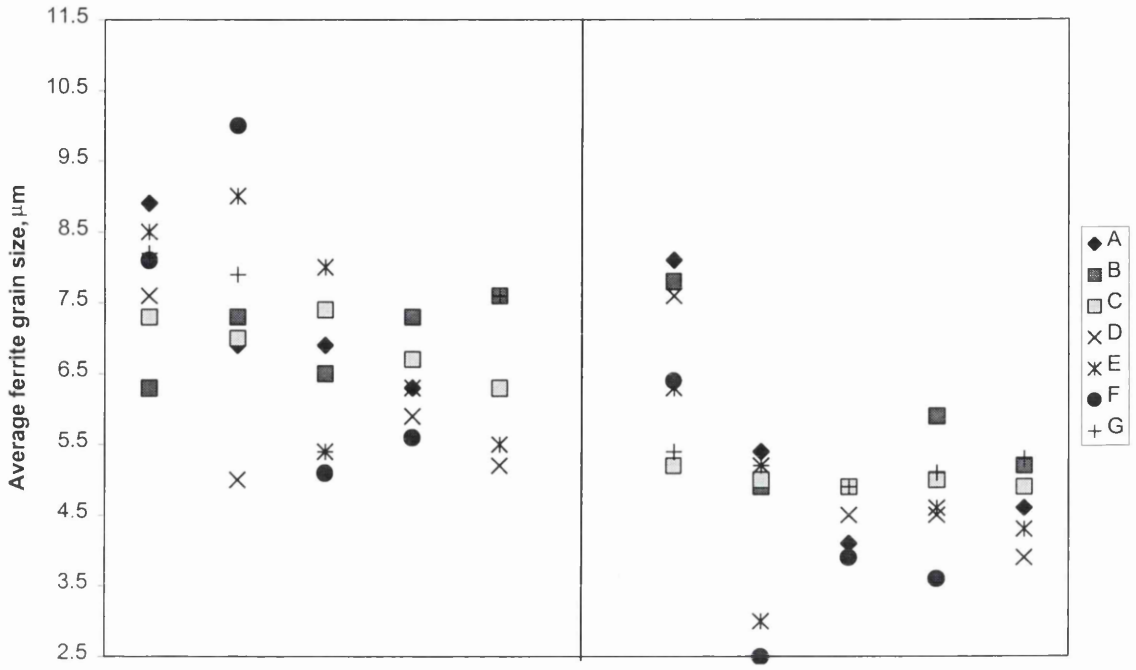

Figure 6.9: Longitudinal (left) and width (right) grain measurements for all steels processed by all cycles.

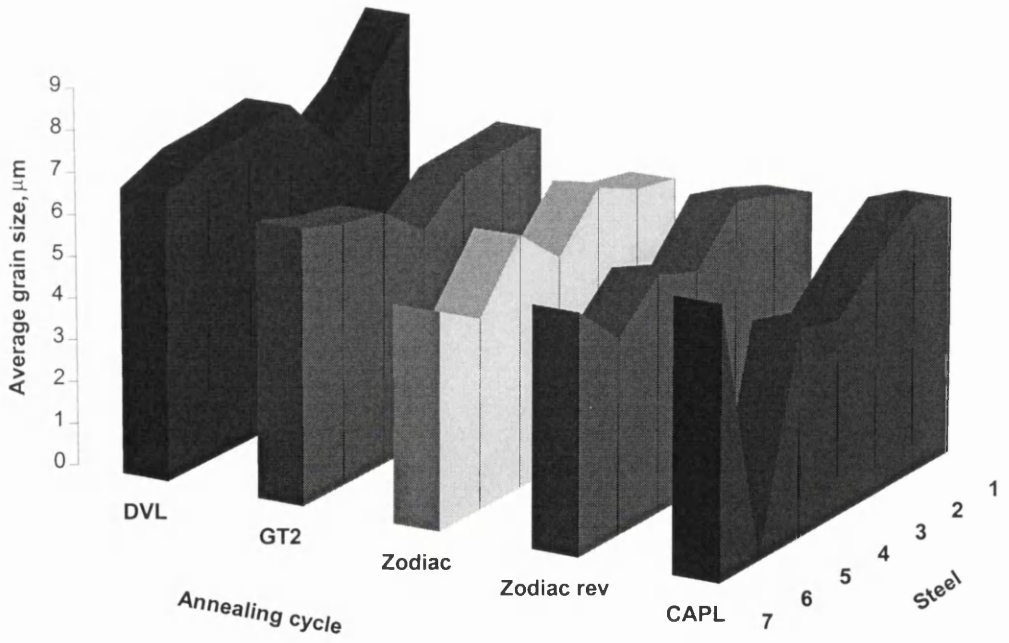

Figure 6.10: The average ferrite grain size for all steels and cycles investigated (Note: Steels 1-7 refer to steels A-G).

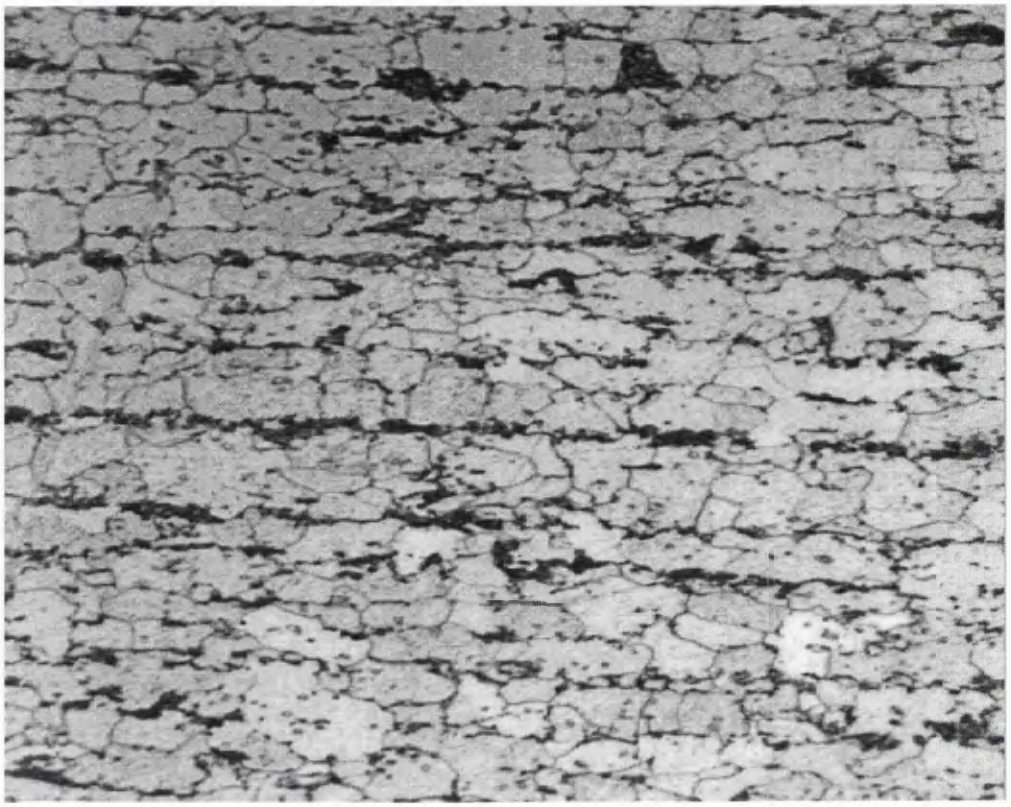

Figure 6.11: A micrograph of steel B processed by the DVL line, which exhibited no martensite (x1000).

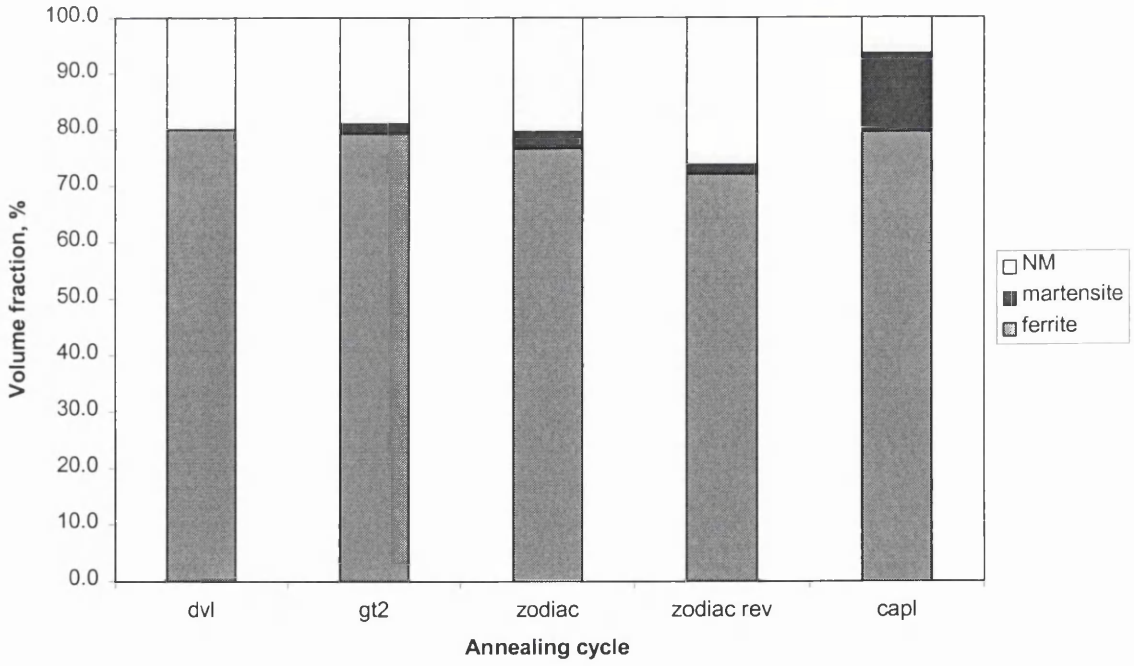

Figure 6.12: A histogram representing volume fraction measurements for steel B for all 5 annealing cycles.

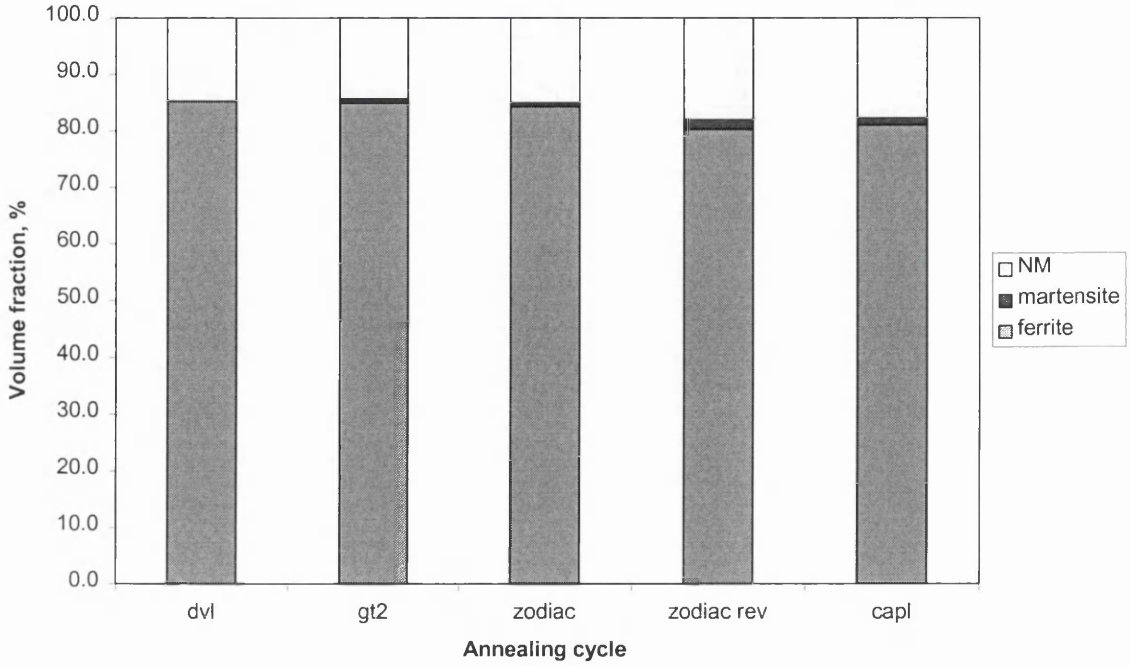

Figure 6.13: A histogram representing volume fraction measurements for steel D for all 5 annealing cycles.

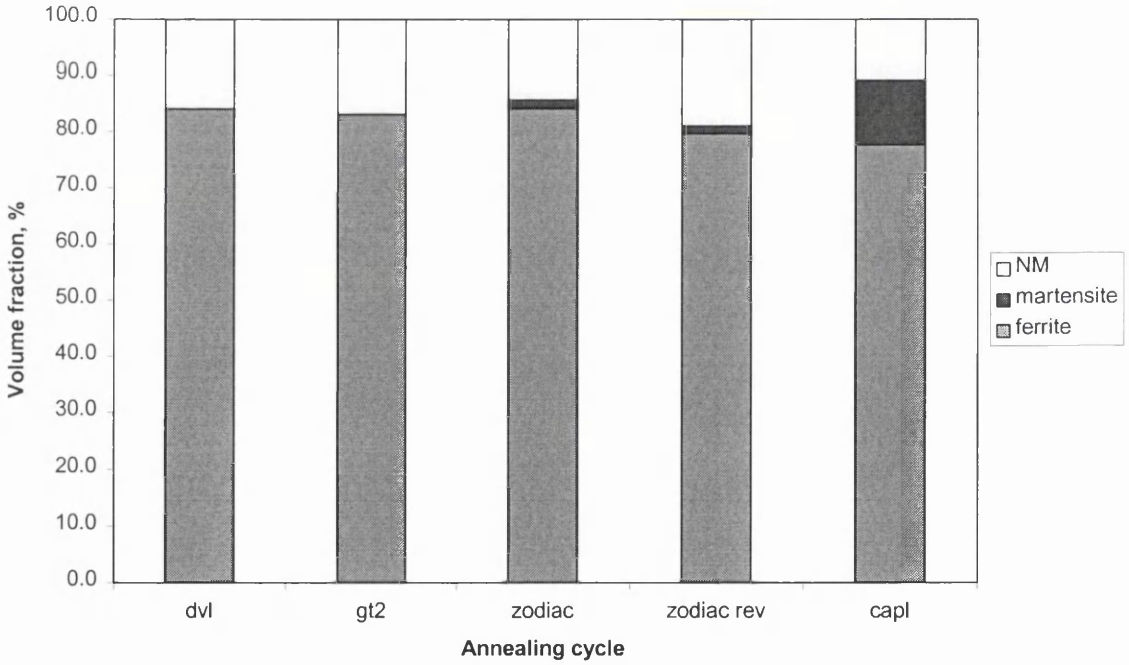

Figure 6.14: A histogram representing volume fraction measurements for steel E for all 5 annealing cycles.

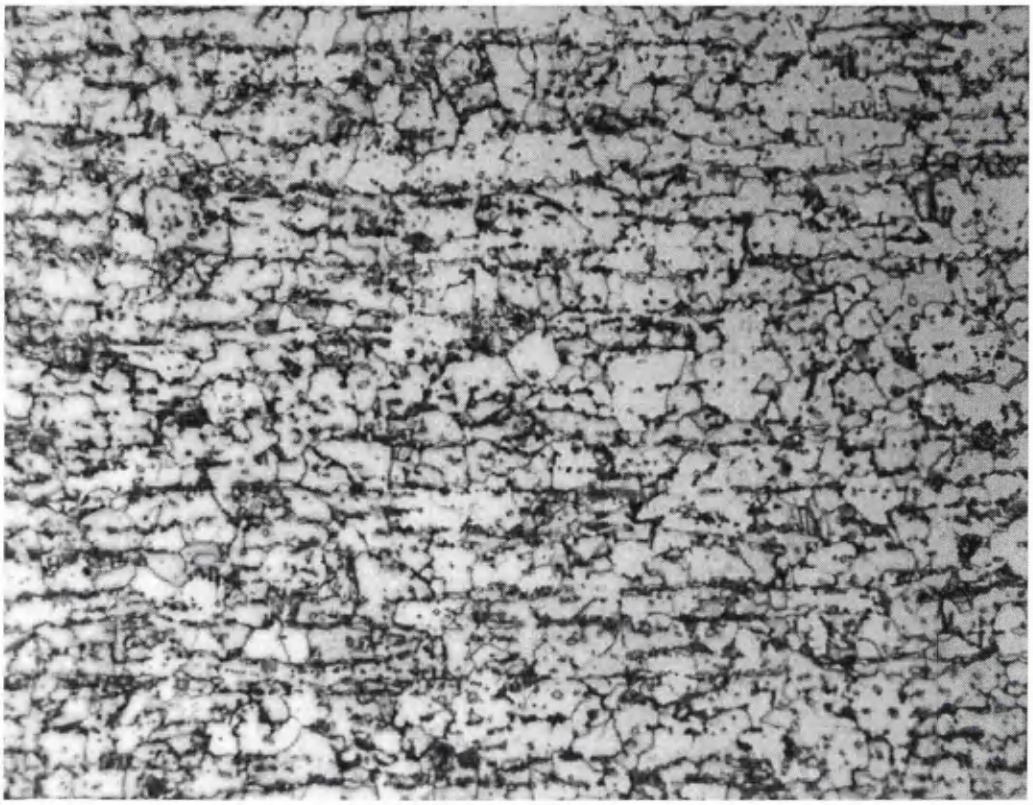

Figure 6.15: A micrograph of steel A processed by the Zodiac line, which exhibited a multi phase microstructure (x1000).

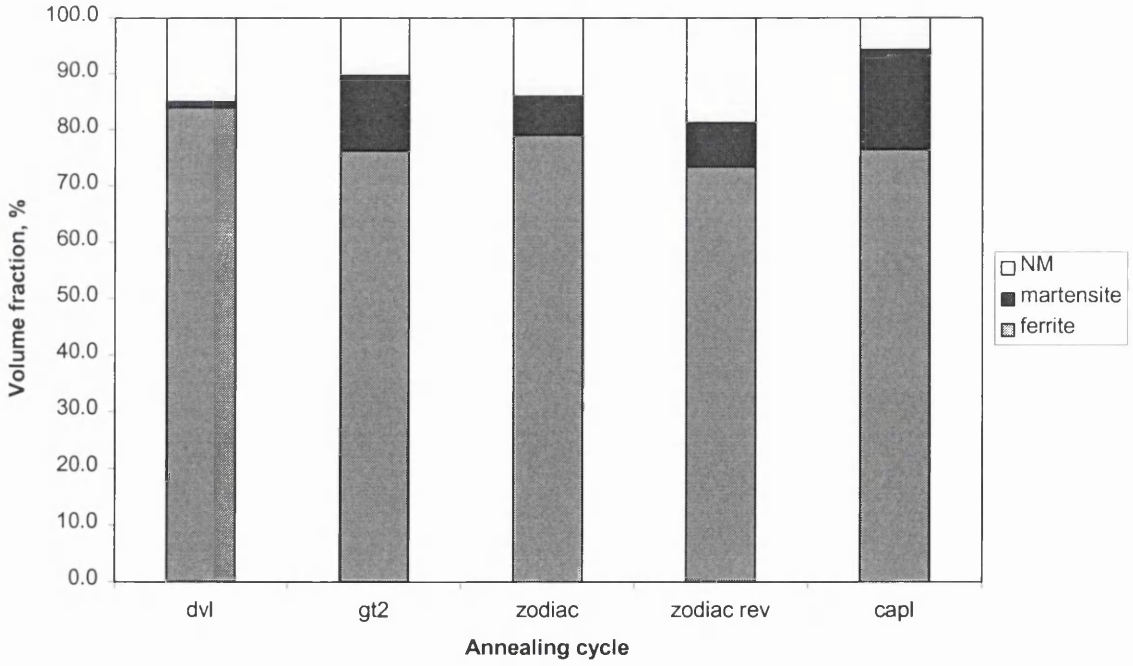

Figure 6.16: A histogram representing volume fraction measurements for steel A for all 5 annealing cycles.

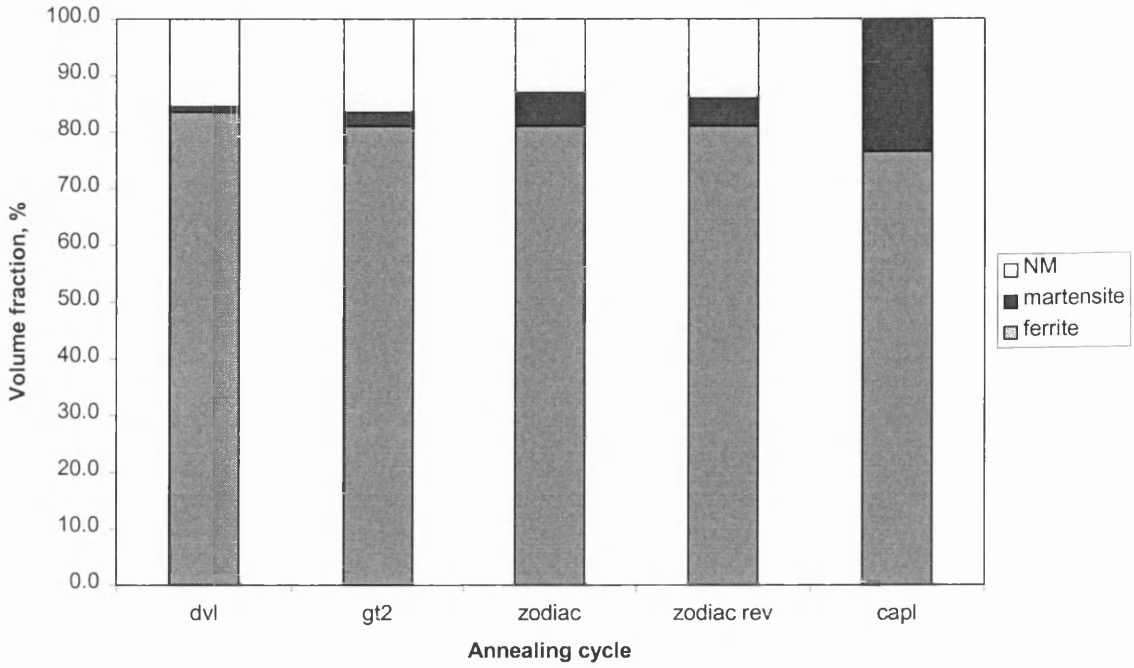

Figure 6.17: A histogram representing volume fraction measurements for steel G for all 5 annealing cycles.

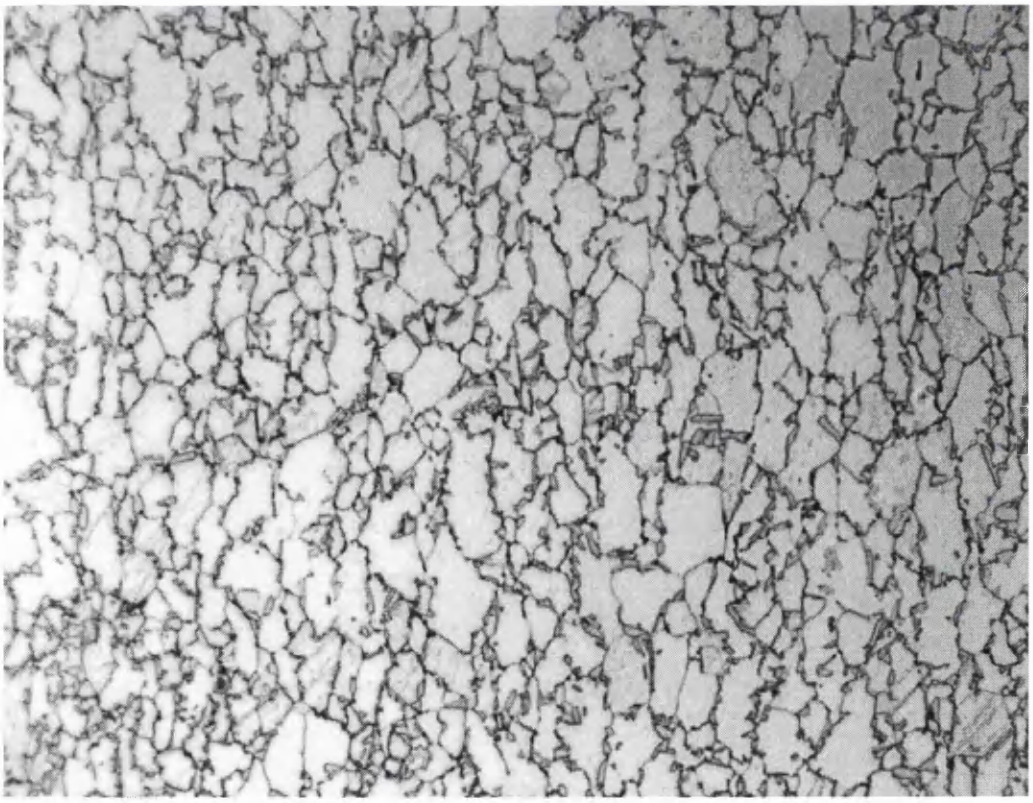

Figure 6.18: A micrograph of steel C processed by the Galtech line, which exhibited a dual phase microstructure (x1000).

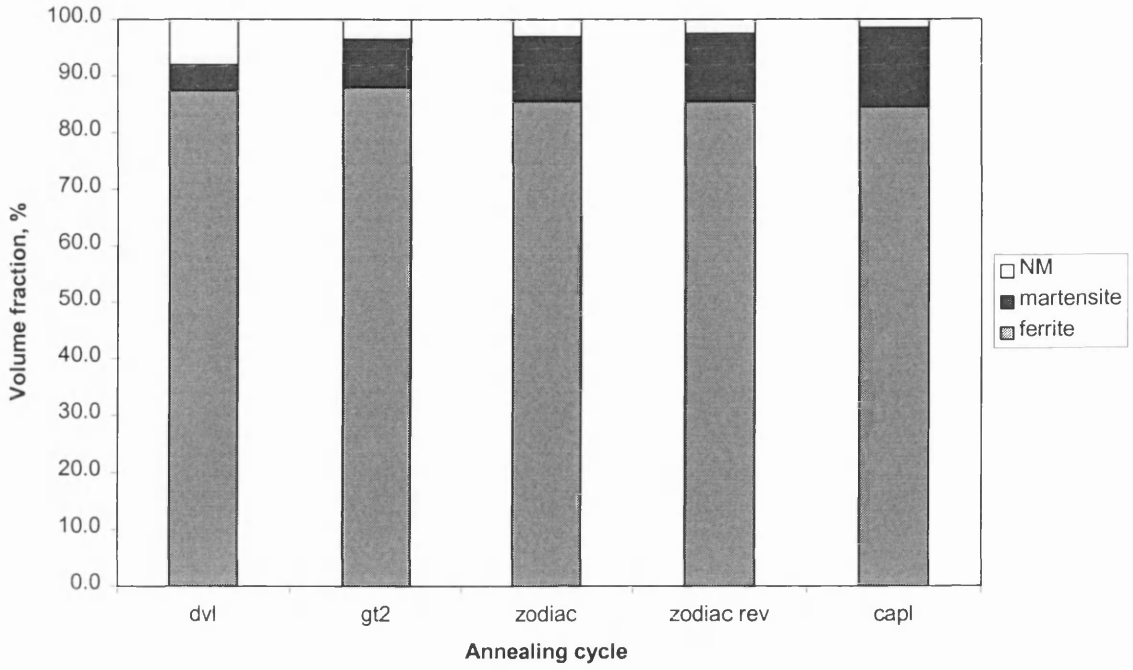

Figure 6.19: A histogram representing volume fraction measurements for steel C for all 5 annealing cycles.

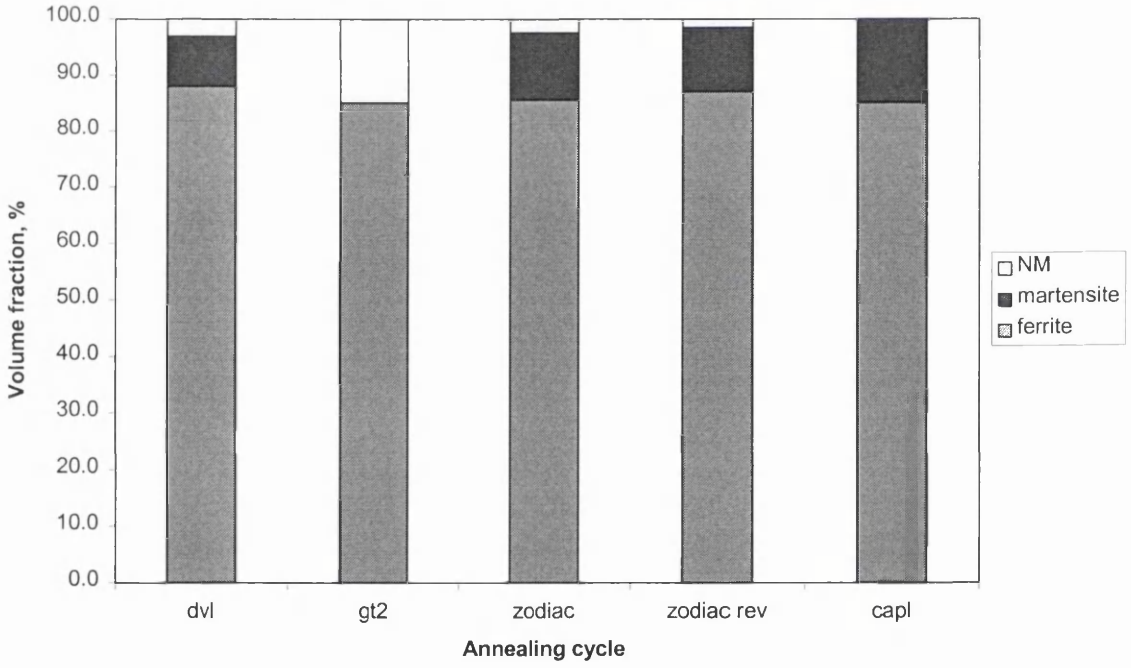

Figure 6.20: A histogram representing volume fraction measurements for steel F for all 5 annealing cycles.

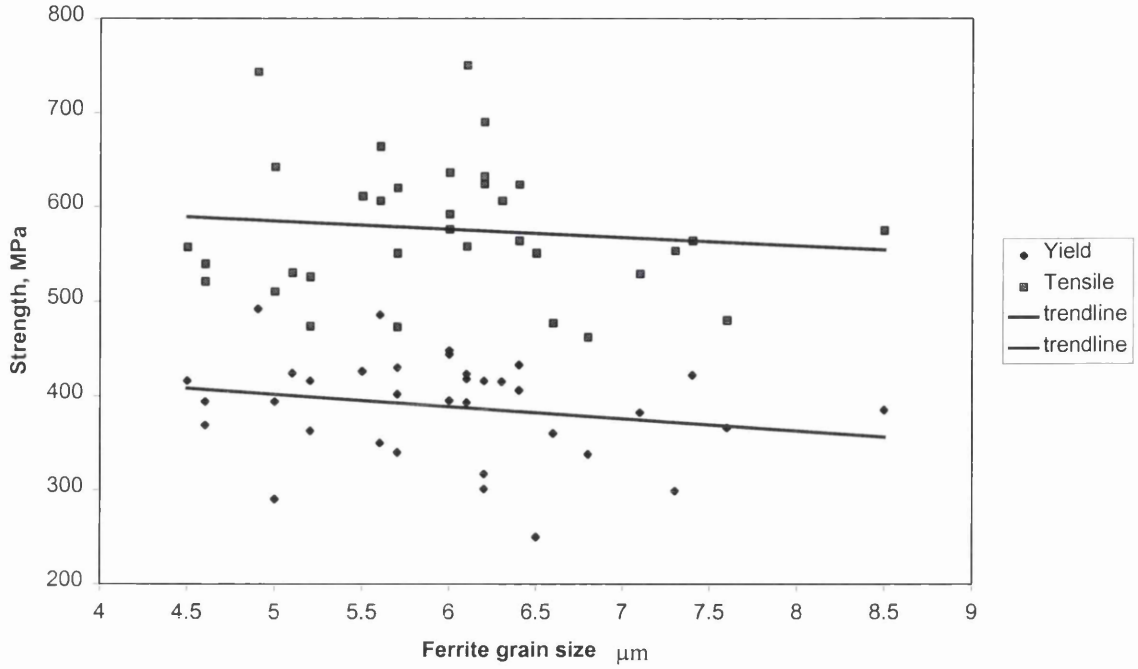

Figure 6.21: Ferrite grain size plotted against strength for all steels processed on all cycles.

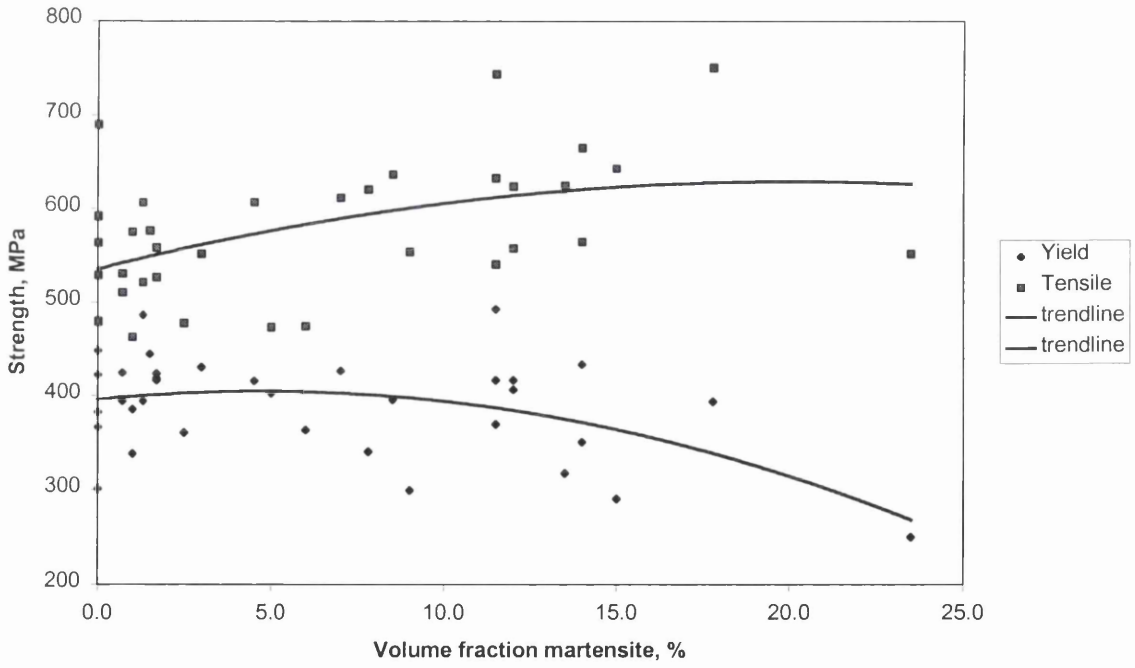

Figure 6.22: Volume fraction martensite plotted against strength for all steels processed on all cycles.

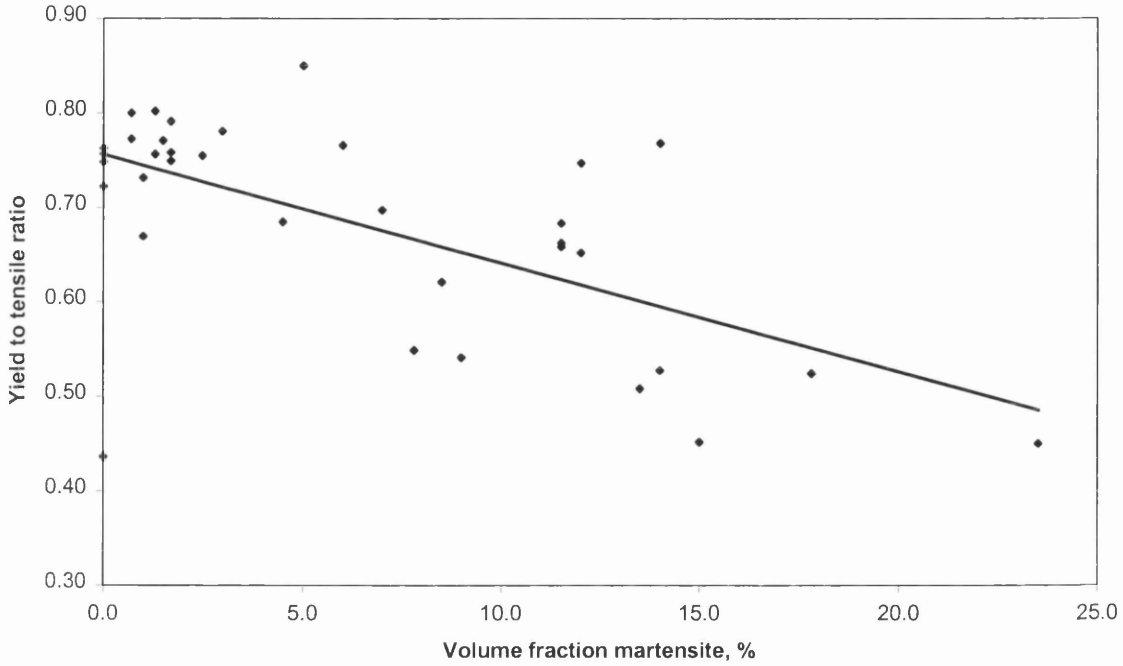

Figure 6.23: Volume fraction martensite plotted against yield to tensile ratio for all steels processed on all cycles.

7.0 INVESTIGATION 3 – THE PRODUCTION OF GALVANISED HIGH STRENGTH STEEL

This section of work focussed on the galvanising process for the high strength steels. Several key process variables were considered, beginning by galvanising all steels using standard processing conditions. The work carried out on the standard conditions made up the majority of investigation 3. Irrespective of coating quality, the steels were then coated with slight variations in galvanising practice to determine whether an improvement could be made. Process parameters that were changed included dew point, annealing cycle, effective aluminium in the zinc bath, strip entry temperature and steel chemistry.

7.1 STANDARD CONDITIONS

All steels were subjected to a galvanising schedule that was explained in the experimental programme. The standard hot dip simulator (HDS) cycle was used (800 °C annealing temperature, 60 s hold time and 30 °C/s cooling rate) as well as standard spelter conditions, i.e., held at 455 °C with effective aluminium of 0.18 %. The main purpose of this part of the study was to evaluate the success in coating these highly alloyed steels. Coating quality was assessed by visual inspection as well as microscopic evaluation. Any defects were subsequently analysed in an attempt to determine the cause.

7.1.1 Wettability & General Visual Evaluation

The first stage and the most difficult to represent scientifically was an attempt to grade the coating quality by means of visual inspection of the panels. A table showing a grading system is represented in table 7.1, poor coating quality was marked as 1 and good coating quality was marked as 5. In view of the fact that the coating quality was determined visually, it would be reasonable to state that repeatability of this technique to be low. However, this approach to analysing the coating was very

good when panels with a great deal of bare spots were seen. Steel C exhibited a degree of de-wetting that was so severe it appeared that the zinc had not adhered at all to the substrate. All other steels displayed average to good coating quality, with those identified as average having generally small bare spots positioned randomly across the panels. Most of the bare spots were large enough to see without the need to examine the panels in great detail. Indeed, figures 7.1 and 7.2, which represent digital images of two panels, shows the variation in coating quality observed. The image taken for steel C shows the total de-wetting with globules of zinc present, whereas the photograph of steel D showed a vastly improved coating quality, apart from the small bare spots.

7.1.2 Coating Weight Evaluation

All samples were subject to coating weight measurement in order to ensure that coating thickness was at the correct levels. This measurement was important because a thicker coating would mask defects more than the thinner coatings. The coating weight measurement was also an opportunity to establish whether the coating was uniform across the panel. The variation in coating thickness is shown in table 7.2 for the steels processed with the standard conditions. Figure 7.3 best describes the variation in coating thickness; values shown are a true reflection of typical zinc coating thickness. The diagram clearly shows that, although there appears to be a great deal of variation, all but one of the samples is 8 μm ± 2. This is the coating tolerance usually associated with laboratory-galvanised samples, even though commercial material would have more stringent constraints. It is also worth noting that the sample closest to the desired coating thickness was selected for further analysis if there were several panels processed under the same conditions. The coating thickness of steel C can effectively be ignored because of the de-wetting evident from figure 7.1. It can be assumed that the coating thickness variation was due to galvanising practice and not due to any other variables, i.e., regardless of steel chemistry, dew point, annealing cycle etc., the same coating pattern was observed.

7.1.3 Coating Chemistry

Examination of all the coated samples revealed a pure zinc coating, consistent with typical galvanised coatings. These results were obtained from the X-ray diffraction studies and were not tabulated because they did not reveal results that were unexpected. Specifically, η zinc (pure zinc) was detected, which means the effective aluminium in the zinc spelter formed the inhibition layer preventing iron-zinc alloying occurring. As discussed in the literature review, the pure zinc coating is desirable because it offers better forming properties than galvannealed (iron-zinc alloy) coatings. Cross-sectional micrographs of the zinc coating confirmed that no iron-zinc alloys were observed, but the inhibition layer was not examined in detail because it fell outside the scope of this investigation.

7.1.4 Defect Analysis

The examination and analysis of the defects in the coated steel from standard conditions formed a large part of this area of investigation. Scanning electron microscopy (SEM) was used for both capturing images of defects as well as analysing the chemical make-up. One of the main reasons for the significant SEM work was to distinguish between coating defects attributed to the steel and processing conditions and those attributed to the HDS practices.

Effects of previous processing must also be take into account, because the surface quality of strip produced by means of the laboratory method very rarely matches the quality of commercial material. For that reason, the incoming surface quality must be considered, especially with steels A, C, D and E.

7.1.4.1 Control Panel

A control panel was analysed first because of the known wetting issues associated with the laboratory produced zinc coated steels, i.e., the interstitial free (IF) steel panels galvanised before each sequence of work was also analysed to assist in

determining defects associated with steel chemistry and HDS factors. Because the IF steel used was known to galvanise without coating problems, any defects could usually be attributed to the HDS practices. Table 7.3 shows the chemical analysis of a pinprick type defect at three random points within the defect, which is shown in figure 7.4. The defect, which was roughly elliptical in shape, measured approximately 10 μm at its longest diameter and 4 μm at its shortest. Both oxygen and iron were detected in large amounts within the defect, which would usually suggest that iron oxide on the surface of the steel would be the most likely cause of this particular de-wetted area. However, the detection of calcium (especially at point 3) in significant amounts, as well as silicon and magnesium to a lesser extent, demonstrates that the root cause of the bare spot was probably not iron oxide. A point analysis was subsequently carried out on the coated area about 5 μm away from the bare spot, which revealed as expected zinc and oxygen with traces of iron and aluminium. Given that no calcium, magnesium or silicon was detected on the coated section, it seems to confirm that the defect cause was either on the substrate prior to dipping or was in the zinc bath.

7.1.4.2 Steel A

Defects observed with galvanised panels of steel A were generally bare spots (figure 7.5) that ranged in diameter from around 5 μm to 50 μm. Analysis of the substrate, which could be seen through the bare spot in the coating, revealed that, as well as iron and zinc, silicon and oxygen were also detected. It can be assumed that silicon oxide and possibly iron oxide was the cause of the bare spots in this case. A number of defects were analysed all of which revealed similar results.

The coating quality, which was of average quality was fairly surprising considering that it was subjected to laboratory hot and cold rolling conditions and was one of the most alloyed steels. There were sufficient levels of both silicon and manganese present that could have presented significant problems in forming a good coating. However, it should be noted that there were a number of coating defects, which would lead to possible coating problems if it was processed on an industrial scale. Analysis revealed that the cause of the defects was silicon oxide in most cases, which supports

work carried out by Bordignon *et al.* 2001. The study found that a steel with similar chemistry had de-wetted areas on the surface, due to the silicon oxide forming a continuous and homogenous film that prevents the zinc from adhering. The explanation why silicon is more problematic than manganese (which also forms oxides on the surface) is that the manganese oxide has a greater tendency to form nodules that can be hidden by the layer of zinc, which gives the appearance of good coating.

7.1.4.3 Steel B

Given that steel B contained the least amount of alloying additions that are known to cause coating defects, it may seem logical that it should yield the best coating quality. In fact, the general coating evaluation was good, but was not the best of all the steels used. Indeed, two types of defects (several more defects were present) were analysed from the galvanised steel B panel, which were identified as an inclusion and a bare spot. The chemical analysis is shown in table 7.4. The inclusion type defect (figure 7.6), which was of a rectangular nature, measured about 25 μm by 15 μm. It appeared to be a defect within the coating rather than a substrate defect, which seemed to be confirmed by the analysis that revealed zinc as the main component with relatively low iron and oxygen levels.

Conversely, the bare spot defect (figure 7.7) could be split into two definite areas, namely a bare spot that was adjacent to a particle in the coating. The bare spot was an uncoated area that meant the substrate was visible, even though the image was taken looking down on the surface of the coated panel. This area when analysed revealed a very high iron percentage, which is not surprising given that it is in fact an analysis of the substrate. However, the particle was analysed at three separate points, revealing that significant levels of silicon were recorded each time (table 7.4). A varying volume of iron, zinc and oxygen was also observed, but it was the silicon levels that were not as expected. It can therefore be assumed that it was the silicon in the form of silicon oxide that caused this defect. Again it appears as though the particle could well have been in the zinc bath and not of substrate origin, because of its position within the coating. Examination of the steel chemistry shows that silicon in the steel

is very low, which means it would be very unlikely that it was silicon in the substrate that had caused the defect.

7.1.4.4 Steel C

The extremely poor coating produced with steel C was discussed in the section describing the visual condition of the panels. It was apparent that the zinc did not adhere to the surface. Therefore, during SEM analysis, a random spot on the panel was analysed as well as a large globule on the surface. Table 7.5 lists the chemical analysis of the two areas analysed. The large globule (figure 7.8) measured about 800 μm by 500 μm and, as expected, it was almost entirely made up of zinc with small amounts of aluminium, iron and oxygen also present.

Analysis was also carried out on an area containing smaller globules but larger in number, as shown in figure 7.9. The first point of analysis hit a zinc drop, which was high in zinc with small amounts of iron, aluminium and oxygen. However, points 2 and 3 were taken from areas free of zinc, i.e., the steel substrate. Both points exhibited significant levels of manganese and silicon, as well as those elements expected (iron, zinc, aluminium and oxygen). At point 3, manganese was detected at almost twice the total weight fraction in the steel, which shows that a manganese rich spot in the steel was identified.

Results have shown that attempting to galvanise C-Mn steel containing 1.3 weight % silicon under standard conditions is hugely problematic. The cause of the extensive de-wetting relates to the silicon that subsequently forms silicon oxide. It is therefore impossible for the zinc to adhere to the surface. A study carried out by Maki *et al.* (2001) also reported that severe de-wetting was a feature of C-Mn-Si steel. Glow Discharge Optical Emission Spectroscopy (GDOES) was used to determine the integral intensity and found that, in some cases, there was more than ten fold increase peak for silicon.

7.1.4.5 Steel D

The defects highlighted with steel D were consistent across the whole panel and were a series of bare spots of various shapes and sizes. Analysis of the defects (table 7.6) revealed that the substrate had been exposed on each occasion because of the high iron levels recorded in each case. An SEM image of the defect is shown in figure 7.10. Both oxygen and zinc were detected, as expected, with manganese also picked up at levels around 1.5 %. Given that the manganese levels in steel D are only slightly higher than some of the other steel used, it would be difficult to apportion the cause of the defect to manganese. However, a comparison between steels B and D may help to explain that this amount of manganese is significant, the difference being an increase in manganese from 1.28 (steel B) to 1.50 (steel D) weight %. All other alloying additions are of comparable levels, but steel D had more bare spots. In view of the fact that this type of defect appeared to be caused by the steel and not by processing conditions, it appears that manganese is the likely cause. If it were the case, then the likely mechanism would be that manganese oxides form as nodules at manganese rich areas of the steel surface during annealing that subsequently cannot be reduced (Bordignon *et al.* 2001). These oxides consequently prevent the zinc adhering.

A feature seen within the aforementioned defect was what appeared to be a galvanneal type structure, which was analysed in greater detail and shown in figure 7.11. The subsequent analysis revealed that iron and zinc were detected at a ratio of nine to one (zinc to iron). If it were a galvanneal structure, then it would appear to be of a delta type structure from the chemical analysis, because of the ratio of iron and zinc. However, from studying the image (figure 7.11), the structure appears to be more like a zeta type alloy. In view of the fact that analysis was conducted looking down on the sample, it is possible that the iron content from the substrate and gamma layer would be picked up to a certain degree. This would explain why the analysis and appearance did not agree with higher volumes of iron being detected.

Given that effective aluminium levels in the zinc bath were set at 0.18 weight % for standard galvanising conditions, a galvanneal reaction taking place would be very

unlikely. An effective aluminium closer to 0.10 weight % would be required to produce a thinner inhibition layer, which would increase the chances of iron – zinc alloys being formed. Even then, a heat treatment would also be required. These factors confirm the unlikelihood of producing galvanneal, as this feature was only observed in a small isolated area and can therefore be overlooked.

7.1.4.6 Steel E

The relatively good coating for steel E meant there were very few defects available for analysis. Indeed, the noteworthy feature was a small degree of alloying occurring on the surface of the coating, which is shown in figure 7.12. The full analysis is presented in table 7.7. Further analysis revealed that up to 4 weight % iron was detected, which could be acknowledged as zeta ($FeZn_{13}$). When considering the processing conditions, there should be no galvanneal reaction taking place. It was similar to the feature seen with steel D, which cannot be attributed to the galvanising process.

7.1.4.7 Steel F

Two types of defects were seen on the galvanised surface of steel F, with neither defect revealing the typical properties associated with bare spots. Chemical analyses of both defect types are shown in table 7.8 and are also shown in figures 7.13 and 7.14.

The first defect was in the form of a cube type crystal that appeared to be in the coating, with the top protruding through the surface. This defect was high in aluminium and iron with some zinc also detected. The ratio in % weight was about one to one, which equates to 2.5:1 (aluminium to iron) atomically. Top dross, which was discussed in the literature review, forms as crystals that are usually cubic in shape and are composed of Fe_2Al_5. It is therefore clear that top dross was picked up from the zinc bath, causing this particular defect. It is also apparent that the zinc detected was either part of the coating or was attached to the top dross particles. Given that a

relatively high effective aluminium (0.18 weight %) was used, top dross was produced in the spelter so, if the bath surface is not skimmed correctly, it will be picked up as the steel is dipped, i.e., in this case the defect was a result of the process and not the steel.

The second defect was very similar to that described with steel E, i.e., a zeta ($FeZn_{13}$) type area on the surface of the galvanised steel. The analysis seemed to confirm this with about 6 weight % iron detected but, as with steel E, it was not found across the whole panel. Clearly, little emphasis should be placed on this zeta type area, because it is was only observed on a few isolated spots.

7.1.4.8 Steel G

Galvanised panels of steel G were of very good coating quality. In fact, SEM analysis did not detect any defects on the panels, only eta (pure zinc) was detected when analysed. Given that chromium levels in this steel were the highest (0.45 weight %) of all current materials, the results are satisfactory. Chromium is known to form oxides on the surface, which gives the same coating issues regarding de-wetting described for silicon and manganese. The relatively high chromium levels coupled with 1.51 weight % manganese mean that the excellent coating was not expected.

7.1.5 Distinguishing Between Substrate and Process Defects

It may seem that very few of the steels produced good coating quality, but the majority of the defects illustrated were due to the process and not the steel. This section aims to distinguish between defects attributed to the steel substrate and processing conditions. By making this distinction, only three of the steels displayed significant defects that were due to the substrate, which were A, C and D.

7.1.5.1 Substrate Induced Defects

With steels A, C and D the coating problems were caused by silicon and manganese, with the degree of de-wetting directly related to the levels of these additions. Unsurprisingly, it was steel C with the greatest volume of the combined additions that encountered the most severe type of de-wetting. This was followed by steel A, which had the second highest volumes of silicon and manganese. Steel D had de-wetted areas due to manganese oxide which, when compared to the steels that coated well, had about the same levels of manganese. The reasons for the problems associated with steel D, which were not seen with some of the others, cannot be explained.

With reference to the steels that did not have substrate induced defects, steel G stands out because of its high chromium levels. The other steels (B, E and F) did not posses high levels of additions that are known to cause coating problems. Therefore, the investigation has shown that C-Mn steel with 0.45 weight % chromium can be galvanised successfully with standard processing conditions.

7.1.5.2 Process Induced Defects

Two types of defect were attributed to the galvanising process. At first glance, it would appear that the coating irregularity could be due to the substrate. However, further analysis revealed that the majority of de-wetted areas were caused by the processing conditions. The two types of defect attributed to the process were the isolated small alloying areas and impurities in the molten zinc that were subsequently found in the coating. The alloying defect was found on the three steels (D, E and F) and in each case, small isolated alloyed areas were detected. No obvious link can be made between the three steels, which therefore signifies that reasons for the alloying effect cannot be given.

The second defect related to contamination in the zinc bath and was found in the control panel as well as steels B and F. Top dross was the reason for the defect in steel F, which does not cause a great deal concern because it is easily rectified by better bath management. However, the calcium-rich defect found in the control panel

and the silicon-rich defect found in steel B was of greater concern. These defects were also seen on some of the panels processed in the next part of the investigation.

The silicon-rich defect could be attributed to either the refractory tile used to cover the spelter when not in use or the quartz tube powder because both contain silicon. Table 7.9 shows these results. The refractory material was a silicon oxide based material whereas the powder for the quartz tube was a silicon-zirconium oxide type material. In view of the fact that zirconium was not detected, the likeliest source of the contamination was the refractory tile.

The calcium-rich defect could not be attributed to the process or to the steels used during the investigation. Calcium oxides produced during industrial steel making and casting can be discounted, because a mixture of laboratory and industrially produced steels were used, i.e., the laboratory-produced steels were not subjected to exactly the same production practice, yet they also displayed the same defect. The likeliest cause of the calcium-rich defects was bath contamination, i.e., debris present in the zinc spelter. Several possible sources for contamination were analysed, which included the refractory material used to cover the spelter when not in use, the powder used to coat the quartz tube and general cement. The results of the analysis are shown in table 7.9 and discount both the refractory material and the powder for the quartz tube. However, cement could explain the calcium detected in the coating on several occasions. In view of the fact that on going building work had been carried out in the vicinity of the laboratory in which the HDS was based, it seems that contamination from cement was probably responsible for the calcium-rich defect.

The discovery that a number of defects could be attributed to contamination should not detract from the fact that there were still a high number of recognisable defects. This investigation has proved that the reliability of the results achieved is not 100 % dependable, with contamination of the zinc spelter giving results that appear to be poorer than the actual situation.

7.2 ANNEALING CYCLE EFFECT

The evidence in the literature described that annealing time and temperature would have an impact on coating quality. However, the range of values needed for this occurrence was greater than those used in the course of this study, i.e., greater temperature ranges than the 800-830 °C used and more of a time range than 40 seconds to 2 minutes. For example, Zhang *et al.* (1995) stated that a temperature greater than 920 °C would be required to prevent manganese oxide forming on the steel surface. This temperature is well over the maximum temperature used in the industrial type annealing cycles.

Considering that the type of annealing cycle used was therefore not expected to have a significant effect on coating quality, only steel B was used for this part of the investigation. Indeed, the results showed that the use of various annealing cycles prior to dipping had no effect on final coating quality. The graph plotted in figure 7.15 helps to prove this point, because it shows that there was no correlation in the results achieved from the different annealing cycles. However, the exercise was carried out for two reasons. The first, which was unlikely, was to determine whether annealing time and temperature would have an influence on coating quality. More significantly, the second was to prove that the type of cycle did not influence final galvanising characteristics, which was the case in this instance.

7.3 EFFECTIVE ALUMINIUM VARIATIONS

A range of effective aluminium values in the zinc spelter did not appear to have any influence on the wettability of the coated steel. Effective aluminium ranged from 0.13 %, which coincided with the minimum galvanising bath levels, to higher more typical levels of 0.18 %. The main consequence that effective aluminium has on bath conditions is to influence the type of dross produced. However, given that its effect on coating quality has not been extensively researched, this aspect of the work attempted to see whether it did affect the coating.

The increase in effective aluminium, which should coincide with a greater volume of top dross, did not appear to increase the top dross picked up within the coating. This statement was made after visual inspection of the panels. Further in depth analysis with the SEM also failed to detect any difference. In fact, there were only a few panels that had dross present within the coating, which makes finding a trend difficult. To be precise, given that there was very little top dross observed regardless of effective aluminium, the error in the calculation could be greater than the variation observed.

Top dross (as well as bottom dross) is an issue that is usually of concern with industrial galvanising. Therefore, in view of these results and the fact that they were obtained from a laboratory study, it would seem very difficult to relate the results to industrial practice.

7.4 STRIP ENTRY TEMPERATURE EFFECT

The effect of strip entry temperature was studied extensively by Le Jeune (2000), which described the change in galvanising kinetics at higher temperatures. Even though strip entry temperatures were not as high as those studied by Le Jeune (2000), the literature raised several issues that could influence the final coating make up.

7.4.1 Wettability & General Visual Evaluation

Generally, there was a slight improvement in coating quality when utilising the higher the strip entry temperature. All steels apart from steel C had either a slight improvement in coating coverage or remained the same across the board. However, steel C displayed a noticeable change in coating quality when the strip entry temperature was raised from 460 °C up to and including 550 °C. Even though a significant improvement was observed, the panels continued to show large uncoated areas that would be unacceptable if produced industrially. Nevertheless, the key factor to note was that a higher than standard strip entry temperature generally had a beneficial result on the final product.

7.4.2 Coating Chemistry

Samples galvanised with a higher strip entry temperature were analysed for iron-zinc alloys, i.e., work carried out in previous studies of zinc quenching (Le Jeune 2000) found that one of the adverse effects was that alloying of iron and zinc was difficult to control. Therefore, even though the strip entry temperatures used in this study were not as high as the aforementioned study, analysis was carried out to be sure that no alloying had taken place. Indeed, the XRD analysis found no iron-zinc alloys in the coating, i.e., only eta zinc (pure zinc) was detected.

7.4.3 Defect Analysis

Many of the defects observed with standard conditions were also seen with the steels dipped with higher strip entry temperatures. In order to avoid describing the same defects, only a summary of the defects is given in this section. Also, the comprehensive analysis carried out for the standard conditions was found to be the same for this batch of tests, i.e., the steels that had substrate-induced defect continued to display the same defects. Silicon oxide was detected for steel C, manganese oxide was detected for steel D and so on. As well as displaying the steel substrate induced defects, the same defects caused by process variables was also seen. The initial defect analysis revealed that steels A and B did not have any significant or unusual features that warranted investigation. Steel C displayed the same top dross type defect described in section 7.1, that is, a defect high in both aluminium and iron. The calcium-rich defect that was most likely caused by bath contamination was observed again with steels D and E, with no defects observed with steels F and G.

7.5 DEW POINT EFFECT

With the investigations by Hertveldt *et al.* (1998) and Lamberigts (1999) describing the significance of changing the dew point, it looked as though the results from this study are also influenced by the changing dew point.

7.5.1 Wettability & General Visual Evaluation

In most cases, the effects of changing the dew point were not significant, apart from the tests involving steel C. Digital images taken of the coated steels revealed that the coating produced with steel D (figure 7.16) was very similar to that of the standard sample, whereas the difference achieved in coating quality for steel C (figure 7.17) was remarkable. When the image of steel C was compared to that of standard conditions, shown in figure 7.1, it is immediately apparent that the dew point had a major impact on the galvanising process.

7.5.2 Defect Analysis

The galvanised coating displayed defects similar to those seen with other conditions, i.e., dross, debris and so on. However, there were defects associated with a change in dew point that were different to those described previously. Generally, defects that were richer in certain elements were observed from the material that utilised a higher dew point in the annealing furnace. Some of the results in this section were placed along side the chemical analysis from the standard conditions in order to make a clearer comparison. Table 7.10 shows the chemical analysis of a selection of steels C and F processed via the standard conditions and with a higher dew point in the annealing furnace. Although there are a number of factors that could influence the chemical analysis taken, the results seem to suggest that the dew point does influence substrate make up. Steel C shows that both silicon and aluminium levels increased significantly while manganese decreased, while the trend with steel F showed very small increases in both silicon and manganese on the steel surface. However, this mode of analysis is only capable of identifying general observations because of the variability associated with analysing such small areas.

An increase in dew point affects the behaviour of elements such as manganese, silicon and aluminium in steel. Maki *et al.* (2001) found that a lower dew point (i.e. standard annealing conditions) had lower levels of elements such as aluminium, silicon and manganese on the surface of the substrate when compared with higher dew points. They proposed that this was due to surface segregation of these key elements when

dew point was changed. However, the results in table 10 appear to show that there was a definite increase in the levels of these elements when the higher dew point was used. The results of this study seem to contradict the findings of Maki *et al.* (2001). In view of the fact that the coating quality had improved, the detection of lower levels of additions that form oxides would be expected. Therefore, if the results given by Maki *et al.* (2001) were mirrored, silicon and manganese levels would have been less, which was not the case. Given that the technique to measure the chemical analysis was questioned because it was too focussed, caution should be taken with the results.

7.5.3 Substrate Analysis

To avoid the degree of inaccuracy associated with taking substrate analysis perpendicular to the coated steel, a cross-sectional analysis was carried out of the steel composition. The results from the steels processed at higher dew points were compared with those taken from the steels galvanised under standard conditions. Results from steel C were analysed in greater detail, because of the degree of de-wetting that had occurred under standard conditions.

7.5.3.1 Steel C

In view of the fact that the change in dew point seemed to have the greatest influence on steel C galvanised panels, emphasis was placed on the analysis from this particular material. Figures 7.18-7.20 are graphs representing the difference in oxygen, silicon and manganese for steel C when comparing standard furnace conditions with an increase in dew point. Of the three graphs, the variation in oxygen was the most significant. The most noticeable feature was that the steel annealed with the higher dew point had a greater volume of oxygen detected when compared with the standard annealing conditions. This was the case regardless of position in the steel cross section. This result helps to prove that the results from the perpendicular SEM analysis appear to be inaccurate, i.e., higher volumes of oxygen found in the substrate when processed at the higher dew point support the theory set out by Maki *et al.* (2001), Lamberigts (1999) & Mahieu *et al.* (2000).

The theory can be explained by referring back to the equations that showed the likelihood of wetting with respect to the contact angle (equation 1.12 & 1.13). An increase in alloying additions such as manganese, silicon and chromium increases the contact angle (θ), therefore, the greater the contact angle the greater the degree of de-wetting. It was also stated that the change in annealing atmosphere would also influence the wetting behaviour.

The significant improvement in wettability for steel C when annealed at +5 °C can therefore be linked to the influence that dew point has on oxygen levels in the annealing furnace. The higher dew point atmosphere contains lower hydrogen levels, which in turn means higher oxygen levels. It has been proposed that the increase in dew point from –40 °C to +5 °C can reduce the selective oxidation on the surface of the steel by up to 75 % (Lamberigts 1999). It has been argued that even though greater oxygen levels are present, there is a significant amount of internal oxidation occurring that in turn decreases oxides on the steel surface. The less surface oxides formed results in a significant reduction in the contact angle, thus improving the wettability of the zinc on steel. Angeli *et al.* (2002) found that as well as reducing the selective oxidation with the higher dew point, more internal oxidation was detected and oxides on the steel surface were reduced substantially.

The clear distinction observed with regards to oxygen levels for the varying dew points was not found with silicon and manganese (figures 7.19 & 7.20) for steel C. Both silicon and manganese levels appeared to be reasonably consistent for the high and low dew points. Also, the levels of silicon and manganese appeared to show no variation in relation to the weight % measured across the steel. Therefore, it appears that no segregation of manganese and silicon was observed during this study.

7.5.3.2 General Trends

Analysis of the other steels showed similar results to those described for steel C. The results from plotting oxygen detected for all steels with standard conditions and high dew point are shown in figures 7.21 and 7.22. First and foremost, all steels had greater volumes of oxygen detected when the steels were processed with a higher dew

point in the annealing furnace. This trend can be related to the promotion of internal oxidation discussed for steel C.

A further trend was that steel E appeared to have the greatest volume of oxygen from both annealing conditions, which was higher than that detected in steel C. Conversely, steel G had the least amount of oxygen detected for both annealing conditions. Assessment of the steel chemistry showed that levels of the additions known to influence oxidation did not vary significantly, which would subsequently give a reason for the difference in oxygen detected for steels E and G. However, these two steels did have the lowest (steel G) and highest (steel E) levels of carbon. This may well have influenced the levels of oxygen, but reasons for this occurrence cannot be ascertained.

Table 7.1: Coating quality for a selection of panels galvanised using standard conditions. (NB 1 = poor coating quality, 5 = good coating quality).

	Panel number		
	(i)	(ii)	(iii)
A	2	4	3
B	4	3	4
C	1	1	1
D	4	2	3
E	5	5	4
F	5	5	4
G	4	4	4

Table 7.2: Variation in coating thickness (μm) across a random selection of the galvanised panels.

	up left	up centre	up right	mid left	mid centre	mid right	low left	low centre	low right
A	12.2	7.2	7.0	6.7	5.1	5.2	7.9	7.2	9.6
B	10.3	9.7	8.4	11	10.5	9.8	9.7	7.4	8.1
C	n/a	n/a	n/a	n/a	n/a	n/a	n/a	n/a	n/a
D	6.0	5.5	6.6	5.4	5.3	10.6	8.7	8.3	8.6
E	10.1	11.0	11.0	9.6	8.5	9.4	11.7	14.8	10.3
F	9.2	6.4	6.6	6.1	5.0	5.6	5.8	7.3	8.2
G	7.4	7.5	8.4	5.5	5.9	6.5	5.7	6.3	10.2

Table 7.3: SEM analysis of the coating defect produced on the IF steel control panel (point 4 refers to analysis carried out away from the defect).

% Element	Point 1	Point 2	Point 3	Point 4
Oxygen	6.52	0.43	27.1	1.92
Magnesium	1.13		1.12	
Aluminium	0.80	0.11	1.30	0.20
Silicon	0.97	0.11	2.08	
Phosphorous			0.20	
Sulphur	1.40	0.19	1.45	
Calcium	3.39	0.64	18.2	
Manganese		0.37	0.27	
Iron	72.4	92.6	31.7	2.61
Zinc	13.4	5.60	16.6	95.3

Table 7.4: SEM analysis of the coating defects produced on steel B (point 1 relates to the 1st defect, points 2, 3 and 4 refer to the 2nd defect).

	Defect 1	Defect 2		
% Element	Point 1	Point 2	Point 3	Point 4
Oxygen	4.94	18.4	56.2	31.3
Aluminium	0.32	5.46	9.73	6.30
Silicon	0.29	15.3	26.7	16.63
Potassium	0.16	0.38	0.10	0.26
Sulphur		0.14		
Calcium		0.76	0.82	0.96
Manganese	0.24	1.33		0.56
Iron	5.46	37.0	1.26	13.8
Zinc	88.2	21.2	5.17	30.2
Molybdenum	0.36			

Table 7.5: SEM analysis of the coating defects produced on steel C (point 1 relates to the 1st defect, points 2, 3 and 4 refer to the 2nd defect).

	Defect 1	Defect 2		
% Element	Point 1	Point 2	Point 3	Point 4
Oxygen	1.93	0.62	0.98	3.45
Aluminium	0.53	0.26	0.18	2.50
Silicon			1.17	0.61
Manganese			1.15	2.80
Iron	0.41	3.52	94.6	24.0
Zinc	97.1	95.6	1.90	66.6

Table 7.6: SEM analysis of the coating defects produced on steel D (points 1 to 4 refer to the 1st defect, point 5 refers to the galvanneal type defect).

	Defect 1				Defect 2
% Element	Point 1	Point 2	Point 3	Point 4	Point 5
Oxygen	1.21	1.70	0.60	2.46	2.47
Aluminium				0.28	0.49
Silicon	0.19	0.18	0.13	0.33	0.20
Calcium				0.15	
Manganese	1.52	1.68		1.68	0.46
Iron	94.5	90.1	4.06	90.9	9.92
Zinc	2.60	6.30	95.2	4.18	86.5

Table 7.7: SEM analysis of the coating defect produced on steel E.

% Element	Point 1	Point 2
Oxygen	1.84	3.26
Aluminium	1.23	1.70
Manganese		0.32
Iron	2.42	3.47
Zinc	94.5	91.3

Table 7.8: SEM analysis of the coating defects produced on steel F (points 1 to 3 relates to the top dross type defect, point 4 refers to the 2nd defect).

	Defect 1			Defect 2
% Element	Point 1	Point 2	Point 3	Point 4
Oxygen	6.47	1.25	1.41	1.89
Aluminium	38.9	41.41	43.9	0.29
Chromium	0.13			
Iron	35.1	35.42	34.6	5.97
Zinc	18.9	21.5	19.5	91.9
Nickel	0.48	0.42	0.51	

Table 7.9: SEM analysis of the possible sources of the calcium rich defects obtained on a number of panels.

% Element	Refractory Tile	Quartz Tube Powder	Typical Building Cement
Oxygen	54.2	38.3	40.0
Aluminium		0.20	3.0
Silicon	45.7	16.4	15.0
Sodium	0.16	0.26	
Magnesium		0.38	
Titanium		0.33	
Zirconium		44.1	
Calcium			40.0

Table 7.10: SEM analysis for steels C and F processed using standard conditions and at a higher annealing furnace dew point.

	Steel C		Steel F	
% Element	Standard	High DP	Standard	High DP
Oxygen	0.98	8.78	1.21	0.96
Aluminium	0.18	9.02		
Silicon	1.17	3.88	0.19	0.58
Potassium		0.16		
Calcium		0.37		
Manganese	1.15	0.69	1.02	1.42
Iron	94.6	64.7	95.0	97.0
Zinc	1.90	12.4	2.60	

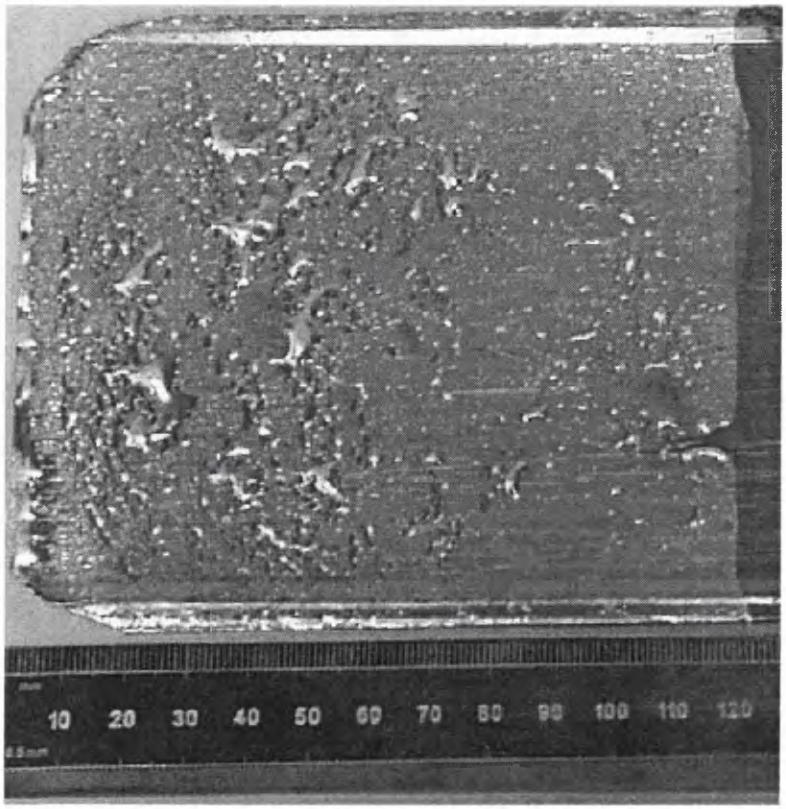

Figure 7.1: A digital image of steel C galvanised using the standard conditions.

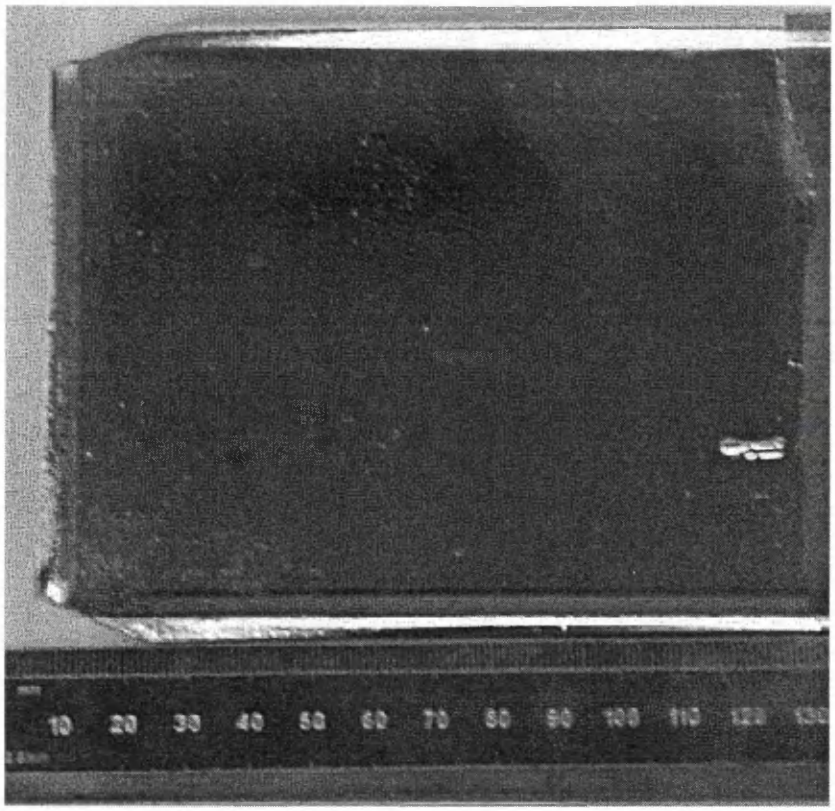

Figure 7.2: A digital image of steel D galvanised using the standard conditions.

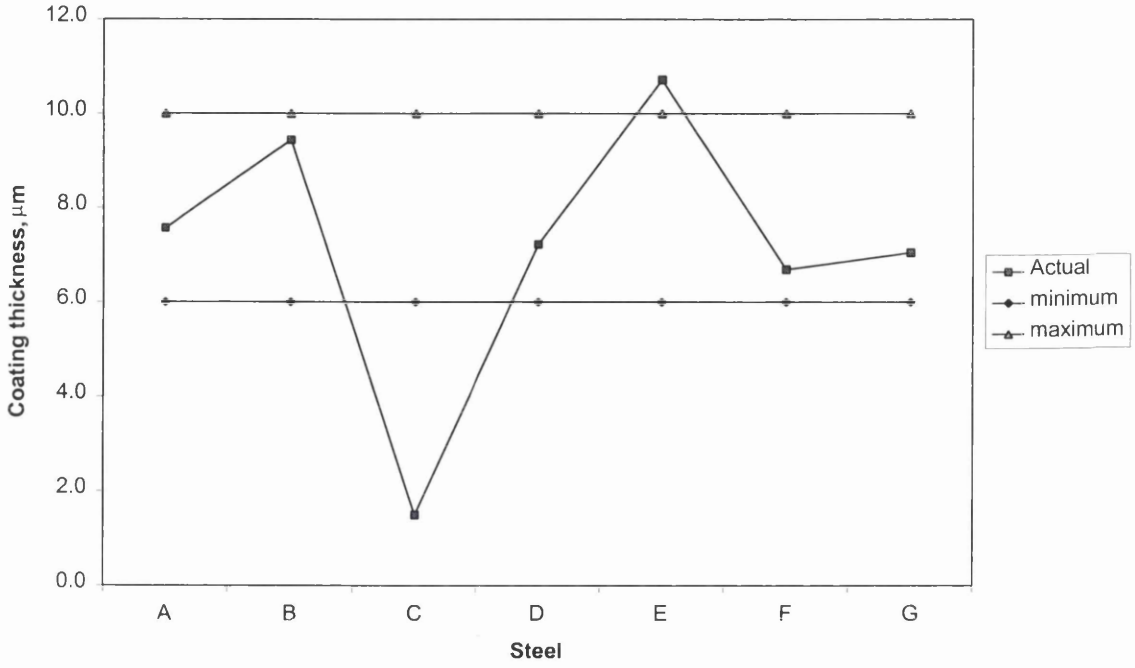

Figure 7.3: Typical coating thickness (average) for a small selection of samples, the minimum and maximum constraints of coating thickness are also shown.

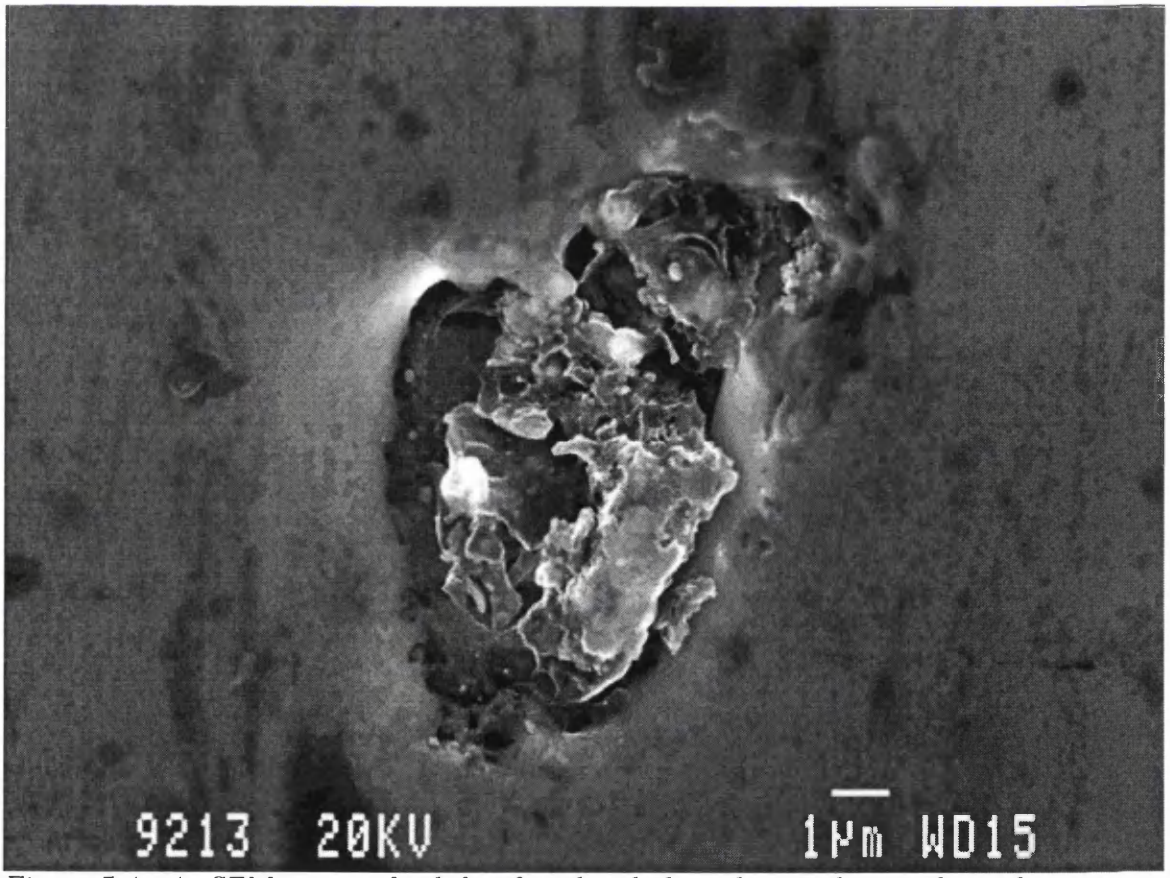

Figure 7.4: An SEM image of a defect found with the galvanised control panel.

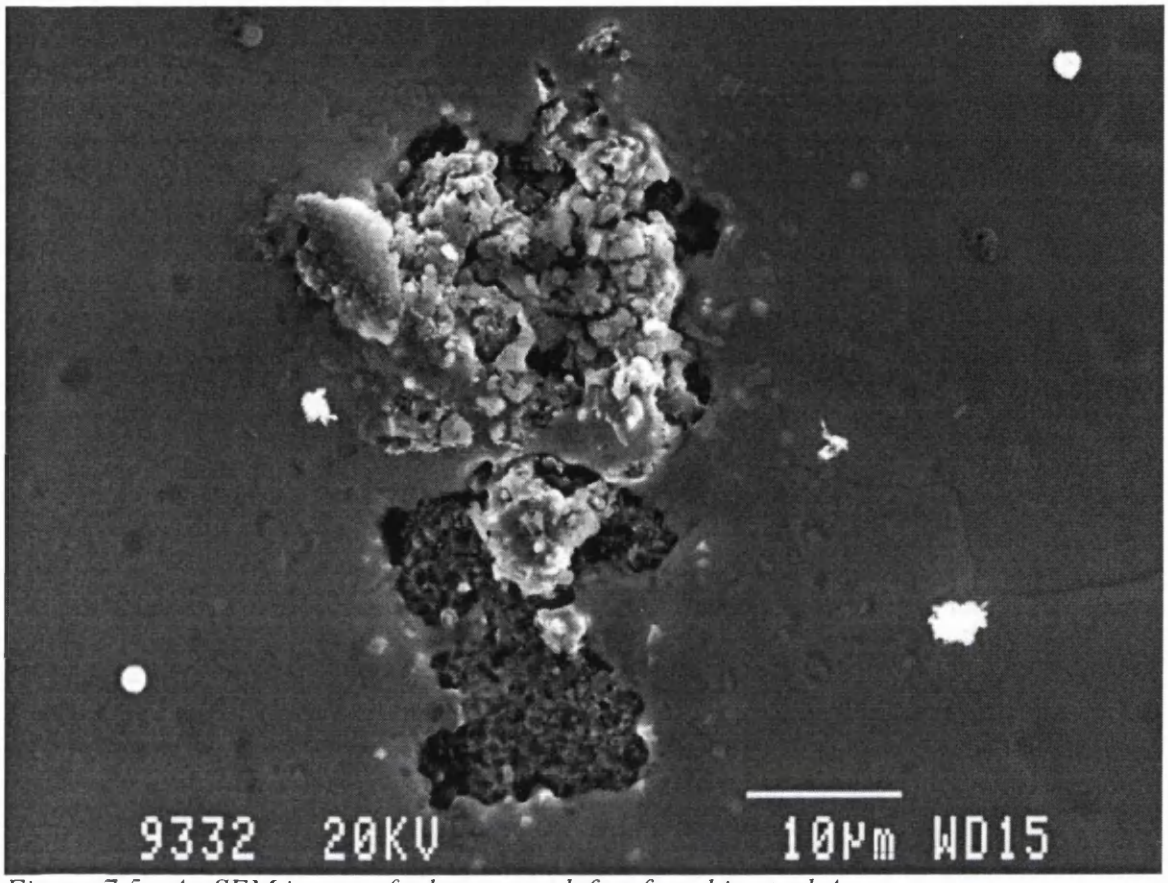

Figure 7.5: An SEM image of a bare spot defect found in steel A.

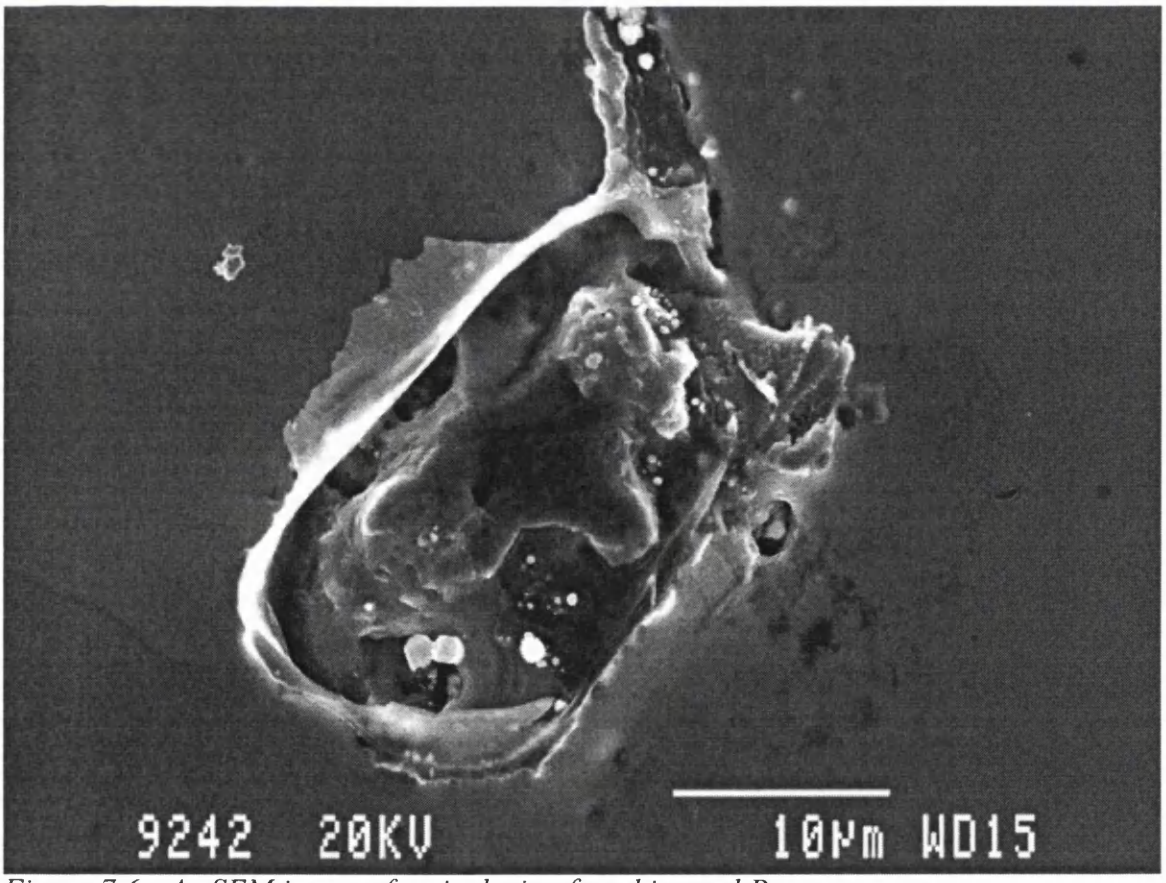

Figure 7.6: An SEM image of an inclusion found in steel B.

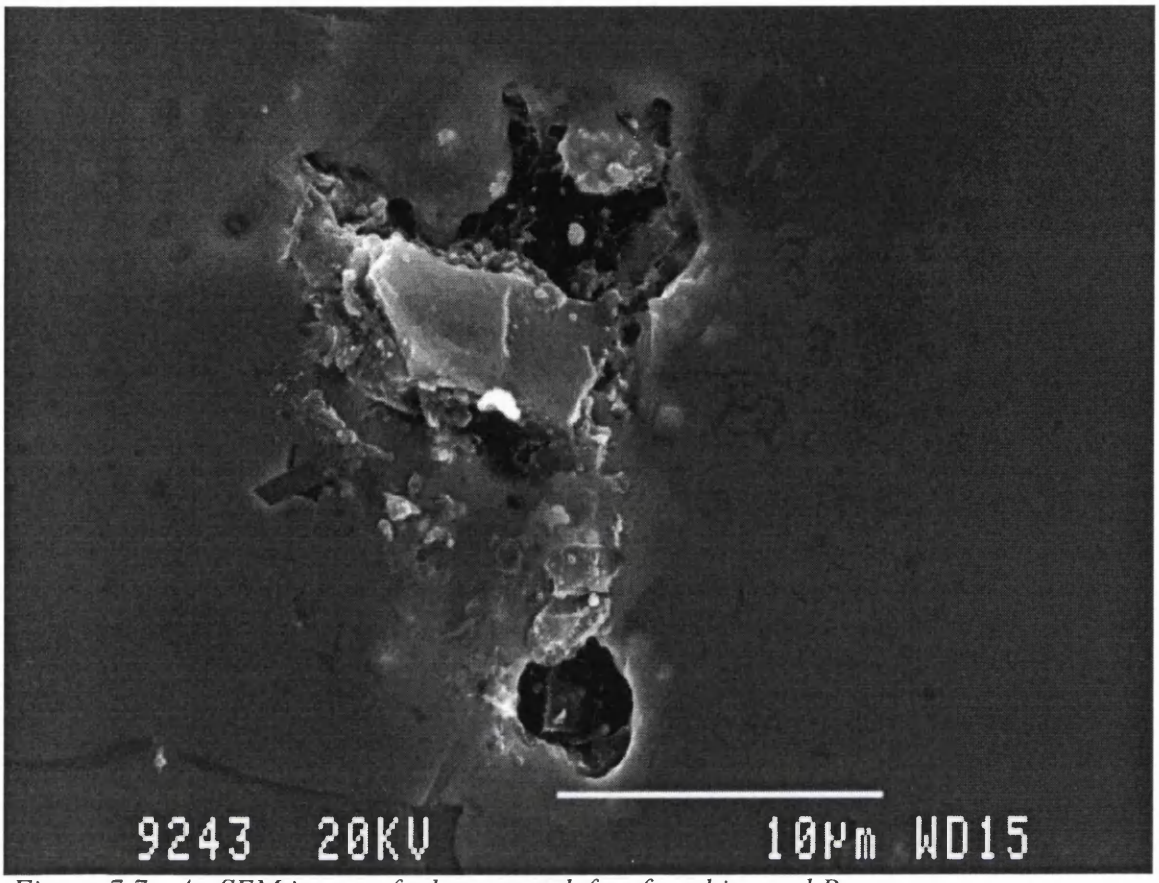

Figure 7.7: An SEM image of a bare spot defect found in steel B.

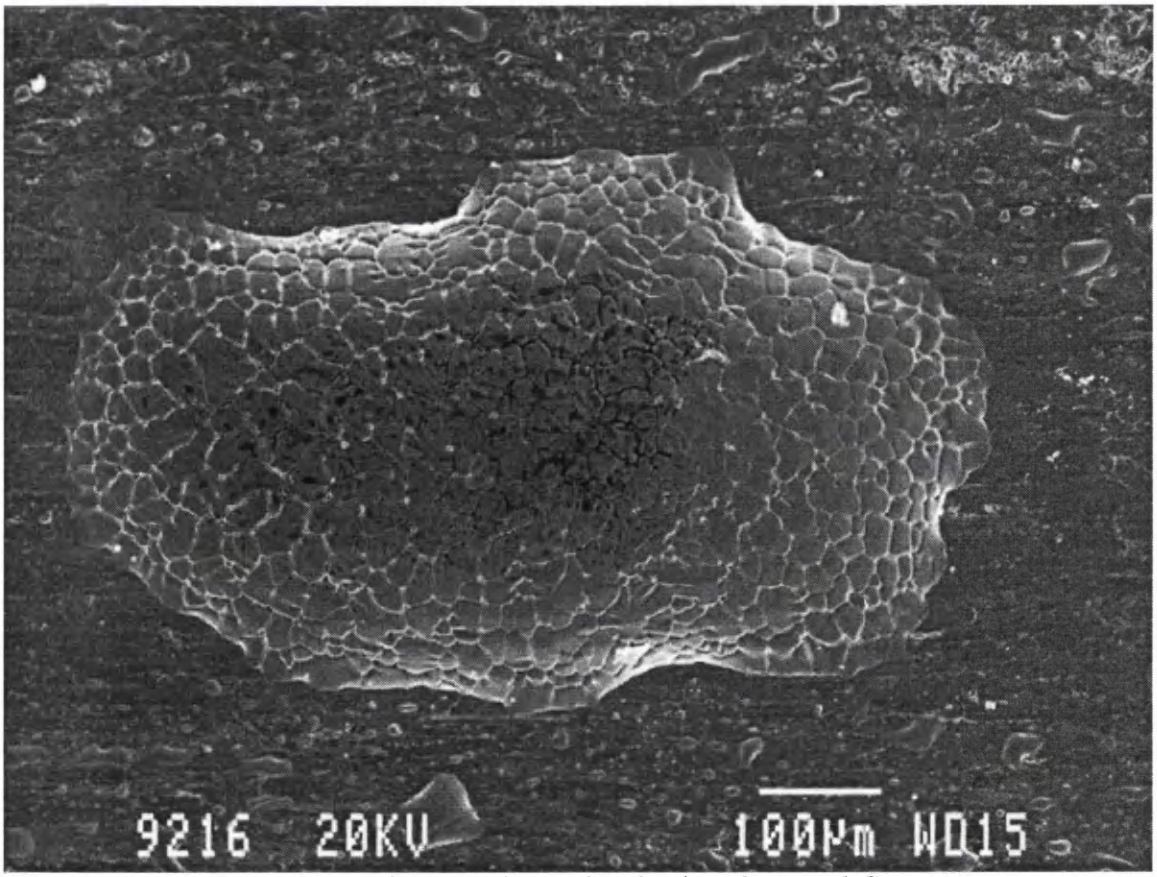

Figure 7.8: An SEM image of a typical zinc droplet found in steel C.

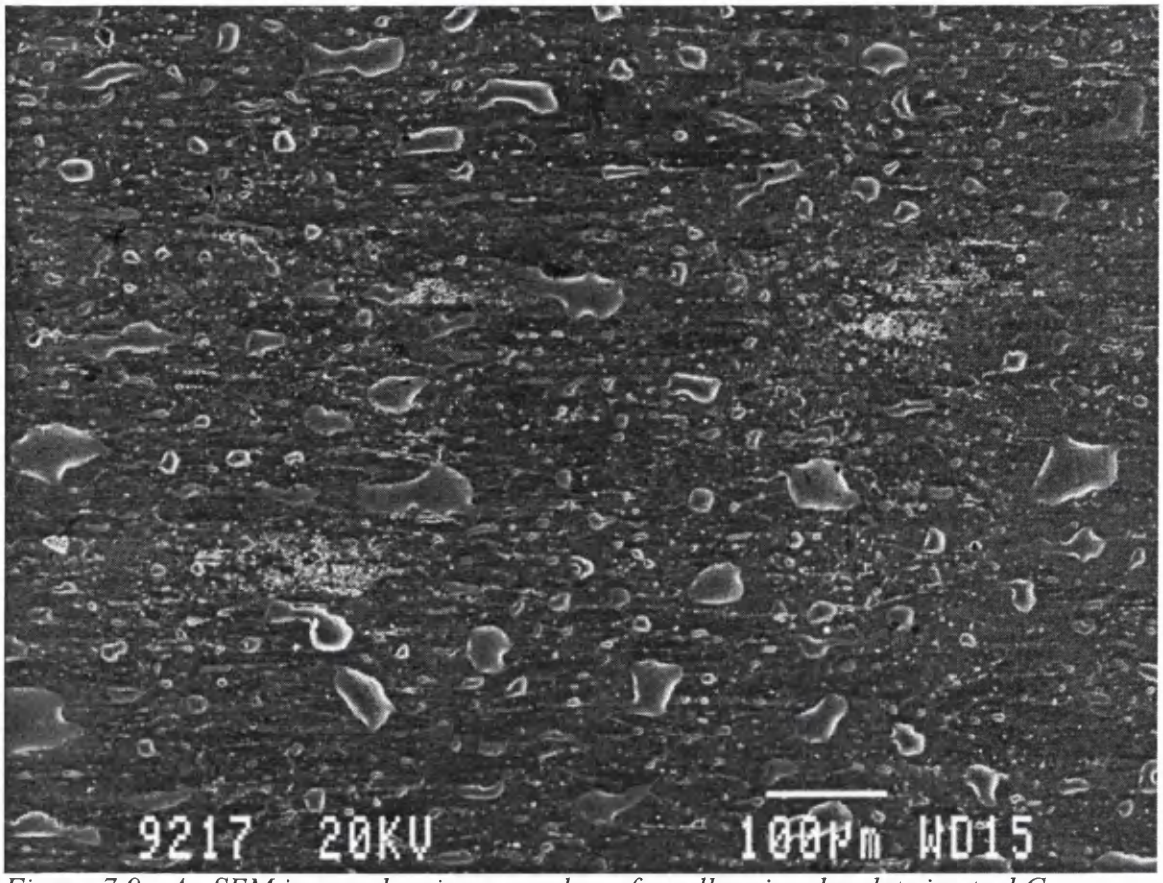

Figure 7.9: An SEM image showing a number of smaller zinc droplets in steel C.

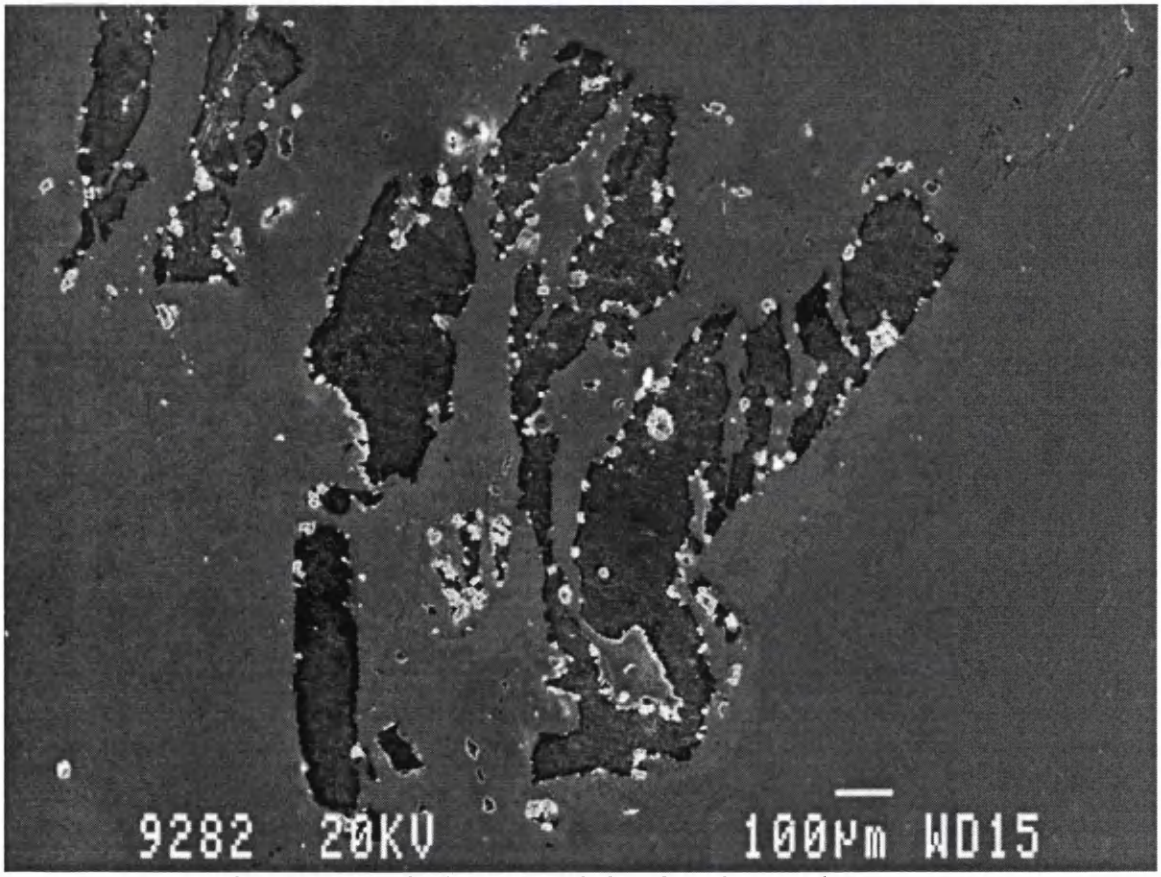

Figure 7.10: An SEM image of a bare spot defect found in steel D.

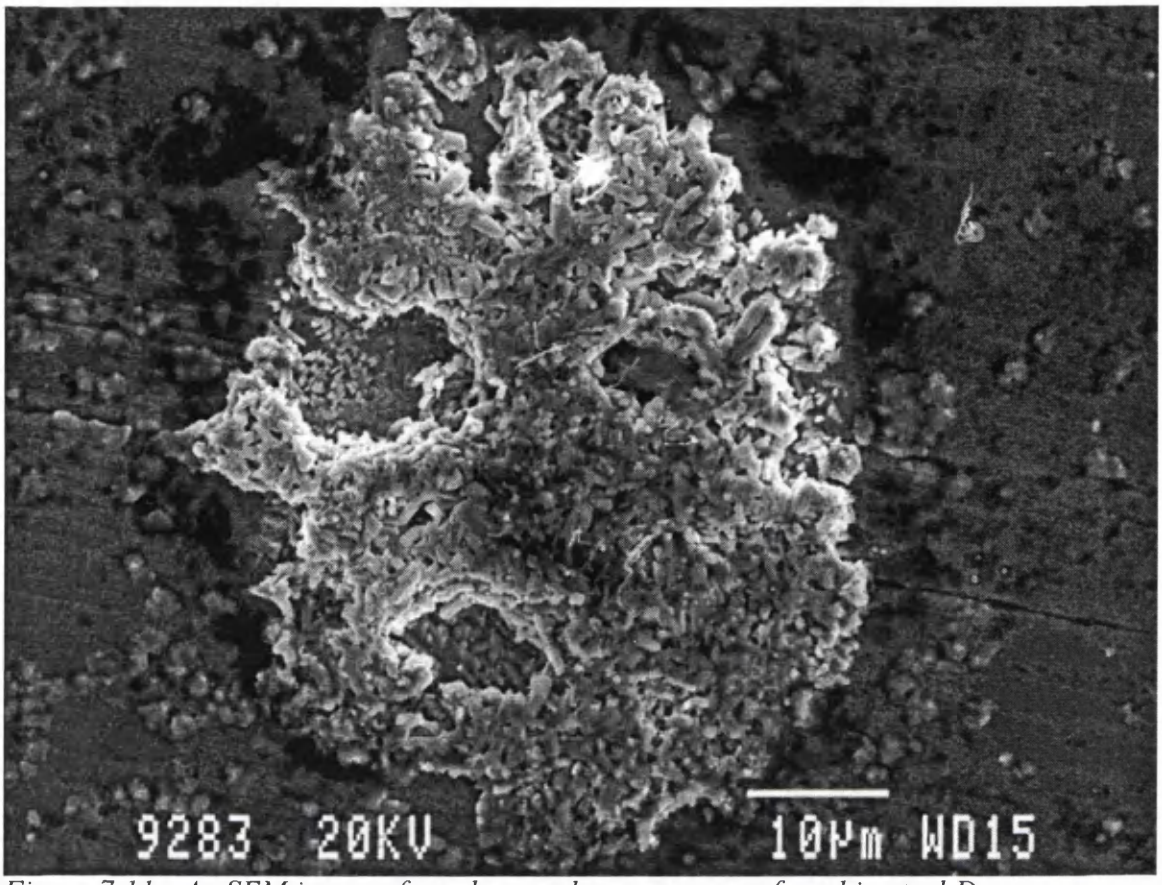

Figure 7.11: An SEM image of a galvanneal type structure found in steel D.

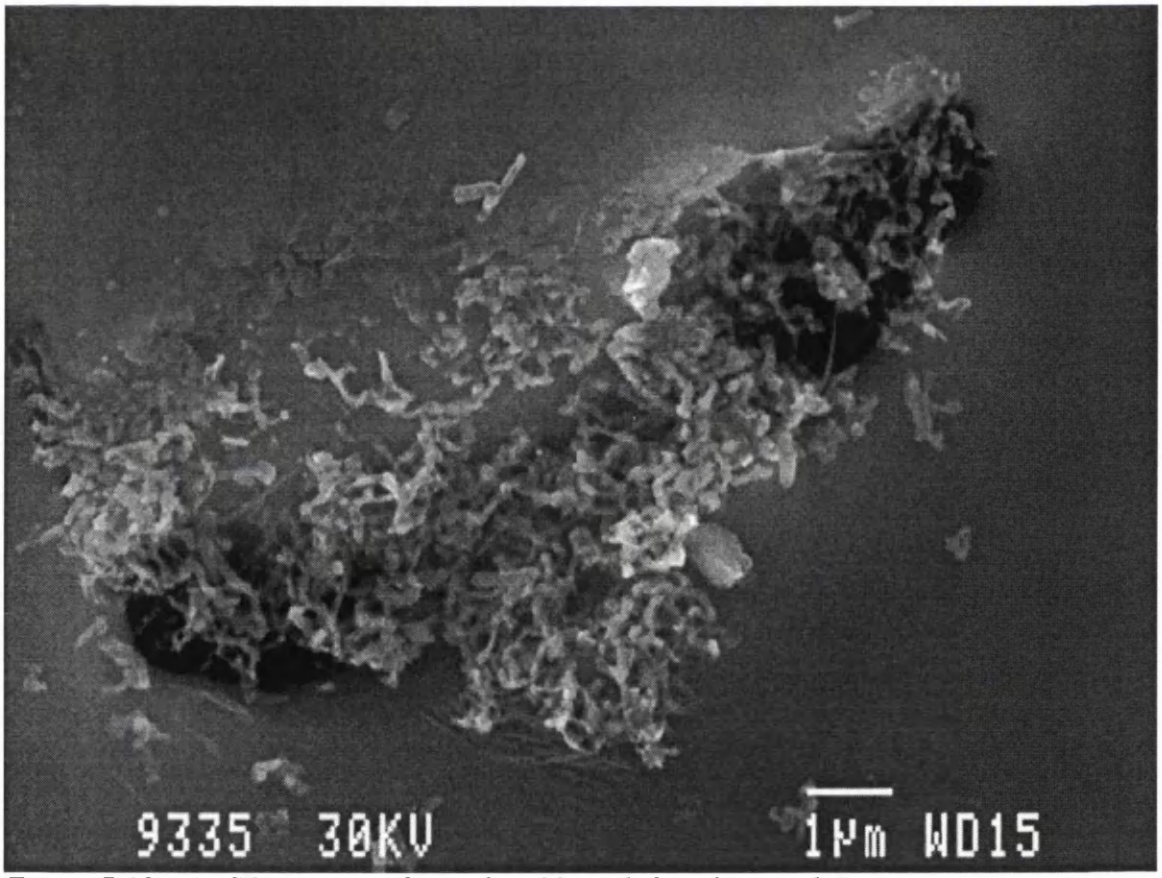

Figure 7.12: An SEM image of a surface blemish found in steel E.

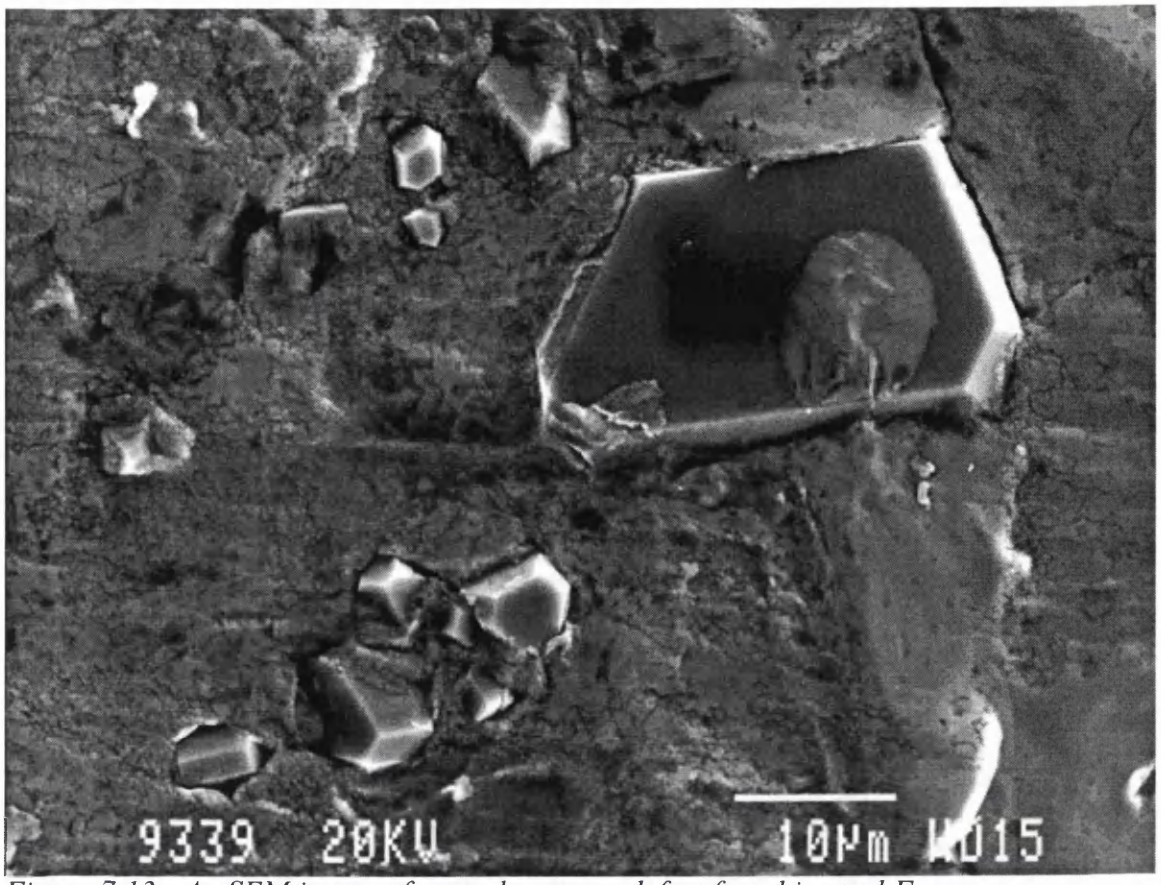

Figure 7.13: An SEM image of a top dross type defect found in steel F.

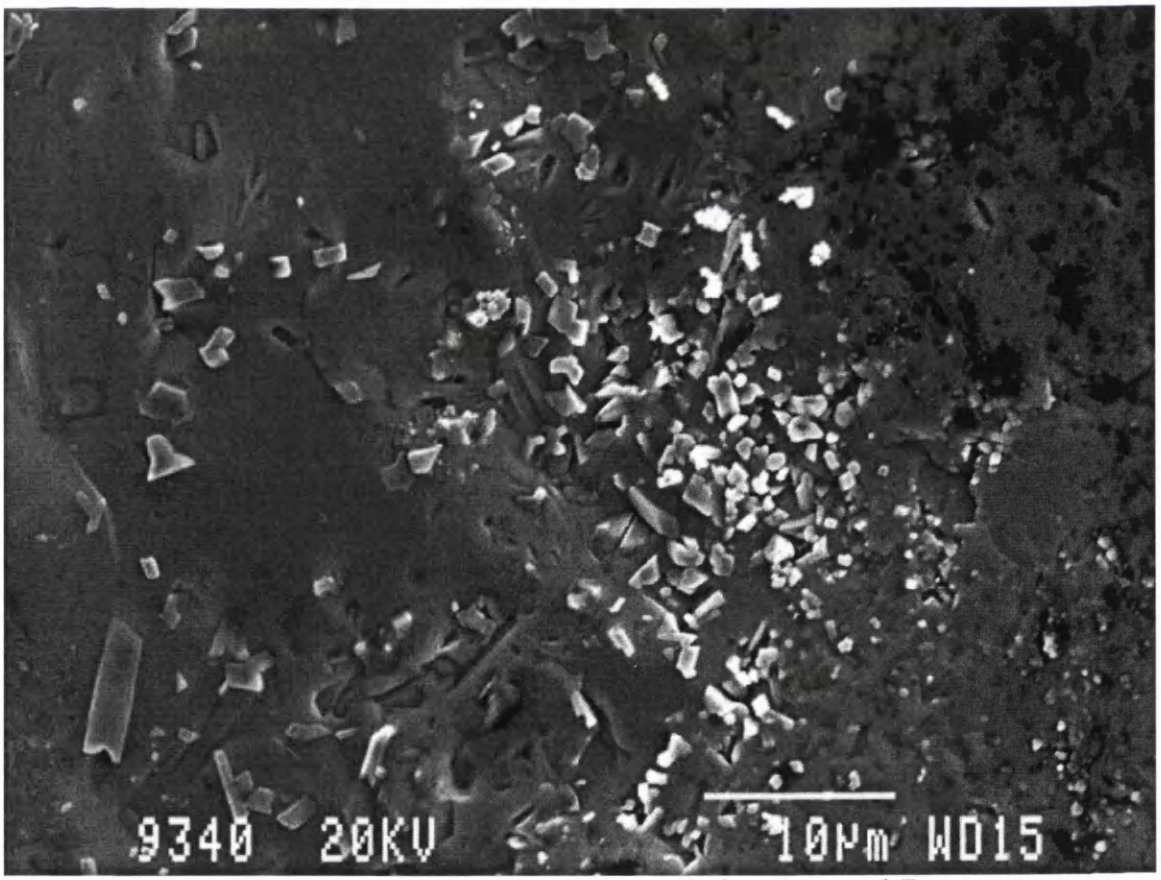

Figure 7.14: An SEM image showing angular crystals found in steel F.

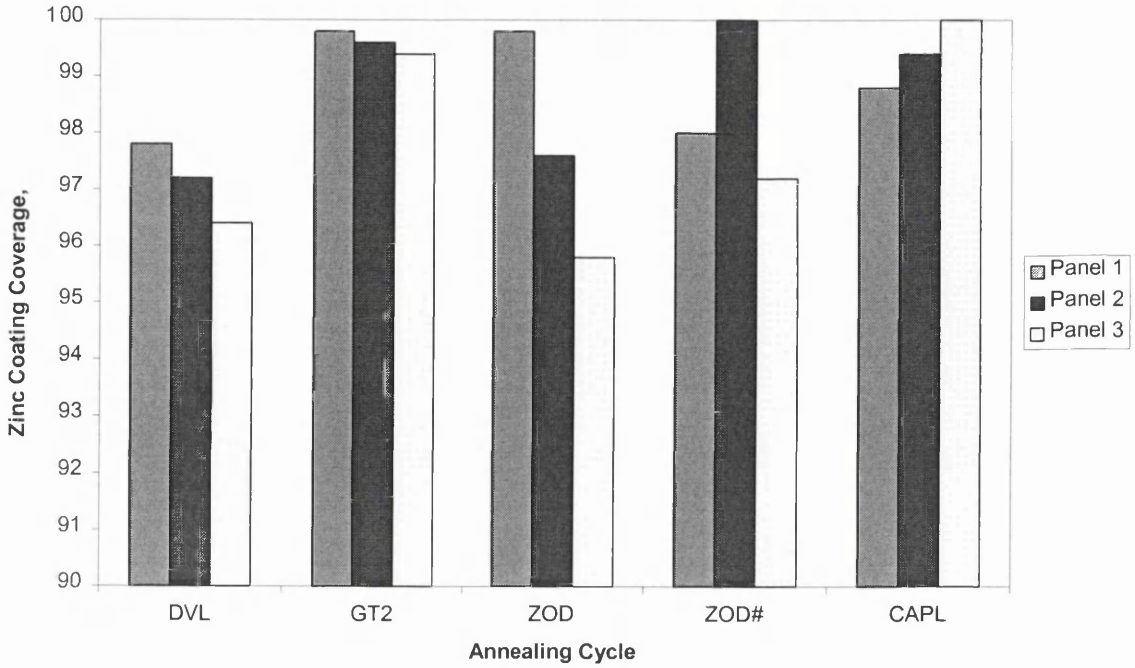

Figure 7.15: Surface area covered by zinc following the galvanising process with various annealing cycles.

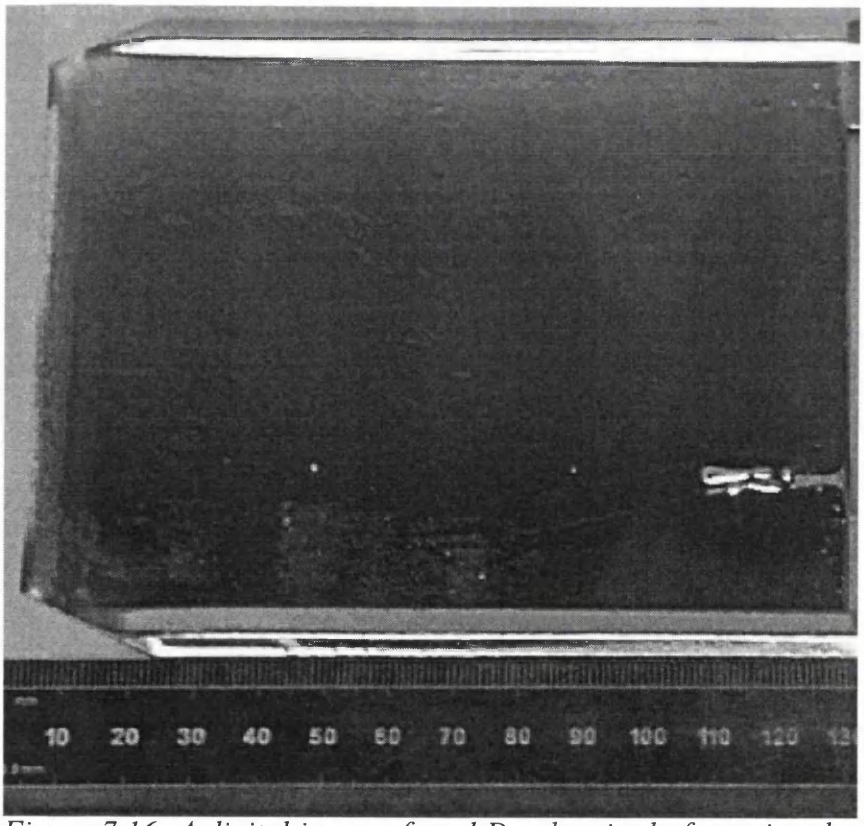

Figure 7.16: A digital image of steel D galvanised after using the higher dew point in the annealing furnace.

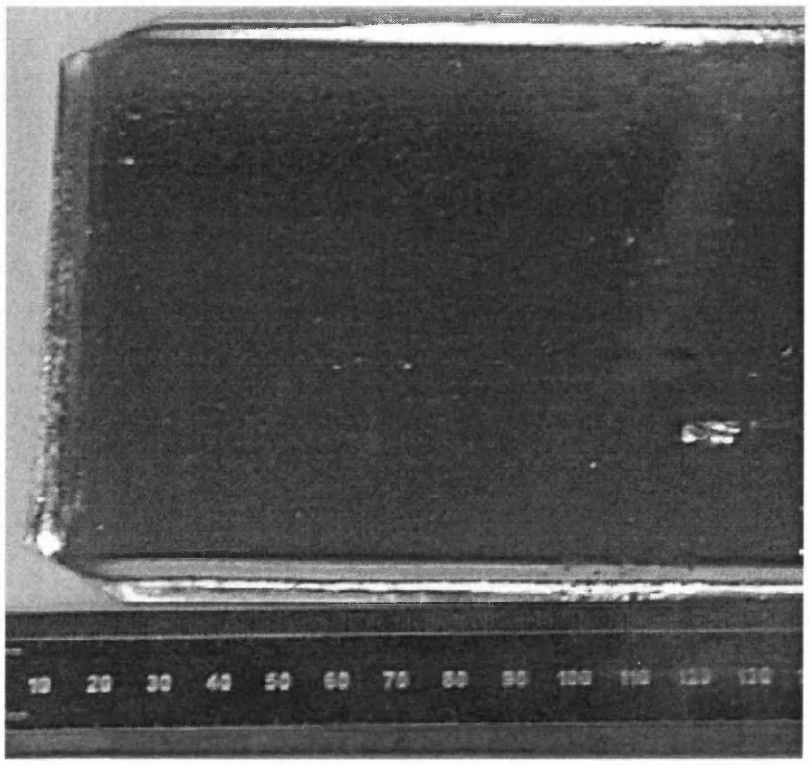

Figure 7.17: A digital image of steel C galvanised after using the higher dew point in the annealing furnace.

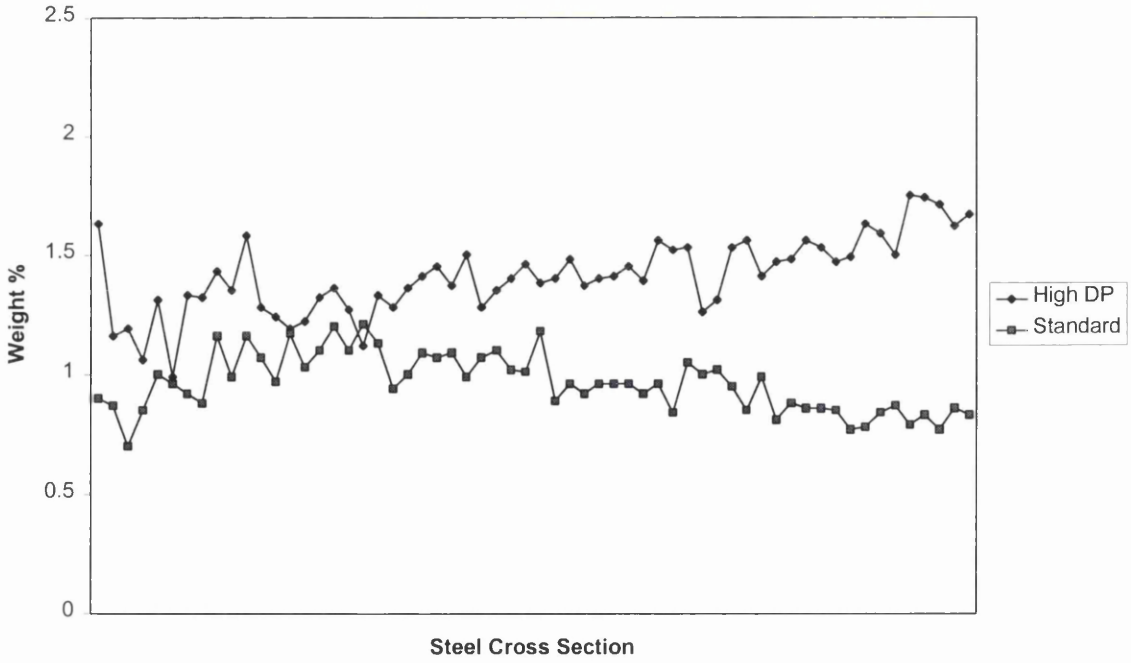

Figure 7.18: Oxygen levels for a cross section of steel C utilising both standard and high dew point annealing conditions from EDS analysis.

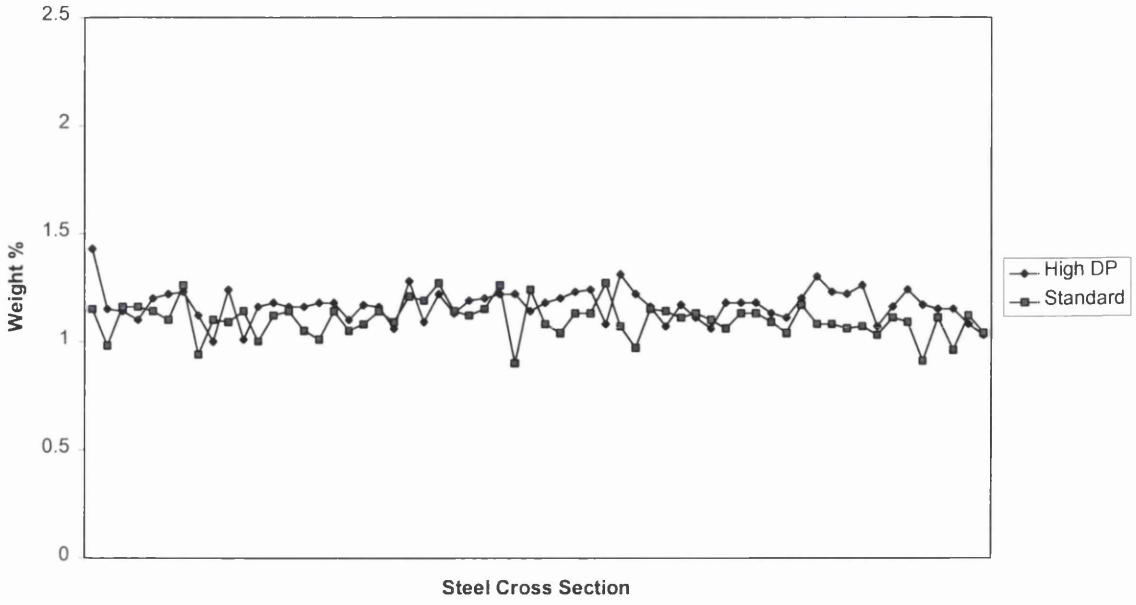

Figure 7.19: Silicon levels for a cross section of steel C utilising both standard and high dew point annealing conditions from EDS analysis.

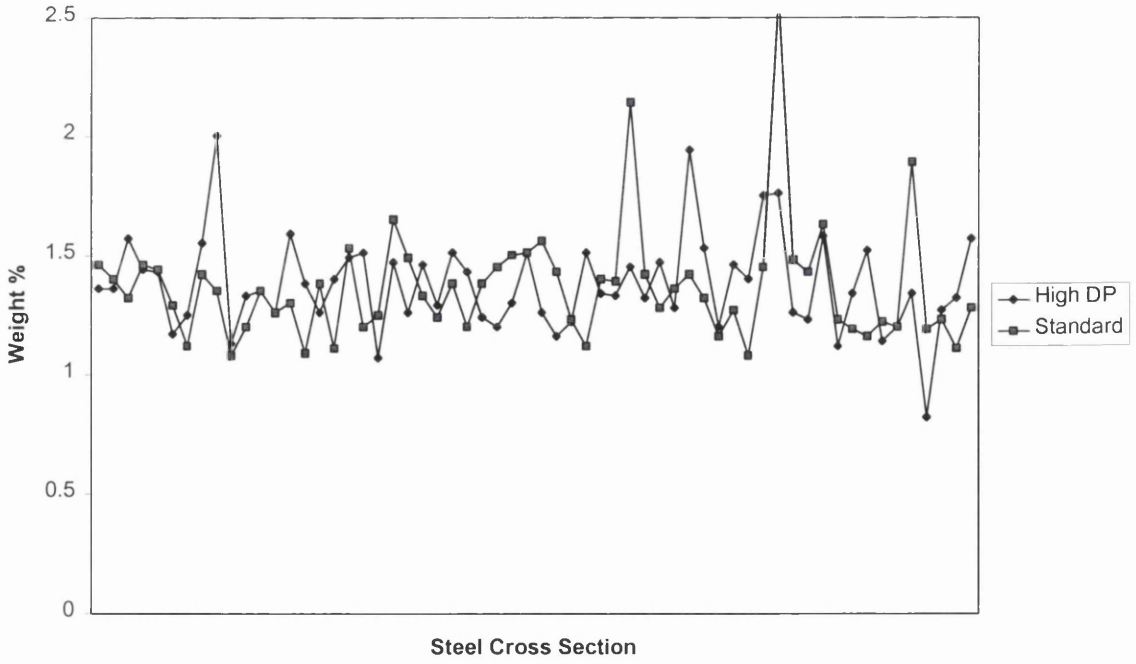

Figure 7.20: Manganese levels for a cross section of steel C utilising both standard and high dew point annealing conditions from EDS analysis.

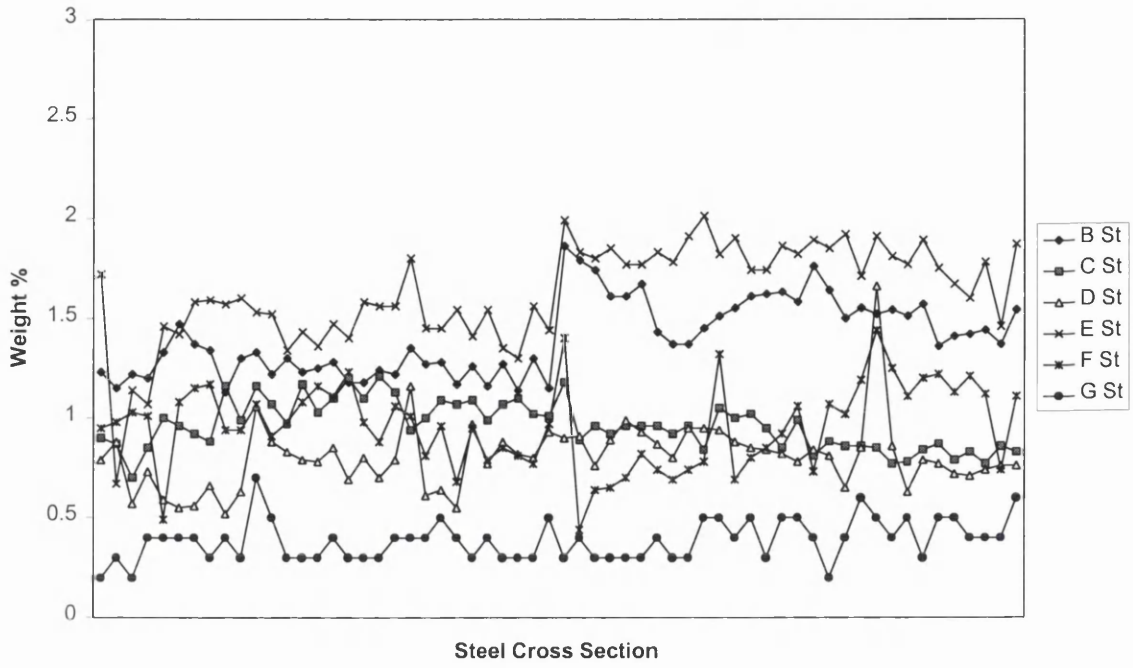

Figure 7.21: Oxygen levels for cross sections of all steels after standard annealing conditions from EDS analysis.

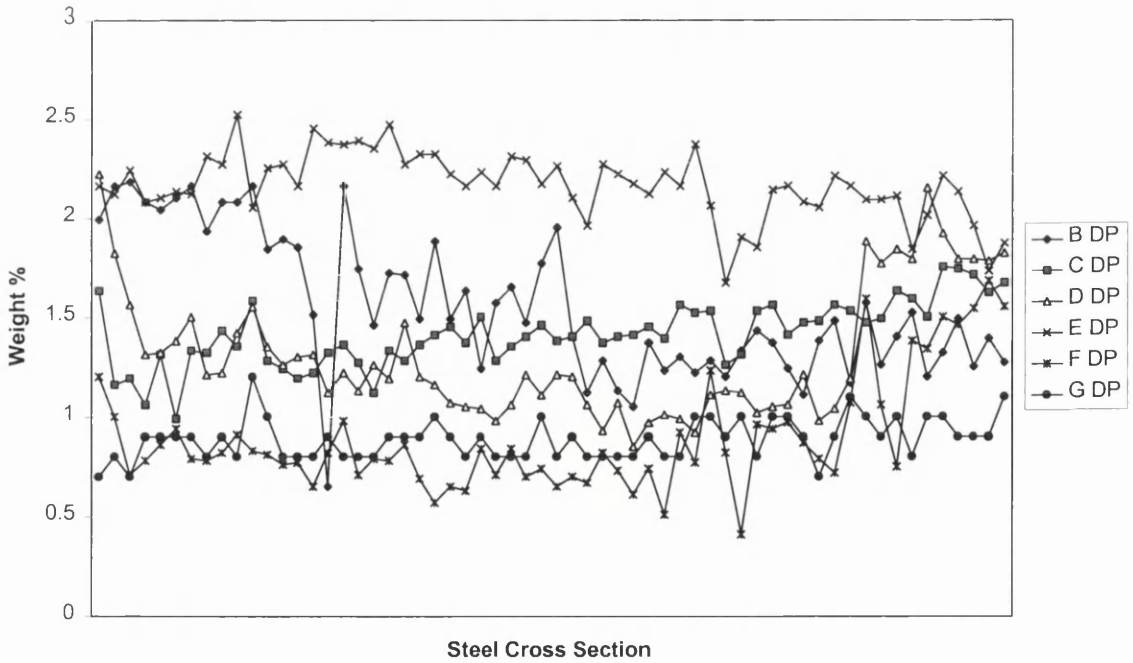

Figure 7.22: Oxygen levels for cross sections of all steels after high dew point annealing conditions from EDS analysis.

8.0 GENERAL DISCUSSION

This section brings together results from the three investigations and describes the all round properties of the steels, i.e., steels with the best mechanical properties and coating properties. The brief of the project was to produce galvanised-high strength steel, with dual phase steel being the preferred option. As a result, the success of steel properties was assessed primarily by whether typical dual phase tensile behaviour and ferrite – martensite microstructures were observed. The literature showed that the highly alloyed steels would be the most likely to produce required mechanical properties and poorest coating quality. With the reverse also being true, an intermediate position was ultimately what was aimed for.

Results will be set out so that the steels with the worst properties are considered first, until the steel with best properties is finally identified. Initially, the results of steels galvanised using a CAPL type cycle were explored. The CAPL line is not a galvanising line, but this exercise was carried out because, theoretically the CAPL line was the most suitable for dual phase production. After exploring the galvanising line that incorporated the CAPL annealing pattern, results from the cycles based on the galvanising lines were considered. These results would be more relevant with regards to current galvanising practice, but mechanical properties would inevitably be inferior to those of CAPL annealed material

8.1 STEEL D (0.1%C - 1.5%Mn – 0.1% Nb)

The steel microstructure and mechanical properties were the primary reason for rating this steel as the poorest steel grade. Even when subjected to the cycle most suitable for dual phase steels, steel D did not exhibit the required properties. This coupled with the problems associated with producing a satisfactory galvanised coating indicated that this steel was the least suitable for galvanised dual phase steel production. Deficiencies in alloying additions that increase hardenability caused the lack of martensite production. In conclusion, this steel possessed neither the steel properties nor coating quality required for galvanised high-strength steel production.

This point was only emphasised further by the results obtained from the steels annealed and galvanised with the galvanising line cycles.

8.2 STEEL B (0.1%C - 1.3%Mn)

As with steel D, steel B did not meet the desired characteristics. The coating quality was generally good for this steel, which shows it is suitable for producing galvanised steel. However, the purpose of the project was to produce galvanised dual phase steel, which this steel did not achieve. The fact that it was the least alloyed of the steels used meant that the results of the metallurgical evaluation were not surprising. The level of alloying additions in the steel was also the reason that a relatively good coating was achieved. Thus, the coating quality showed that steel B could be used for galvanised high strength steel, but would not meet the mechanical property standard set out for this project. Yet again, the galvanised steels produced from the galvanising line cycles had mechanical properties that were below standard.

8.3 STEEL E (0.2%C - 1.5%Mn)

Steel E displayed results that were only marginally better than those of steels B and D with regards to steel microstructures and mechanical properties. This was the only reason it was ranked above the aforementioned steels, because steel E also displayed a satisfactory galvanised coating. The higher carbon levels were proposed as the principal reason for the slight improvement in mechanical properties, which did not have an adverse effect on galvanisability. Yet again, the suitability of this steel grade would be questionable with reference to galvanising high-strength steel. Dual phase properties were not observed even when the cycle most conducive to dual phase steel production was utilised. In view of the mechanical properties and coating quality achieved, steel E could be used as galvanised high-strength steel. However, there would be limitations in its application because of the very high strength and low total elongation, the most likely use for steel E would be for non-formable components. Given that the CAPL type cycle produced a high-strength low formability product, it may seem feasible that some of the galvanising lines would be more appropriate. This

is because they produced steels with better elongation values, coupled with reasonably good strength.

8.4 STEEL C (0.1%C – 1.5%Mn – 1.3%Si)

Dual phase properties were produced for steel C from most of the heating/cooling regimes employed. In fact, from a metallurgical viewpoint, this steel grade was a near perfect material for dual phase steel. However, the coating produced during standard annealing conditions prior to galvanising was extremely poor, because of inadequate wetting. Silicon levels in this steel were the reason for both the excellent mechanical properties, as well as the poor coating. Hardenability was increased significantly because of the silicon in the steel and severe de-wetting was observed because of the silicon oxides produced on the surface of the steel. The poor coating quality was the primary reason for ranking this steel grade so low, given that the mechanical properties had been satisfied.

Nevertheless, the investigation did show that, by varying certain parameters within the annealing furnace, namely dew point, the galvanisability could be significantly improved. This improvement did not yield a perfect coating, but the work has shown that galvanisability can be greatly improved. Whether the results of this investigation could be recreated on an industrial scale remains to be seen. Theoretically it would be possible, but there may well be manufacturing or processing issues that would make it very difficult to achieve these conditions. Therefore, because of the uncertainty with regards to industrial annealing processes, it seems steel C could be used as a non-galvanised dual-phase product.

8.5 STEEL A (0.15%C – 1.5%Mn – 0.4%Si)

Results for steel A demonstrated that certain aspects of mechanical properties and steel microstructures were in line with those expected for dual phase steel. This coupled with a reasonable coating quality suggests that steel A could be utilised for galvanised dual phase production. Care must be taken with regards to the coating

quality, because it was not the best quality observed. This was probably due to the levels of silicon present that produced silicon oxide, which was significantly less than that observed with steel C. Even after considering the less than perfect coating, steel A displayed enough of the characteristics to maintain that it could be used for galvanised dual phase steel. This steel did exhibit dual phase properties when annealed using the galvanising line cycles on a couple of occasions, i.e., steel A could, in theory, be used for DP600 type galvanised grade on current lines provided that the minor coating issues were resolved.

8.6 STEEL G (0.1%C – 1.5%Mn – 0.5%Cr)

Steel G satisfied the required conditions for both steel properties and galvanisability for zinc-coated dual-phase steels. A classic ferrite-martensite dual phase microstructure was observed, as well dual phase mechanical properties. This steel also had a galvanised coating that displayed a good and consistent quality. The chromium increased the hardenability of the steel, which subsequently meant that martensite was formed when cooled. Moreover, wettability issues that were identified as a common feature associated with chromium containing steels did not occur. The only negative issue with this steel was the relatively low tensile strengths observed, even though it met the requirements of dual phase steel. Tensile strengths below 600 MPa were recorded, which would be problematic given that DP600 was one of the major products highlighted in the ULSAB project. In conclusion, steel G displayed almost perfect properties, i.e., good coating and dual phase properties, but the low tensile strength may well be an issue if it were produced commercially. In fact, the low tensile strength was even worse for steel produced on the galvanising line cycles.

8.7 STEEL F (0.1%C – 1.5%Mn – 0.01%Mo – 0.01%V)

There were two main differences between steels F and G, which were both positive differences for steel F. The mechanical properties and coating quality were very similar to that described for steel G, i.e., steel F displayed classic ferrite-martensite dual phase structure and mechanical properties as well as good galvanised coating

properties. The differences in steel F compared with steel G relate to the higher tensile strength and an even better coating quality. Steel F had tensile strength in excess of 600 MPa and was the only steel that did not produce any coating defects. Both the molybdenum and vanadium increase the hardenability of the steel and also limit the production of surface oxides that have an adverse effect on coating quality. Crucially, steel F could be used as a DP600 grade even though total elongation was a little less than required for this type of material. With regards to the galvanising line cycles, steel F could also be utilised to produce galvanised dual phase steels. The only drawback being tensile strengths too low for DP600 production.

9.0 CONCLUSIONS

The present study shows that galvanised dual phase steels could be produced when utilising the annealing cycles used in existing industrial galvanising lines. The matrix of results from the steel chemistries and annealing cycles showed that a range of metallurgical features were observed. A classic ferrite-martensite dual phase microstructure was produced on several occasions. In addition, the results have shown that the mechanical properties met criteria set out for dual phase grades.

Steel chemistry was a critical factor in determining whether the second phase produced was martensite. Three of the steels used in the investigation did not meet the criteria set out for dual phase classification. A steel substrate containing 0.1 weight % carbon and 1.3 weight % manganese did not exhibit sufficient hardenability to produce martensite during cooling from the intercritical temperature. An increase in manganese levels to 1.5 weight % was unsuccessful in impacting on hardenability. The addition of 0.01 weight % niobium to the substrate also failed to increase hardenability sufficiently for significant martensite to be produced.

When the cooling rate from the intercritical region was rapid, four of the steels met the desired dual phase characteristics. An addition of 0.5 weight % chromium to the C-Mn steel increased hardenability enough for martensite production when cooled from the intercritical region. Silicon levels set at 0.4 and 1.3 weight % to the C-Mn steel, both produced martensite because of the increased hardenability. A C-Mn steel with 0.01 weight % of both molybdenum and vanadium displayed hardenability levels that were also conducive to martensite formation.

The investigation has shown that the annealing cycle was a very significant factor for dual phase production. Cooling rate was underlined as the major factor, although holding conditions were also influential. Cycles that had cooling rates in the order of 60 °C/s produced dual phase steels in the majority of cases. Conversely, cycles that employed a cooling rate of around 10 °C/s did not develop dual phase steels.

Several of the steels produced in the investigation met the requirements set out for DP600 classification, i.e., tensile strengths greater than 600 MPa and sufficient total elongation values.

Generally, steels that contained less than 0.4 weight % silicon produced galvanised coating ranging from mediocre to good, whereas those with higher silicon levels produced poor coating quality. Furthermore, C-Mn steel containing 0.5 weight % chromium did not have an adverse affect on galvanisability.

Varying dew point in the annealing section of the galvanising process has a significant impact on coating quality. A dew point of 10 °C significantly improved coating quality of the steel that produced severe de-wetting during processing at the standard dew point (- 40 °C).

10.0 RECOMMENDATIONS FOR FURTHER WORK

The project set out to produce galvanised high strength steels and even though the brief of the project was ultimately met, there were several key issues that could have also been carried out. If a greater time scale were granted the following further work would have been carried out. Several of the points raised fell outside the scope of the project; nevertheless, they were subjects that could have enhanced the overall results.

The seven steel grades utilised during the project were suitable for dual phase production, which is one of several steel types that fall under the high strength steel umbrella. However, a study into the galvanisability of Transformation Induced Plasticity (TRIP) steels would have been beneficial. This is especially true for this research project because of the annealing cycles utilised, i.e., the overageing sections associated with a couple of the cycles could have been manipulated to incorporate a bainitic holding temperature. Also, an investigation into galvanising ultra high strength steels could well be carried out following the results achieved with investigation. Steels with tensile strengths in excess of 800 MPa could be investigated.

For industrial relevance, it was decided that annealing based on those available or possible in the near future were used. However, it may have been useful to utilise cycles that were not as variable in order to investigate the results of holding conditions and cooling cycle in greater detail. This would have enabled a larger matrix of steels and cooling rates to be investigated.

The literature review had described that previous processing steps had influenced the steel properties of the as-annealed material. It would have been interesting to vary conditions in the laboratory rolling experiments. The effects of coiling temperature in the hot mill and volume cold reduction during cold working could have been studied.

Given the current limitations on the industrial galvanising lines, innovative processes variations involving the annealing furnace conditions could be made. They include varying the hydrogen/nitrogen gas mix of the cooling sections so that greater cooling

rates could be achieved. Also, utilising thinner gauge material would increase the maximum cooling rate and an increase in pressure during the cooling section may increase the cooling rate. These are all suggestions that should be passed on to the relevant personnel involved with these lines.

In view of the fact that some of the steels were dual phase steels that were successfully galvanised, an industrial trial would have been extremely advantageous. The cost of producing a trial coil and subsequently processing it would have been vast, which makes meeting this recommendation very unlikely. However, in view of the current drive towards galvanised high strength, this aim could well be met. Nevertheless, the results of this investigation would be of interest to the Product Market Development business unit.

REFERENCES

Published Literature

[Abdalla *et al.* 1999]
Abdalla AJ, Hein LRO, Pereira MS, Hashimoto TM, Mechanical Behaviour of Strain Aged Dual Phase Steels, Material Science and Technology, Vol. 15, p1167-1170, 1999.

[Anderson 2003]
Anderson C, Weldability of High Strength and Ultra High Strength Steels, Engineering Doctorate Thesis, p23-31, 2003.

[Andrews 1965]
Andrews KW, Empirical Formaulae for the Calculation of Some Transformation Temperatures, JISI, Vol. 203, p721-727, 1965.

[Angeli *et al.* 2002]
Angeli G, Deinhammer H, Fadrel J, Angeli J, Papst I, Wolpers M, Distribution and Composition of Surface Oxides on High Strength IF-Steels After Recrystallisation Annealing, 44th MWSP Conference Proceedings, Vol. XL, p825-832, 2002.

[Berenger & Charbonnier 1992]
Berengier G, Charbonnier J-C, Book of Steel, Part 4 – Surfaces, Chapter 20, 1992.

[Bordignon *et al.* 1984]
Bordignon P, Hulka K, Jones B, High Strength Steels for Automotive Applications, Niobium Technical Report, December, 1984.

[Bordignon *et al.* 2001]
Bordignon L, Crahay J, Dynamic Effects in Galvanising of High Strength Steels, Galvatech 2001 Conference Proceedings, Brussels, p573-580, 2001.

[CRM 1998]
CRM, Effects of Cold Rolling Reduction and Cooling Rate After Annealing on As Galvanised Properties, ILZRO Project ZCO 1, 1998.

[El-Sesy *et al.* 1990]
El Sesy I, Klaar H-J, Hussein A-H, Effect of Intercritical Temperature and Cold-Deformation on the Kinetics of Austenite Formation During the Intercritical Annealing of Dual Phase Steels, Steel Research 61, No. 3, p131-135, 1990.

[Erdogan *et al.* 1999]
Erdogan M, Priestner R, Effect of Epitaxial Ferrite on Yielding and Plastic Flow in Dual Phase Steel in Tension and Compression, Materials Science & Technology, Vol. 15, p1273-1284, 1999.

[Evans *et al.* 1997]
Evans PJ, Hillis DJ, High Strength Formable Strip Steel, Lean Weight Vehicles Conference, 1997.

[Gallagher *et al.* 2002]
Gallagher MF, Speer JG, Matlock DK, Fonstein NM, Microstructure Development in TRIP Sheet Steel Containing Si, Al and P,44th MWSP Conference Proceedings, Vol. XL, p153-172, 2002.

[Gavard 2001]
Gavard L, Laboratory Investigation for a Dual Phase DP450 Grade, Corus R, D & T Report, 2001.

[Goodwin 1997]
Goodwin FE, ILZRO Worldwide Survey on Zinc Coated High Strength Steel, ILZRO ZCO 1, 1997.

[Goodwin et al. 2000]
Goodwin FE, Venkataraman R, Simpson TC, An Overview of Trends in Continuous Galvanized Sheet Products, Galvanised Sheet Steel Forum Automotive, London, p47-56, 2000.

[Hashimoto *et al.* 1986]
Hashimoto S, Sudo M, Mimura K, Hosoda T, Effect of Microstructure on Mechanical Properties of C-Mn High Strength Hot Rolled Sheet Steel, Transactions ISIJ, Vol. 26, p985-992, 1986.

[Heller *et al.* 2000]
Heller T, Engl B, Stich G, Thiemann G, Thermomechanical Rolling of Hot Rolled Multiphase Steels, Steel World, No. 1, p26-30, 2000.

[Herdveldt *et al.* 1998]
Herdveldt I, DeCooman BC, Classens S, Properties of Galvannealed Coatings on Ti-Nb IF Steels Strengthened with Manganese, Galvatech 1998 Conference Proceedings, Chiba, p230-235, 1998.

[Hillis 1999]
Hillis D, Rapid Annealing of Dual Phase Steels, Engineering Doctorate Thesis, 1999.

[Honeycombe & Bhadeshia 1995]
Honeycombe RWK, Bhadeshia HKDH, Steels: Microstructure and Properties, 2nd Edition, 1995.

[Jenkins *et al.* 1992]
Jenkins GA, Burrows LJ, Investigation of Zn/Fe Alloying in Various Commercial Galvanised Steels During Experimental Galvannealing by Radiation and Induction Heating, Galvatech 1992 Conference Proceedings, Amsterdam, p209-214, 1992.

[Jestin 2003]
Jestin N, Chemical & Physical Constitution of the Bath During the Galvanneal to Galvanise Transition, Engineering Doctorate Thesis, 2003.

[Jin *et al.* 2001]
Jin YS, Baik SC, Kim HT, Electroplating Characteristics of Cold Rolled TRIP Steel Sheets with TS 60 kgf/mm^2, Galvatech 2001 Conference Proceedings, Brussels, p568-580, 2001.

[Jordan *et al.* 1995]
Jordan CE, Marder AR, Alloy Layer Growth During Hot Dip Galvanising at 450 °C, Galvatech 1995 Conference Proceedings, Chicago, p319-325, 1995.

[Lamberigts 1999]
Lamberigts M, Galvanisability of High Strength Steels for Lightweight Automobiles, ILZRO Project ZCO 1, 1999.

[Lamberigts *et al.* 2001]
Lamberigts M, Goodwin FE, Development of Hot Dip Galvanised High Strength, Deep Drawing IF Steel for Modern Automotive Applications, Galvatech 2001 Conference Proceedings, Brussels, p560-572, 2001.

[Le Jeune *et al.* 1999]
Le Jeune D, Jenkins GA, Parker JD, Coating Microstructure Development During Zinquench Galvanising of Sheet Steel, Iron & Steelmaking, Vol.26, p470-476, 1999.

[Le Jeune 2000]
Le Jeune D, Zinc Quenching Dual Phase Steels, Engineering Doctorate Thesis, 2000.

[Llewellyn *et al.* 1996]
Llewellyn DT, Hillis DJ, Dual Phase Steels, Iron & Steelmaking, Vol.23, p471-477, 1996.

[Llewellyn *et al.* 1998]
Llewellyn DT, Hudd RC, Steels: Metallurgy and Applications, Third Edition, p1-137, 1998.

[Mahieu *et al.* 2000]
Mahieu J, Claessens S, De Meyer M, De Cooman BC, Galvanizability of High Strength Steels for Automotive Applications, Galvanised Sheet Steel Forum Automotive, London, p185-196, 2000.

[Mahieu *et al.* 2001]
Mahieu J, Claessens S, De Cooman BC, Influence of the Surface State of TRIP Steels on their Galvanizability, Galvatech 2001 Conference Proceedings, Brussels, p644-651, 2001.

[Maki *et al.* 2001]
Maki J, Mahieu J, Claessens S, De Cooman BC, Hot Dip Galvanising of Si-Free CMnAl TRIP Steels, Galvatech 2001 Conference Proceedings, Brussels, p623-630, 2001.

[Maruta 1999]
Maruta A, Advances in Automotive Sheet Steel, Steel Times International, p26-32, 1999.

[Matthews 1997]
Matthews A, The Competition in the Automotive Industry to Design REV's, Intergalva 1997 Conference Proceedings, Birmingham, 1997.

[McMurray 1999]
McMurray HN, Coated Steel Products, Engineering Doctorate Centre in Steel Technology, 1999.

[Mintz 2001]
Mintz B, Review of the Hot Dip Galvanisability of Low Si TRIP and Dual Phase Steels With 590MPa Strengths, Galvatech 2001 Conference Proceedings, Brussels, p551-559, 2001.

[Okada *et al.* 1996]
Okada S, Sakata K, Imanaka M, Kyono K, Hanazawa T, Development of High Formability High Strength 440MPa Grade with Excellent Formability, JSAE, Vol. 17, p313-318, 1996.

[Ouchi 1985]
Ouchi C, High Strength Low Alloy Steel, Proceedings of Wollongong International Conference, p17, 1985

[Porter *et al.* 1992]
Porter DA, Easterling KE, Phase Transformations in Metals & Alloys, Second Edition, p317-349, 1992.

[Rege *et al.* 2002]
Rege JS, Inazumi T, Nagataki Y, Urabe T, Smith G, Zuidema B, Denner S, Development of HDGI/HDGA Dual Phase Steel Family at National Steel Corporation, 44th MWSP Conference Proceedings, Vol. XL, p391-404, 2002.

[Rigsbee *et al.* 1979]
Rigsbee JM, Vanander PJ, Structure and Properties of Dual Phase Steels, AIME Conference Proceedings, New York, p56-86, 1979.

[Sarwar et al. 1998]
Sarwar M, Priestner R, Hardenability of Austenite in a Dual Phase, JMEPEG, Vol. 8, p380-384, 1998.

[Schumacher *et al.* 2000]
Schumacher B, Meurer M, Biele P, Macherey F, Measures to Improve the Performance of Hot-Dip Galvanized Steel Sheet, Galvanised Sheet Steel Forum Automotive, London, p163-171, 2000.

[Siebert *et al.* 1977]
Siebert CA, Doane DV, Breen DH, The Hardenability of Steels, ASM, Metals Park, Ohio, 1977.

[Soto *et al.* 1999]
Soto R, Saikaly W, Bano X, Issartel C, Rigout G, Charni A, Statistical and Theoretical Analysis of Precipitates in Dual Phase Steels Micro-alloyed with Titanium and their Effect on Moechanical Properties, Acta Metallurgica Inc., Vol. 47, p3475-3481, 1999.

[Steven *et al.* 1956]
Steven WS, Haynes AG, JISI, Vol. 183, p349, 1956.

[Stiaszny *et al.* 2000]
Stiaszny P, Pichler A, Spindler H, Tragl E, Hot Dip Galvanised High Strength Steel Grades for the Automotive Industry, Galvanised Sheet Steel Forum Automotive, London, p7-16, 2000.

[Sun *et al.* 2000]
Sun S, Pugh M, Manganese Partitioning in Dual Phase Steel During Annealing, Materials Science & Engineering A, p167-174, 2000.

[Tanaka *et al.* 1979]
Tanaka T, Nishida M, Hashiguchi K, Kato T, Formation of Ferrite plus Martensite Dual Phase Steels, AIME Conference Proceedings, New York, p221-241, 1979.

[Tang *et al.* 1998]
Tang NY, Dubois M, Goodwin F, Progress in Development of Galvanizing Bath Management Tools, Galvatech 1998 Conference Proceedings, Chiba, p76-83, 1998.

[Thomson *et al.* 1995]
Thomson RC, Miller MK, The Partitioning of Substitutional Solute Elements During the Tempering of Martensite in Cr & Mo Containing Steels, Applied Surface Sciences, 87/88, p185-193, 1995.

[Traint *et al.* 2002]
Traint S, Pichler A, Stiaszny P, Werner EA, Silicon and Aluminium in Low Alloyed TRIP Steels, 44th MWSP Conference Proceedings, Vol. XL, p139-152, 2002.

[Vrieze *et al.* 2000]
Vrieze J, Dekker A, Winter H, Zwetsloot R, Cold Rolled Hot Dip Galvanised Multi Phase Steel with 600-900 MPa Tensile Strengths, Galvanised Sheet Steel Forum Automotive, London, p17-26, 2000.

[Winchell & Cohen 1962]
Winchell PG, Cohen M, ASM 55, p347, 1962.

[Winklegrund 1994]
Winklegrund R, Lightweight Construction with Steel in the Automotive, Intergalva 1994 Conference Proceedings, Paris, psb2/1-5, 1994.

[Zhang *et al.* 1995]
Zhang L, Bensinger TR, Hot Dip Galvannealing of Interstitial Free Steel Strengthened by Manganese, Galvatech 1995 Conference Proceedings, Chicago, p115-120, 1995.

Web Pages

[www.audi.co.uk]

[www.lafargecement.co.uk]

[www.ispat.com]

[www.thyssen-krupp-stahl.com]

[www.ulsab.org]

[www.uss.com]